UNIVERSITY OF BIRMINGHAM

UNDERSTANDING THE ROLE OF THE LIPOPROTEIN DolP IN CELL ENVELOPE BIOGENESIS

by

GABRIELA BOELTER

A thesis submitted to the University of Birmingham for the degree of DOCTOR OF PHILOSOPHY

Institute of Microbiology and Infection
School of Biosciences
College of Life and Environmental Sciences
University of Birmingham

August 2022

Abstract

The bacterial cell envelope protects the cell against environmental threats, maintains the cell shape and contributes to metabolism and growth. The Gram-negative bacterial envelope is composed of three-layers, the outer membrane (OM), a peptidoglycan (PG) layer, and the inner membrane. The coordination of proteins involved in cell growth and septation is essential to avoid cell lyses. The aim of this thesis is to study the lipoprotein, DolP (formerly YraP) and its role in the cell envelope biogenesis of the Gram-negative bacterium *Escherichia coli*. DolP is a dual-BON domain lipoprotein localised in the OM. Studies have suggested that DolP might be a component of the BAM (β-barrel assembly machinery) complex and be a player in cell division. The BAM complex is formed by a β-barrel lipoprotein BamA and four accessory components, BamB, BamC, BamD and BamE. To test the first hypothesis, we deleted the non-essential genes *bamB, bamC* and *bamE* in a ∆*dolP* background. We observed a reduction in cell fitness and increase in the number of lysed cells in Δ*bamB*Δ*dolP* and Δ*bamC*Δ*dolP* mutants compared to the single mutants. The results suggest that DolP impacts the OM proteins assembly machinery. The second hypothesis is based on a study that suggested that DolP is an upstream regulator of NlpD. NlpD is the activator of the amidase AmiC. Amidases cleave the shared PG layer of adjunct cells to separate into daughter cells. In *E. coli*, amidases (AmiA, AmiB and AmiC) are regulated by NlpD, EnvC or ActS. To verify DolP's link to this process, we first observed that DolP does not regulate amidases activity *in vitro* and does not interact with NlpD in pull-down and MST (MicroScale Thermophoresis) assays. In addition, the mutant Δ*dolP* did not phenocopied Δ*nlpD* in a range of envelope stresses. Next, we tested the morphology of a panel of double deletion mutants of amidases and

amidase regulators with *dolP.* The analysis showed that *ΔamiAΔdolP* and Δ*envC*Δ*dolP* mutants present longer chain length compared to their parental strains indicating a role for DolP in cell division. In conclusion, we suggest that DolP might not be a NlpD regulator. However, DolP may impact daughter cell separation by interacting with AmiA and AmiC, or by a yet unknown mechanism.

Dedication

I would like to dedicate this thesis to my parents, João and Tânia, who gave me all the tools to build my path.

Acknowledgments

I would like to acknowledge my supervisor, Dr Manuel Banzhaf, for all his support and teaching. Thanks for the advice in helping to shape my future career and thanks for making our lab a good environment to work in.

I would like to acknowledge Prof Ian Henderson who was my first contact at the University of Birmingham and who firstly selected me as a PhD candidate. Thank you for your collaboration in this process.

Thanks to Dr Jack Bryant, who was there since the beginning helping and guiding me throughout the project.

Thanks to everyone in IMI, who helped me in different ways, to get good quality results to build up my thesis. Specially to Dr Patrick, Dr Andrew, Dr Tim, and the people of the 7th floor. Thanks to all students' part of the department. I had a great time during the IMI seminars, forums, and JAM talks with you.

Thanks to the first integrands of the Banzhaf group, Coral, Tejwant, Mindi and Coni, who faced the first challenges when I arrived in Birmingham with me.

Thanks to the all the students who later joined the group, Adam, Luca, Dimitra. Thanks for the moments of fun and learning. Thanks to Jaya, who, even for just a few months, appeared to help me to push the project.

Thanks to the current students in Banzhaf lab, Dema, Hannah, Micheal, Rudi, Annika, and Sotirios who helped me to release the pressure of being a PhD student, sharing our good and bad moments.

Thanks to all the people from T101, who I saw leaving and arriving in the lab during my time as PhD student.

Thanks to my mom and dad, who always motivated me to go after my dreams and to seek for knowledge to become a good person and professional. I am really grateful for all your support. Thanks to my brother, for the support and for all the visits enjoying our time in England together.

I would like to thank my love, Alexis, who, firstly, faced the adventure of moving to a foreign country with me. Secondly, thank you for all the support during the ups and downs of these four years leading me to arrive here today, to the completion of this thesis.

Thanks to all my friends in Brazil, who supported me from the other side of the ocean. Thanks to all friends I met in Birmingham. You were my family here and I will never forget all our experiences together.

I would like to thank The Darwin Trust of Edinburgh, for the funding and opportunity to complete a PhD degree in a well-recognised institution in England.

List of papers

Results and methodology of the following paper are incorporated in this thesis:

- Bryant JA, Morris FC, Knowles TJ, Maderbocus R, Heinz E, **Boelter G**, et al. Structure of dual BON-domain protein DolP identifies phospholipid binding as a new mechanism for protein localisation. Elife. 2020;9.

The following paper is incorporated in this thesis:

- **Boelter G**, Bryant JA, Doherty H, Wotherspoon P, Alodaini D, Ma X, Alao MB, Moynihan PJ, Moradigaravand D, Glinkowska M, Knowles TJ, Henderson IR, Banzhaf M. The lipoprotein DolP affects cell separation in *Escherichia coli*, but not as an upstream regulator of NlpD. Microbiology. 2022; 168

The following papers were also published during the PhD study period:

- Wątroba M, Bednarczyk W, Kawałko J, Mech K, Marciszko M, **Boelter G**., ... & Bała P. Design of novel Zn-Ag-Zr alloy with enhanced strength as a potential biodegradable implant material. Materials & Design. 2019; 183, 108154.
- Condren AR, Kahl LJ, **Boelter G**, Kritikos G, Banzhaf M, Dietrich LE, & Sanchez LM. Biofilm inhibitor taurolithocholic acid alters colony morphology, specialized metabolism, and virulence of *Pseudomonas aeruginosa*. ACS infectious diseases. 2019; 6(4), 603-612.
- Bryant JA, Cadby IT, Chong ZS, **Boelter G**, Sevastsyanovich YR, Morris FC, ... & Henderson IR. Structure-function characterization of the conserved regulatory

mechanism of the *Escherichia coli* M48 metalloprotease BepA. Journal of bacteriology. 2020; 203(2), e00434-20.

- Goodall EC, Isom GL, Rooke JL, Pullela K, Icke C, Yang Z., **Boelter G,** ... & Henderson IR. Loss of YhcB results in dysregulation of coordinated peptidoglycan, LPS and phospholipid synthesis during *Escherichia coli* cell growth. PLoS genetics. 2021; 17(12), e1009586.
- Verheul J, Lodge A, Yau HC, Liu X, **Boelter G**, Liu X, ... & den Blaauwen T. Early midcell localization of *Escherichia coli* PBP4 supports the function of peptidoglycan amidases. PLoS Genetics. 2022; 18(5), e1010222.
- Goodall EC, Morris FC, McKeand SA, Sullivan R, Warner IA, Sheehan E, **Boelter G** ... & Henderson, I. R. LI-Detector: a Method for Curating Ordered Gene-Replacement Libraries. Microbiology Spectrum. 2022; e00833-22.

Table of Contents

List of Figures

List of tables

List of abbreviations

BAM - β-barrel assembly machine
DAPI - 4′,6-diamidino-2-phenylindole
DNA - deoxyribonucleic acid
EDTA - ethylenediaminetetraacetate
IM – Inner membrane
LPS – lipopolysaccharides
MST – MicroScale Thermophoresis
OM – Outer membrane
OMP – Outer membrane protein
PBP - penicillin-binding proteins
PCR – Polymerase Chain Reaction
PG – Peptidoglycan
POTRA - polypeptide transport-associated
SDS - sodium dodecyl sulphate
SDS-PAGE - SDS-polyacrylamide gel electrophoresis
SEDS - shape, elongation, division and sporulation
TEMED – tetramethylethylenediamine
TraDIS – Transposon Directed Insertion Site Sequencing
WT – wild-type

Chapter 1. Introduction

1.1 Bacterial cell envelope

The bacterial cell envelope acts as a first line of defence against antimicrobial insults and therefore understanding its biogenesis is important to address antimicrobial resistance. Among the most important bacterial cell biology discoveries was the description of cell envelope composition. Most bacteria are divided in two groups according to its cell envelope composition: Gram-negative and Gram-positive. The Gram-negative cell envelope is constituted by an outer membrane (OM), a thin layer of peptidoglycan (PG), and an inner membrane (IM). The Gram-positive cell envelope contains a thick layer of PG and an inner membrane; however, it lacks the OM (Vollmer & Seligman, 2010). As the bacterial cell envelope is unique to bacteria, its components are effective drug target, with limited side effects outside the human gut microbiome. For example, penicillin, and later developed antibiotics as cephalosporins, and vancomycin, affect cell wall synthesis, leading to cell lysis and death (Patrick, 2013). Evaluating the most frequent infections by bacteria, it was observed that Gram-negative bacteria are often more resistant to antibiotics than Gram-positive bacteria due to their asymmetric OM that repels antibiotics from reaching their cellular target within the cell (Delcour, 2009). Therefore, in my project I focus on Gram-negative bacteria identifying proteins that contribute to envelope biogenesis as this may lead to the identification of novel drug targets. The Gram-negative cell envelope layers work against chemical and mechanical affronts, preventing hydrophobic compounds and large hydrophilic compounds from penetrating the cell. These layers are also crucial for the maintenance of cell shape during growth (Rojas *et al*, 2018).

The OM consists of an inner leaflet with phospholipids and an outer leaflet with lipopolysaccharides (LPS) (Ebbensgaard *et al*, 2018) (Figure 1). In the inner leaflet of the OM there are three types of phospholipids: phosphatidylethanolamine, phosphatidylglycerol and cardiolipin (Raetz & Dowhan, 1990). These phospholipids are also present in the IM (Wu *et al*, 2014). In the outer leaflet, there is LPS which is a barrier against cationic antimicrobial peptides and also serves as one of the primary targets of the innate mammalian immune system (Maldonado *et al*, 2016). The LPS core structure can change depending on the species (Erridge *et al*, 2002). LPS in *E. coli* is formed by (i) lipid A (highly hydrophobic, responsible for endotoxicity), (ii) core-OS (outer core consists of sugars as glucose and galactose, and inner core consists of a high concentration of Kdo (3-deoxy-D-manno-octulosonic acid) and Hep (L-glycero-D-manno heptose) sugars) and (iii) O-antigen (polymer of repeating saccharide subunits composed commonly of hexoses and hexosamines) (Widmalm, 2019). The negative charge interaction of lipidA and core oligosaccharide creates an ionic binding with divalent cations which is important for membrane stability (Rietschel *et al*, 1994).

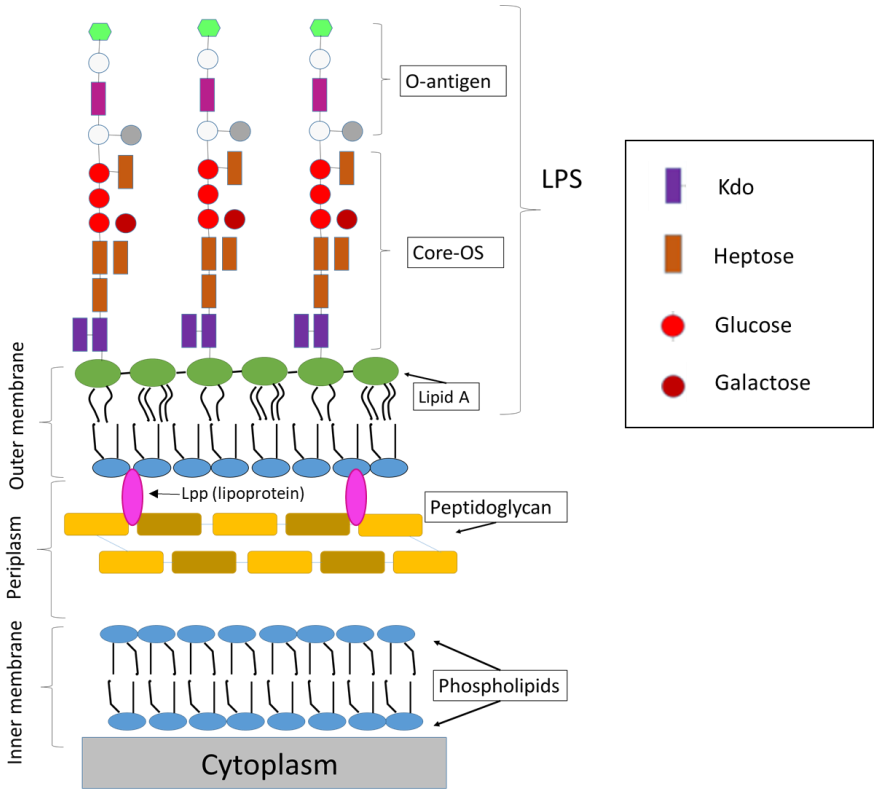

Figure 1. Schematic view of the cell envelope of Gram-negative bacteria showing the inner membrane, periplasm, outer membrane and LPS portion
(Figure based on (Ebbensgaard *et al.*, 2018))

The OM and IM are separated by the periplasm, which contains a thin layer of PG, the cell wall. The stabilization of the cell envelope is mediated by PG lipoproteins, Lpp, that are covalently attached in the cell wall and binds OM to PG (Bernstein, 2011). The cell wall is responsible for maintaining the cell shape and osmotic homeostasis, and serves as scaffold to anchor proteins of the cell envelope (Dramsi *et al*, 2008). PG contains repeating glycan strands of the disaccharide N-acetylglucosamine (GlcNAc) and N-acetylmuramic acid (MurNAc), which are cross-linked by pentapeptide side chains. Oligomerization of monomeric disaccharide units forms the glycan strand. Cross-linking of the glycan strands generally occurs between the carboxyl group of D-

Ala and the amino group of the diaminoacid, either directly or through a short peptide bridge (Vollmer *et al*, 2008).

The IM is a phospholipid bilayer. In *E. coli*, the main phospholipids are phosphatidylethanolamine and phosphatidylglycerol (Raetz & Dowhan, 1990). The IM proteins either span the lipid bilayer via one or more hydrophobic transmembrane helices (integral) or are bound directly to phospholipid molecules or by protein:protein interaction to the surface of the membrane (peripheral) (Papanastasiou *et al*, 2013). Since bacteria do not have organelles, besides ribosomes, this membrane encloses the cytoplasm and contains the main proteins involved in energy and lipid synthesis, environmental sensing, protein secretion and transport, trafficking of ions, molecules, and macromolecules (Silhavy *et al*, 2010).

The homeostasis of all three layers of a Gram-negative bacteria is crucial along cell life cycle. Specific to separation into daughter-cells, proteins of the cell envelope involved in elongation, division, invagination and septation must be well coordinated to avoid cell lysis. I will introduce the key players that are relevant to this thesis in the following paragraphs.

1.2 Cell elongation

Bacteria elongate the cell envelope in order to grow leading them to separate into two daughter cells. To maintain shape and to resist the turgor pressure during growth, the elongation of the PG sacculus must be well coordinated. The sacculus grows with the insertion of newly synthesized PG into the pre-existing sacculus, while

hydrolases cleave PG to allow space for the newly synthesized material (Burman & Park, 1984). PG hydrolases are discussed in section 1.6.

PG synthesis happens in three stages. First, nucleotide precursors (UDP-*N*-acetylglucosamine and UDP-*N*-acetylmuramyl pentapeptide) are synthesized in the cytoplasm by the Mur proteins (MurA, MurB, MurC, MurD, MurE MurG, MraY and MurZ (Barreteau *et al*, 2008). Second, the nucleotides are assembled with undecaprenyl phosphate in the inner surface of the IM, forming lipid II (lipid-anchored disaccharide-pentapeptide monomer subunit) (Bouhss *et al*, 2008; Mohammadi *et al*, 2011) and are flipped across the membrane presumably by MurJ (Qiao *et al*, 2017; Ruiz, 2008) or RodA and FtsW (Ehlert & Holtje, 1996). Third, lipid II is polymerized, liberating undecaprenyl pyrophosphate, and the subsequent glycan chains are inserted into the cell wall via a glycosyltransferase activity to polymerise the glycan strands and a transpeptidation activity to cross-link the peptides of adjacent strands (Vollmer & Bertsche, 2008). PG hydrolases (see 1.5) activity allows the enlargement of the cell wall for insertion of new glycan chains.

PG synthases are classified as glycosyltransferases (GTases), DD-transpeptidases (DD-TPases) and TPases or penicillin-binding proteins (PBPs). PBPs originally have this nomenclature since they are able to covalently bind penicillin. PBPs have bifunctional GTase–TPases (the class A PBPs), monofunctional TPases (the class B PBPs) and DD-carboxypeptidase (DD-CPase) and endopeptidase (EPase) activities (Vollmer & Bertsche, 2008). In *E. coli*, the PG synthases present are three bifunctional synthases (PBP1A, PBP1B and PBP1C), a GTase (MgtA) and two TPases (critical either for cell elongation (PBP2), or for cell division (PBP3; also known as FtsI) (Figure 2). Monofunctional GTases are the SEDS (shape, elongation, division and

sporulation) proteins and GT51 GTase (Terrak *et al*, 2008). The SEDS proteins constitute a family of PG polymerases with ten transmembrane helices which are involved during sporulation, growth and division of the cell (Meeske *et al*, 2016). The lipoproteins LpoA and LpoB regulate PBP1A and PBP1B activity, respectively. PBP1A is coded by *mrcA* and PBP1B by *mrcB*. These genes have redundant function but have a synthetic lethal phenotype when knocked out in combination (Yousif *et al*, 1985). Synthetic lethality happens when the deletion of two genes lead to cell death, while when those same genes knocked out alone would not.

PBP1A/PBP1B forms, along with other proteins, a dynamic multi-enzyme complex called the elongasome. The elongasome is a multiprotein complex present in most rod-shaped bacteria, which inserts PG into different sites in the lateral wall of the cell (Egan *et al*, 2020). The elongasome proteins are scaffolded by the actin-like protein MreB throughout the lateral cell. The MreB filaments are anchored to the IM via association with RodZ (cytoplasmic domain) (van den Ent *et al*, 2010) and an N-terminal amphipathic helix (Salje *et al*, 2011). MreB forms filaments and interacts with MreC, MreD, RodZ, RodA, and PBP2. To span cell length, MreB forms small filaments patches that move around the cell perpendicularly to its long-axis (Dominguez-Escobar *et al*, 2011; Garner *et al*, 2011; van Teeffelen *et al*, 2011). At the end of the cell elongation, the elongasome is associated with tubulin-like protein FtsZ during the 'preseptal' phase of cell elongation, followed by septum synthesis, which allows cell division. FtsZ will be discussed in more detail in the cell division section (see 1.3).

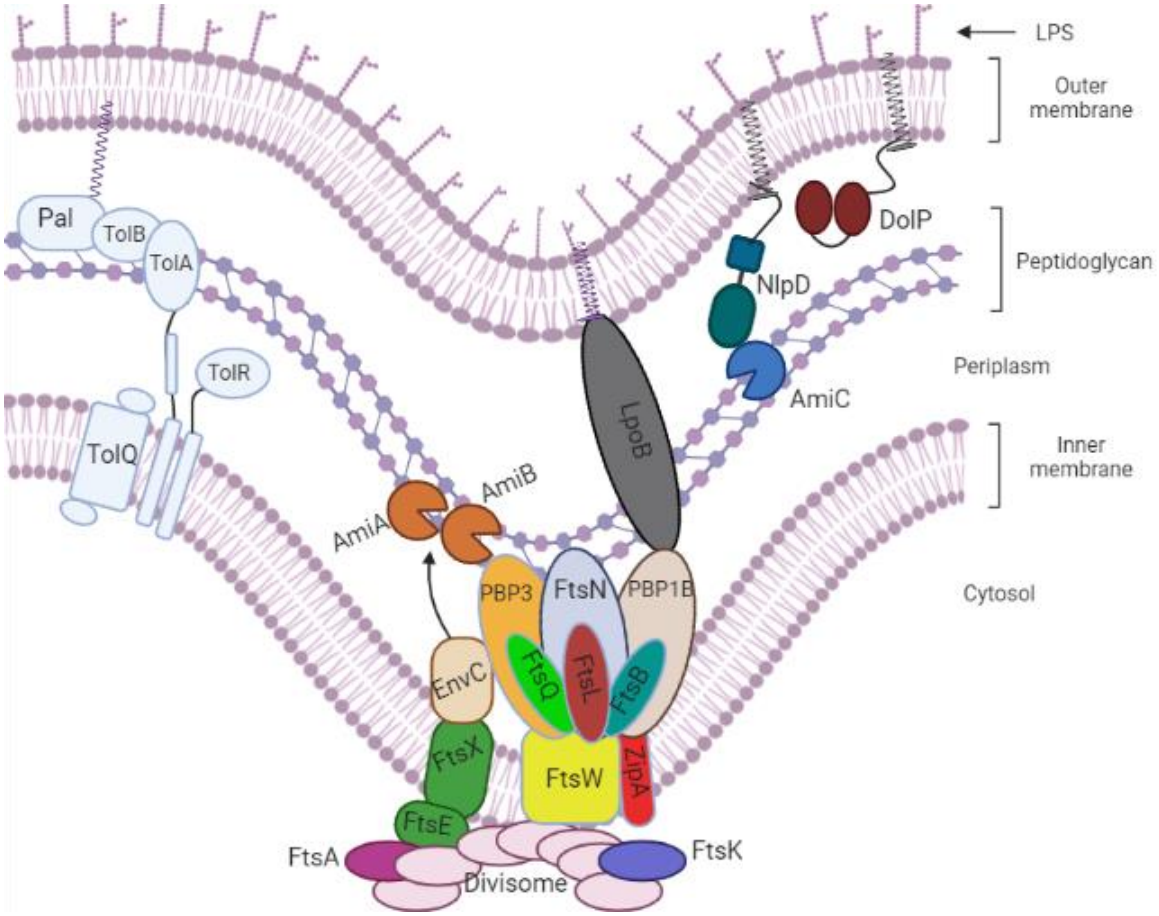

Figure 2. Schematic view of proteins involved in the cell division of Gram-negative bacteria. The main protein interaction and activation for peptidoglycan elongation and splitting, and invagination are represented. (Figure based on (Tsang *et al*, 2017), (den Blaauwen & Luirink, 2019) and (Nierhaus *et al*, 2022)). Created with BioRender.com

1.3 Cell division

Cell division is the process when a parent cell separates into two daughter cells. Cell division comes with two major challenges: (i) the cell needs to divide exactly at its centre to ensure a coherent cell shape over time and (ii) coordinate the division process avoiding cell lysis. Cell division is mediated by a protein complex called divisome.

To ensure the divisome is assembled at midcell the regulation of cell division is led by the Min system. The Min system regulates cell division in *E. coli* not only by inhibiting cell division close to the cell poles (de Boer *et al*, 1991), but also by increasing

the precision of Z-ring position at midcell. This system consists of three proteins, MinC, MinD and MinE. MinC and MinD form a cap-like structure at the cell poles, which block FtsZ assembly and limit the cell division to midcell (de Boer *et al.*, 1991; de Boer *et al*, 1989). MinC and MinD oscillate from one pole to the other until one half of the oscillation cycle. A cap of membrane-bound MinD begins to grow from the pole to the midcell and shrinks back to the same pole. Once the polar zone disappears, a new one is settled in the opposite site pole. MinE avoids MinCD complex establishment in the midcell by creating a ring that oscillates through the cell (Loose *et al*, 2011).

Division starts with the formation of the Z-ring, that over time recruits and scaffolds all proteins that contribute to division. Together, this dynamic multiprotein complex forms the divisome. Z-ring formation starts with the polymerization of FtsZ into a ring shape in the mid-cell. FtsZ is homologous of the eukaryotic protein tubulin and is the main cytoskeletal protein in cell cytokinesis. FtsA (actin-like protein) and ZipA (bitopic membrane protein) interact and stabilize the Z ring at the IM (Bi & Lutkenhaus, 1991; de Boer, 2010; Pazos *et al*, 2018). Division proteins are recruited to the division site to promote cell constriction (de Boer, 2010) and synthesise the septal PG material that will fortify the pole of the daughter cells (Typas *et al*, 2012; Uehara, 2011).

The Fts proteins are recruited to the divisome to assist division. The FtsQLB complex are bitopic membrane proteins that act as scaffold for the recruitment of downstream divisome proteins and are regulator of divisome activation (Ikeda *et al*, 1989; Tsang & Bernhardt, 2015a, b). FtsN triggers for septal PG synthesis. FtsW is a putative PG GTase and is part of the SEDS (shape, elongation, division and sporulation) family of membrane proteins (Ikeda *et al.*, 1989). FtsW works together with FtsI, a PG TPase to synthesize septal PG (Botta & Park, 1981). FtsEX have a role in

divisome activation besides FtsA and FtsQLB (Du & Lutkenhaus, 2017). Also, FtsEX coordinates cell wall hydrolyses at the septum by regulating amidase activity via EnvC (Figure 2) (Gerding *et al*, 2007). During this process the cell constricts, led by the Tol-Pal system (see 1.4), and the final step is done by hydrolases (see 1.5).

1.4 Invagination or constriction

When the bacterial OM folds at the mid-cell to start the separation process, it is called invagination or constriction. The Tol-Pal system is a complex of proteins responsible for invagination (Gerding *et al.*, 2007), and has most recently been shown to promote cleavage of cell wall glycans at the division site (Yakhnina & Bernhardt, 2020). This machinery is broadly conserved in Gram-negative bacteria and is composed of TolQ, TolR and TolA IM localised proteins, the periplasmic protein TolB, and the Pal PG-binding OM lipoprotein (Figure 2) (Sturgis, 2001).

The elements of the divisome that promote OM invagination are not completely defined, but it is believed that the Tol-Pal system has a major role in this process (Egan, 2018; Gerding *et al.*, 2007). Microscopy analysis shows that depletion of the Tol-Pal system leads to a cell separation defect and a cell chaining phenotype (Dubuisson *et al*, 2005; Gerding *et al.*, 2007). Fluorescence microscopy of tagged proteins also demonstrates that the Tol-Pal system is localised to the site of cell division (Szczepaniak *et al*, 2020). Pal stabilises OM during constriction by mobilization and capture by Tol system. Tol mobilizes Pal molecules in dividing cells, afterwards, captures and deposits them at the division septum (Szczepaniak *et al.*, 2020).

The Tol-Pal system has also been implicated in retrograde phospholipid transportation and maintenance of OM lipids homeostasis (Shrivastava *et al*, 2017). Additionally, Tol-Pal system synchronises PG synthase activation with OM constriction during cell division (Gray *et al*, 2015). The authors demonstrated that the periplasmic protein CpoB coordinates physically and functionally PBP1B/LpoB and Tol system. CpoB is an accessory protein of Tol-Pal system, interacting with TolA and also interacts with PBP1B/LpoB modulating the stimulation of TPase activity. CpoB allows PBP1B activity respond to the presence, assembly and energy state of Tol permitting a potential feedback regulation of PG synthesis related to the status of OM invagination. These Tol-Pal functions connects the system to cell division.

Inactivation of the Tol-Pal system in combination with the amidase regulators EnvC and NlpD results in severe cell division defects and causes a chaining phenotype. Amidases are PG hydrolases responsible for daughter cell separation at the end of the division and are discussed in detail in section 1.5. This result indicates that Tol-Pal can be a requisite for amidase activation by NlpD (Tsang *et al.*, 2017). However, recently, Yakhnina and authors (Yakhnina & Bernhardt, 2020) showed that the cell chaining phenotype of a unique Tol-Pal system deletion is caused by a failure in septal PG splitting and not just from a defect in NlpD and amidases activation. This phenotype is explained by a reduction in activity of OM lipoproteins capable of cleaving the glycan strands of PG and cannot be explained just based on an OM constriction defect. Instead, the authors suggested that Tol-Pal system is required for the activity of many other OM-localised enzymes with cell wall remodelling activity. Further investigations are necessary to link this complex to PG septation.

1.5 Septation or splitting

PG septation or splitting occurs when proteins cleave bonds that link stem peptides to the glycan strands and result in cell separation (Heidrich *et al*, 2001). This class of proteins is called PG hydrolases (Figure 3). The hydrolases are classified depending on their substrate specificity as muramidases, endopeptidases, carboxypeptidases and amidases. (Typas *et al.*, 2012). This thesis will focus on amidases that are autolysins which cleave amide bonds. *E. coli* encodes three main amidases: AmiA, AmiB, and AmiC, which are autoinhibited and require activation by divisome proteins. In addition, there are other two amidases AmiD and AmpD, that are not well described. The amidases activators EnvC, NlpD and ActS are LytM (lysostaphin/peptidase M23)-domain containing factors (or LytM factors) proteins in *E. coli* along with MepM, a DD-endopeptidase (Singh *et al*, 2012; Uehara *et al*, 2009). EnvC activates AmiA and AmiB (Uehara *et al*, 2010); and NlpD activates AmiC by promoting the release of the regulatory helix from the active site (Tsang *et al.*, 2017). Amidases can also be activated by ActS (formerly YgeR). It was recently described that ActS is able to activate all the three amidases; however, *in vitro* results show that it interacts and preferably activates AmiC (Gurnani Serrano *et al*, 2021). In conditions of acidic pH ActS activates AmiB along with NlpD and EnvC and at some extent, activates AmiC (Mueller *et al*, 2021).

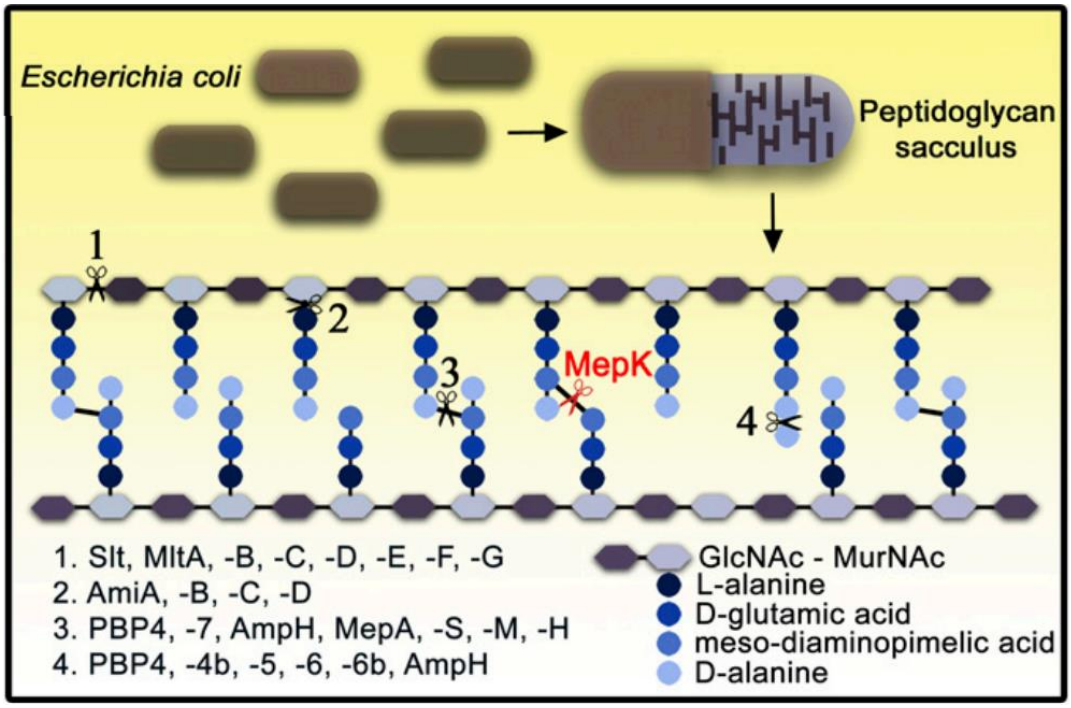

Figure 3 Schematic view of hydrolases activity in PG sacculus of *E. coli*..
The figure shows the different hydrolases presented in *E. coli*. Their activity is represented by scissors. The structure and composition of the glycan strands and peptide chains are demonstrated. (Figure obtained from (Chodisetti & Reddy, 2019)).

PG synthases and hydrolases in the divisome form the septum and pushes the IM, providing enough pressure for constriction (Xiao & Goley, 2016). However, inactivation of multiple amidases or activators demonstrate a long chain phenotype with complete IM constriction and fusion, however layers of septal PG are still connected, interrupting the OM invagination (Figure 4) (Heidrich *et al.*, 2001; Priyadarshini *et al*, 2007; Uehara *et al.*, 2009). The most severe chain phenotype is observed for mutants lacking both AmiA and AmiB (Chung *et al*, 2009).

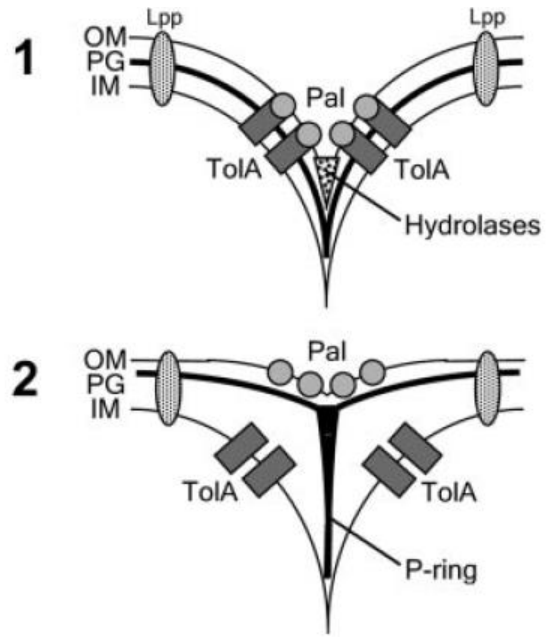

Figure 4. Schematic view of invagination and septation.
(1) Invagination of OM by Tol-Pal and hydrolases splitting the PG layer. (2) In the absence of hydrolases, the OM invagination is blocked by unsuccessfully split of PG. Accumulation of PG in the septa forms a P-ring (peptidoglycan ring). (Figure obtained from (Priyadarshini *et al.*, 2007)).

1.5.1 Regulators of amidases

Most amidases are autoinhibited and require activation to function. To date, EnvC, NlpD and ActS are the three well described amidases' activators. EnvC is anchored to the outer surface of the IM and FtsEX recruits EnvC to the septal ring by an interaction between EnvC and a periplasmic loop of FtsEX and its coiled-coil (CC) domain (Cook *et al*, 2020; Yang *et al*, 2011). The CC domains are suggested to be involved with EnvC regulation because variants of FtsEX that lack ATPase activity can still recruit EnvC, but not promote septal splitting (Du & Lutkenhaus, 2017; Cook *et al.*, 2020).

NlpD must be localised in the OM for its proper function, even if it is localised in the midcell. As a result, the cell can lyse if NlpD is produced as a soluble periplasmic

protein. This event is linked to AmiC, indicating that NlpD can activate AmiC in the periplasm, however it will cause disruption in the cell wall and septal PG splitting. NlpD recruitment is delayed until the septal ring is maturated, indicating that it is activated and promotes AmiC activity for PG cleavage in a certain time during the division cycle (Tsang *et al.*, 2017). Tsang and authors study suggests that DolP is NlpD activation promoter. In our work, we will try to confirm this interaction.

ActS is an OM-anchored protein which localizes unevenly on the periphery of the cell and have a mild enrichment in the division site. The ActS subcellular localization is not as clear as EnvC and NlpD localization, as these two proteins display a more important role in the division cell and their fluorescent signal is stronger when detected by mCherry (monomeric red fluorescent protein) (Uehara *et al.*, 2009). Regarding the activation of ActS, a recent study has shown that under envelope stress, cells show division defect and lysis in a *ldtF* (LD-transpeptidase) mutant. The defects are then alleviated by depletion of ActS, indicating a corelation of cell envelope biogenesis and proper PG remodelling (Gurnani Serrano *et al.*, 2021).

In summary, a well coordination of protein localization and activation is important for proper cell maintenance and separation into daughter cells. However, cell envelope integrity also relies on the proper assembly of the proteins that compose it, depending on the BAM (β-barrel assembly machine) complex.

1.6 Outer membrane protein assembly

Transmembrane β-barrel proteins cover a major part of the OM and they play distinct roles such as selecting entrance of nutrients and acting as virulence factors

and receptors (Hagan & Kahne, 2011; O'Neil *et al*, 2015). The components of the BAM (β-barrel assembly machinery) complex are related to the assembly of β-barrel proteins into the OM of Gram-negative bacteria (it is also found in eukaryotic mitochondria and chloroplasts) (Tommassen, 2010; Voulhoux *et al*, 2003). The proteins BamA (β-barrel protein) and accessory lipoproteins BamB, BamC, BamD and BamE form the complex (Figure 5) (Knowles *et al*, 2009). The OM proteins (OMPs) after being synthetized in the cytoplasm are transported across the IM by the SecYEG translocon. In the periplasm, they are escorted to the inner surface of the OM by chaperones (e.g. SurA or DegP-Skp pathways) to interact, be folded and be inserted in β-barrel form in the OM by the BAM complex. DegP, a protease, recycles the unfolded proteins.

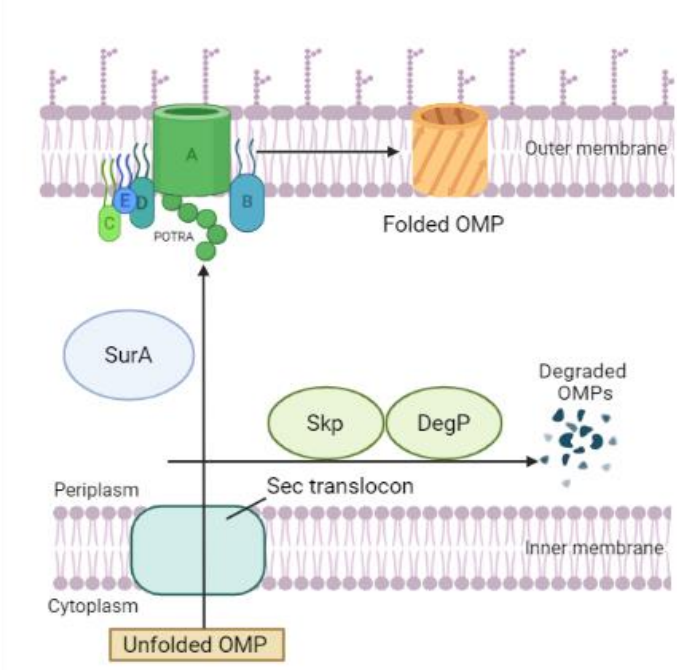

Figure 5. Schematic representation of BAM complex structure in *E. coli.*
The Sec translocon targets the unfolded OMP synthesised in the cytoplasm and exports them to the periplasm. The chaperone SurA transports the OMP to the BAM complex where the pore of BamA offers its pore for insertion of the OMP into the membrane. The POTRA (polypeptide transport-associated) domains and/or accessory lipoproteins BamB,C,D,E lace the OMP into the pore to then be folded, assembled, and inserted as β-barrel in the OM. The OMPs that fail to be transported and folded, are degraded by Skp and DegP. (OMP = outer membrane protein). (Figure based on (Knowles *et al.*, 2009)). Created with BioRender.com

The catalytic function of the BAM complex depends on one of the subunits, BamA. Probably, BamA interacts with all the other BAM complex subunits; BamC exposed on the outer surface of the OM and BamB, BamD and BamE, exposed to the periplasm. BamA belongs to Omp85 family of proteins that contains an N-terminal periplasmic domain that encompasses five polypeptide transport-associated (POTRA) domains (Sanchez-Pulido *et al*, 2003). POTRA domains interact with folding substrates using β-augmentation, which provides the scaffold to BAM subunits associate with BamA. The BamA flexible pairing of β-strands 1 and 16 controls a lateral gate which links the inner part of the barrel to the lipid bilayer, supporting insertion of new OMPs to the OM (Bakelar *et al*, 2016; Gu *et al*, 2016). Recently, a study showed that BamA capacity to catalyse outer membrane protein insertion is mediated by the PG assembly, meaning that most of its insertion happens at the division site (Mamou *et al*, 2022).

Besides BamA, the BAM subunits contribute to the complex in different forms, but it is not yet well described the individual impact of each component. The accessory components could function as independent chaperones or docking site for other chaperones (Knowles *et al.*, 2009). Also, it is known that deletion of *bamB, C* or *E* increases the cell sensitivity to antibiotics such as rifampin, an inhibitor of RNA polymerase (Onufryk *et al*, 2005; Sklar *et al*, 2007). In addition, *bamB and bamC* deletion increases cell permeability (Wu *et al*, 2005) and *bamD* deletion decreases cell density (Malinverni *et al*, 2006).

The BAM complex has been related to the lipoprotein DolP by protein interactome studies, suggesting that DolP is a component of the complex (Babu *et al*,

2018; Carlson *et al*, 2019). A study developed in our lab demonstrates further connections. The results are demonstrated in chapter 3.

1.7 Lipoproteins and regulation

Bacterial lipoproteins are hydrophilic proteins anchored to bacterial cell membranes by a conserved N-terminal lipid-modified cysteine residue, which is derived from phospholipids. It can be localised in different portions of the cell, such as the cell surface, the periplasmic side of the IM or OM, or the external milieu (Szewczyk & Collet, 2016). These proteins have important functions in bacterial physiology, such as virulence, nutrient uptake, cell wall metabolism, cell division, transmembrane signal transduction, antibiotic resistance, adhesion to host tissues during infection, and inducing innate immune response in mammalian receptors (Hantke & Braun, 1973; Nakayama *et al*, 2012). Lipoproteins synthesis occurs in the cytoplasm with a conserved sequence called a lipobox (Leu-(Ala/Ser)-(Gly/Ala)-Cys) (Hayashi & Wu, 1990). Lipoprotein modifications happen on the periplasmic side of the IM by three membrane-bound enzymes, phosphatidylglycerol:prolipoprotein diacylglyceryl transferase (Lgt), prolipoprotein signal peptidase (Lsp) and apolipoprotein N-acyltransferase (Lnt) (Wu *et al*, 1982). Lipoproteins have been studied for several years. A compilation of this class of proteins in *E. coli* can be found in Braun and Hantke *et al.* (Braun & Hantke, 2019). Nevertheless, in recent years, it became evident that lipoproteins are involved in cell envelope biogenesis regulation. Among others, the lipoproteins identified involved in this envelope biogenesis to date are Lpp, Lol, LpoA, LpoB, NlpD, Pal, DolP, NlpI, Lpt and most BAM components (Banzhaf *et al*, 2020;

Bernstein, 2011; Chimalakonda *et al*, 2011; Magnet *et al*, 2007; Onufryk *et al.*, 2005; Paradis-Bleau *et al*, 2010; Szczepaniak *et al.*, 2020; Tsang *et al.*, 2017).

The most abundant lipoprotein in *E. coli* is Lpp. Lpp has a key role in cell envelope integrity. Its deletion causes sensitivity to EDTA (ethylenediaminetetraacetic acid), cationic dyes and detergents. It is an elongated trimer formed by long α-helical domains that presents a coiled coil, giving a repetitive structural feature. It is covalently linked to PG, being one-third of its structure related to this binding and the other two-thirds are the free form, anchored to OM but not to cell wall. Lpp fixes the OM to the PG wall (Braun & Rehn, 1969). This reaction is catalysed by three L,D-transpeptidases, LdtA, LdtC, and LdtB (Magnet *et al.*, 2007). The transfer of Lpp from the IM to the OM is mediated by the chaperones of Lol pathway (LolA, LolB, LolC, LolD, and LolE) (Okuda & Tokuda, 2011). LolB is itself a lipoprotein and the Lol pathway also contributes to other lipoproteins insertion into the OM (Szewczyk & Collet, 2016).

Transportation of LPS from the cytoplasm to the cell surface is mediated by lipoproteins of the Lpt pathway (Choi *et al*, 1986; Ruiz *et al*, 2009). To allow transport and OM insertion of LPS, LptE is connected inside the β-barrel structure of LptD. Then LptD is inserted into the OM by the BAM complex (Chimalakonda *et al.*, 2011). BAM complex is formed by four lipoproteins BamB-E, mediating β-barrel proteins assembly (Malinverni *et al.*, 2006).

Lipoproteins also have a role in PG synthases and hydrolases. PG synthases are mediated by the activators LpoA and LpoB, besides other proteins. LpoA stimulates TPase activity of PBP1A and LpoB activates PBP1B (Paradis-Bleau *et al.*, 2010; Typas *et al.*, 2012). Considering the role of lipoproteins within hydrolases, NlpD

is OM localised and is the activator of amidase AmiC. DolP and Tol proteins are other lipoproteins that may be involved in amidase activation (Tsang *et al.*, 2017), which are described in this introduction. NlpI is described as an OM lipoprotein that targets MepS, a PG EPase, for proteolytic degradation (Ohara *et al*, 1999; Singh *et al*, 2015). NlpI also scaffolds proteins to form complexes between PG synthases and EPases (Banzhaf *et al.*, 2020).

The study of different classes of proteins and their interaction is essential to understand how bacteria build and maintain their cell envelope. In my thesis I intend to characterize a key player in OM biogenesis, the lipoprotein DolP.

1.8 Structure of DolP, a lipoprotein involved in maintenance of cell envelope integrity

DolP (**d**ivision and **O**M stress-associated **l**ipid-binding **p**rotein - formerly YraP) is a non-essential OM lipoprotein that is conserved among Gram-negative bacteria (Goodall *et al*, 2018; Onufryk *et al.*, 2005). To identify genes involved in OM homeostasis, the Henderson group screened the KEIO collection, a library of *E. coli* single-gene in-frame deletion strains of all non-essential genes, aiming to detect mutants incapable of growth in the presence of SDS (sodium-dodecyl sulphate) and vancomycin. The screen revealed many genes that were previously associated with OM biogenesis, however many of the genes had unknown functions. One of these genes was *dolP* and was selected as a case for study.

Previous studies revealed that cells lacking *dolP* in *Salmonella enterica* and *E. coli* present OM defects, being sensitive to SDS, vancomycin and EDTA (Morris *et al*,

2018; Onufryk *et al.*, 2005). Perturbations in OM homeostasis lead to σ^E-mediated alteration in the expression of genes that are necessary for envelope homeostasis under stress conditions and for cell viability. The gene *dolP* is upregulated by σ^E in *E. coli* (Figure 6) and in *S. enterica,* (Dartigalongue *et al*, 2001; Onufryk *et al.*, 2005; Skovierova *et al*, 2006), which is another indication of DolP having a role in OM biogenesis.

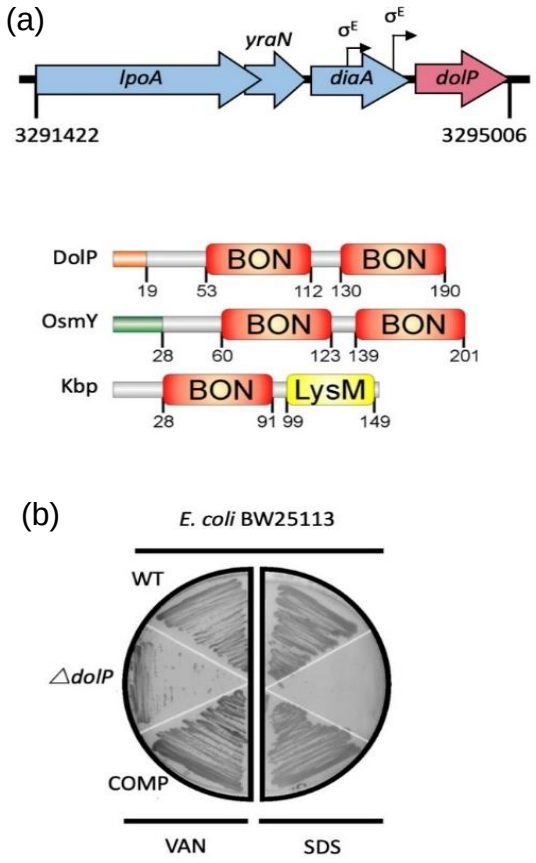

Figure 6. DolP is a dual-BON domain protein related to OM integrity.
(a) In *E. coli*, *dolP* is located downstream of *diaA* and encodes a lipoprotein with a signal sequence (orange) and two BON domains (red). (b) The mutant Δ*dolP* is sensitive to SDS and vancomycin, while the WT (wild-type) or the complemented mutant (COMP) are not. Cells are grown in LB agar with vancomycin (100 mg/ml) or sodium dodecyl sulphate (SDS; 4.8%). Figure obtained from (Bryant *et al*, 2020).

Structurally, DolP is formed by a dual BON (bacterial and OsmY nodulation) domain. BON domain is a conserved protein region named after it was found in a series of protein groups such as the bacterial osmotic-shock-resistance protein OsmY and a

group of nodulation specificity proteins (Yeats & Bateman, 2003). Our research group (Bryant *et al.*, 2020) solved the structure of the DolP dual-BON domain fold (BON1 and BON2) (Figure 7). Three-stranded mixed parallel/antiparallel β-sheet packed against two α-helices yielding a αββαβ topology forms the structure of each domain. The two BON domains interact with each other via their β-sheets through contacts mediated by the residues Y75 and V82 in BON1 and T150, G160, L161 and T188 in BON2. In addition, we defined a conserved membrane:protein interface centred on BON2α1 through which DolP binds to anionic phospholipids. Therefore, the C-terminal BON domain (BON2) facilitates interaction of the C-terminus of the protein with the membrane at sites that are enriched with anionic phospholipid. The study also showed that the phospholipid-binding guides DolP to localise to the division site. It was demonstrated that introducing a mutation in tryptophan W127 (W127E) eliminates binding of DolP to phosphatidylglycerol micelles and prevents localisation of DolP to the division site. These data demonstrate that DolP localisation to the division site is dependent upon interaction with anionic phospholipid via BON2:α1, and this interaction and the sub-cellular localisation are required for DolP function (Bryant *et al.*, 2020).

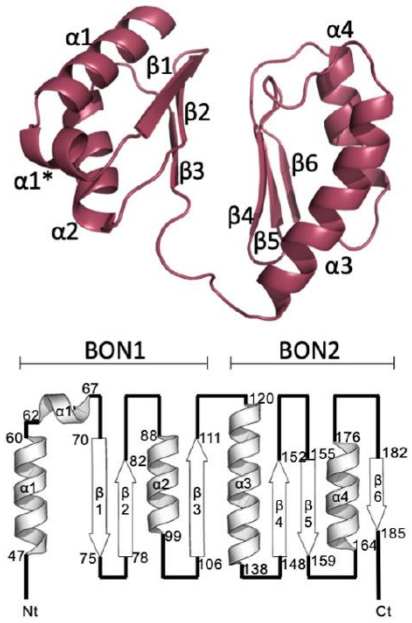

Figure 7. Solution structure and topology of DolP.
Dual-BON domain DolP structure with α helices, β strands and termini labelled. Figure obtained from (Bryant *et al.*, 2020).

DolP has also been linked to the BAM complex, responsible for folding and insertion of OM proteins into the OM (Babu *et al.*, 2018; Carlson *et al.*, 2019). Previous protein interactome studies captured DolP as interactor of two components of the BAM complex, BamD and BamE. Genetic studies also showed synthetic lethality of *dolP* with the gene encoding the periplasmic chaperone SurA, which delivers unfolded substrate of OMPs to the BAM complex (Onufryk *et al.*, 2005; Typas *et al*, 2008; Yan *et al*, 2019). Based on this evidence, a recent publication has confirmed the DolP link with the BAM complex and shown that DolP contributes to folding and proper function of BamA (Ranava *et al*, 2021). The authors showed that in a Δ*bamB*Δ*dolP* strain, the levels of BamA were reduced when visualised by SDS-PAGE and immunoblotting. When BamA was overproduced in a Δ*dolP* strain, the cells showed growth defect in solid media supplemented with vancomycin, indicating that DolP contributes to cell fitness in this condition. The defect was shown to be due to an excess of uncomplexed

BamA, which was found in the absence of the other components of the complex. To confirm this interaction, overproducing DolP rescued the growth defect. In addition, the overproduction of both DolP with BamA induced the proper folding of BamA (Ranava *et al.*, 2021).

It has also been shown that DolP contributes to cell division and it was suggested that DolP could be a regulator of cell-wall amidases, directly activating AmiC either directly or via NlpD (Tsang *et al.*, 2017). The authors created a transposon inserting library in an Δ*envC* genetic background to identify mutants with cell-chaining defects when the EnvC pathway was inactivated. This screen identified Δ*dolP*Δ*envC* as having a cell elongation defect, implicating DolP in the process of cell division. Microscopy revealed that Δ*dolP*Δ*envC* has the same severe chaining phenotype as an Δ*nlpD*Δ*envC* mutant, indicating that DolP could be in the same pathway as NlpD. My studies aimed to experimentally examine this interaction to validate the role of DolP in the amidase regulation pathway. In addition, we aimed to confirm and further investigate the correlation between DolP and the BAM complex.

1.9 Aim of the thesis

Approaches to weaken envelope integrity can contribute to combat infectious diseases. As a result of this study, we hope to define the importance of proteins in Gram-negative bacteria cell envelope biogenesis. This may lead to the identification of new drug targets.

The aim is to describe a protein involved in cell envelope biogenesis, the lipoprotein DolP. The structure of DolP was recently solved by researchers in our lab

within identification of potential partners. I will better investigate the correlation of DolP with other cell envelope related proteins and clarify its function.

Chapter 2. Material and Methods

2.1 Microbial methods

2.1.1 Strains used in this work

Escherichia coli BW25113 is the parental strain used in this study. *E. coli dolP*::*kan*, *bamB*::*kan, bamC*::*kan, bamE*::*kan, amiA*::*kan*, *amiB*::*kan, amiC*::*kan*, *envC*::*kan, nlpD*::*kan*, *actS*::*kan* mutants were obtained from the KEIO library (Baba *et al*, 2006) and the mutations transduced by P1 transduction into a clean parental strain.

E. coli Δ*dolP* was created by resolving the Kan^R cassette (Datsenko & Wanner, 2000) by previous students in our lab and stocked in the lab collection. Double mutants were created by P1 transduction. The chromosomal modification was confirmed by PCR when a Kan^R cassette was transduced.

The pET17b DolP::mCherry plasmid was constructed to contain an 11 amino acid flexible linker and a codon optimised mCherry gene at the 3' end of the *dolP* gene. Strains were routinely cultured on LB agar and LB broth.

2.1.2 Growth of *E. coli* strains

E. coli strains were cultivated in Luria Bertani (LB) medium (5 g/L NaCl (unless otherwise specified), 5 g/L yeast extract, 10 g/L peptone, pH 7.2) and shaken at 180 rpm, or on LB agar plates (5 g/L NaCl, 5 g/L yeast extract, 10 g/L peptone, 1.5% agar, pH 7.2) at 37°C. The medium pH varied as indicated in session 2.4.1. Strains

overproducing proteins were grown at 30°C. Growth was monitored by measuring the optical density (OD) at a wavelength of 600 nm (OD_{600}).

2.1.3 Strain's storage

To keep bacterial strains temporarily, strains were plated on LB agar with or without addition of the appropriate antibiotic, incubated overnight at 37°C and stored at 4°C. For long-term storage, overnight cultures were mixed 4:1 with sterile 50% glycerol and stored at -80°C.

2.1.4 Competent cells

An overnight culture was diluted 1:100 in 50 mL LB medium and grown until reach mid-exponential phase (OD_{600}= 0.4-0.6). The culture was transferred to a centrifuge tube and centrifuged for 10 min, at 4ºC, 13,000 rpm. The pellet was resuspended in 0.1 M $CaCl_2$ and incubated on ice for 30 min. The culture was centrifuged (10 min, at 4ºC, 13,000 rpm) and resuspended in 2 mL of 0.1 M $CaCl_2$ and 1 mL 50% glycerol and placed on ice for 30 min. Aliquots of 100 µL of the culture were made.

2.1.5 Transformation of competent cells

An aliquot of 100 µL was placed on ice and 1 µL of plasmid was added. The sample was incubated for 30 min on ice and incubated for 30 sec at 42°C in a water bath. The samples were transferred back to ice for 2 min. After the incubation, 1 mL of LB media was added. The sample was incubated at 37°C, in 180 rpm shaker incubator, for 60 min. The tube was centrifuged for 2 min at 6000 rpm and cells were resuspended in 100 µL of LB. The cells were plated on LB agar plate containing the suitable antibiotic.

2.2 Standard DNA methods

2.2.1 Oligonucleotides

Oligonucleotides were purchased from Merck in a final concentration of 100 pmol/µl resuspended in H_2O.

2.2.2 Colony PCR

A small portion of a colony was picked with a sterile tip and placed in a tube containing PCR reagents. For PCR reactions MyTaq Red Mix 2x (Bioline) was used in accordance with manufacturer's instructions. Oligonucleotides used in this study are described in appendix and were used in a final concentration of 10 µM. The conditions

of the thermocycler programme are 95ºC for 5 min; 95ºC for 30 sec; 54ºC 30 sec (35 cycles); 72ºC for 1 min; 72ºC for 5 min; and hold for 4ºC.

After PCR, the products were loaded in 1% agarose gel in 1x TAE buffer (50x TAE buffer = 2 M Tris, 1 M acetic acid, 0.05 M EDTA in water) and stained with 0.07 µL/mL Midori Green (Nippon Genetics). Hyperladder 1 kb (Bioline) was used as a marker to confirm the DNA fragments size. The gels were run at 110 V for 60 minutes and visualized using BioRad system in UV light.

2.2.3 Isolation of plasmid DNA from *E. coli*

Plasmid DNA was isolated using the QIAprep Spin Miniprep Kit - QIAGEN according to the manufacturer's instructions. Plasmids were stored at -20°C.

2.3 Advanced DNA methods

2.3.1 Isolation of the phage P1

The protocol is based in a methodology previously described (Thomason *et al*, 2007). A culture of the donor strain was grown overnight and diluted 1:100 in 5 mL LB medium containing 50 µL glucose and 25 µL 1 M $CaCl_2$ in 50 mL Erlenmeyer flask and incubated with aeration in 37°C for 40 min. 100 µL of P1 phage stock were added to the culture and incubated until the cells were lysed (~3 hours). After incubation, 100 µL of chloroform was added and the culture was incubated for extra 5 min. The samples were pelleted (13000 rpm, 1 min). The supernatant was transferred to new glass tubes. The phage lysate was stored at 4°C.

2.3.2 P1 transduction

The protocol was followed as previously described (Thomason *et al.*, 2007). A culture of the recipient strain was grown overnight. The following day the samples were centrifuged at 13,000 rpm for 2 min. The pellet was resuspended in one-half of the original volume in P1 salt solution (10 mM $CaCl_2$; 5 mM $MgSO_4$). A volume of 100 µL of cells/P1 salt solution and 100 µL of P1 lysate was added to sterile glass flask. The phages were absorbed by the cells for 30 min at 37°C. As control, a flask with no phage was incubated in similar way. After incubation, 1 mL of LB medium and 200 µL of 1 M sodium citrate were added. The samples were incubated for 1 h at 37°C. The samples were centrifuged (13,000 rpm, 2 min). The supernatant was discarded, and the cells were resuspended in 50-100 µL LB medium and plated in agar plates containing the suitable antibiotic.

2.4 Phenotype and growth analysis assays

2.4.1 Microscopy

DolP::mCherry imaging and BAM mutants: Cultures were grown at 37°C to OD_{600} = 0.4-0.5. Cells were harvested by centrifugation at 7000 x g for 1 min before being applied to agarose pads, which were prepared with 1.5 % agarose in PBS and set in Gene Frames (Thermo Scientific) (de Jong *et al*, 2011). Cells were immediately imaged using a Zeiss AxioObserver equipped with a Plan-Apochromat 100x/Oil Ph3 objective and illumination from HXP 120V for phase contrast images. Fluorescence

images specifically were captured using the Zeiss filter set 45, with excitation at 560/40 nm and emission recorded with a bandpass filter at 630/75 nm. For localisation analysis and generation of demographs, the MicrobeJ plugin for Fiji 600 was used and >500 cells were used as input for analysis (Ducret *et al*, 2016).

Live imaging cells: Overnight cultures were diluted to initial OD_{600}=0.01 in LB. The cells were incubated at 37°C until OD_{600}= ~0.4. Cells were harvested by centrifugation at 7000 x g for 1 min and 2.5 µL were added to agarose pads, which were prepared with 1.5 % agarose in LB and set in Gene Frames. The samples were imaged on a Nikon Ti-E inverted widefield microscope. Images were acquired using a Plan-Apochromat 100x/Oil Ph3 objective. Temperature was maintained at 37 °C using an environmental enclosure. After a 20 min acclimatization period, cells were imaged at a 7.4 min acquisition frame rate for a total observation time of 185 min.

DolP and amidases/regulators fluorescence imaging: To visualise membrane and DNA of the cells, FM1-43 FX dye (Invitrogen) and DAPI (Stratech Scientific) were used, respectively, according to (Uehara *et al.*, 2009). Overnight cultures were diluted to initial OD_{600}=0.01 in LB. The cells were incubated at 37°C until OD_{600}= ~0.4. A volume of 0.5 mL of the culture was stained with 5 µg/mL of FM1-43FX at room temperature for 10 min. The cells were adjusted to 33 mM sodium phosphate pH 7.4. Fixation was made adding 2.4% formaldehyde and 0.04% glutaraldehyde to the culture. Cells were imaged using a Zeiss AxioObserver equipped with a Plan-Apochromat 100x/Oil Ph3 objective and illumination from HXP 120V for phase contrast images. FM1-43 images were captured using the Zeiss filter set 38. For DAPI images we used the Zeiss BFP filter set. For shape analysis the MicrobeJ plugin for Fiji 600 was used according to Ducret et al. (Ducret *et al.*, 2016). To analyse elongated cells

that could not be visualised in one image we applied a stitching plugin of Fiji 600 software (Preibisch *et al*, 2009) to provide a complete view.

Cells grown in acidic pH imaging: The protocol was adapted from (Mueller *et al.*, 2021). An overnight culture in 37°C was grown in LB media pH 6.9. From this culture, an over-day culture was prepared in LB media pH 6.9 until the culture reached early-exponential phase (OD_{600}= ~0.2). The cultures were back-diluted either in media with pH 5.2 (containing MMT (1:2:2 molar ratio of D,L-malic acid, MES, and Tris base) buffer) or pH 6.9. The culture was washed with pH 5.2 before being transferred to a new flask with pH 5.2 media. Then the cells were grown until OD_{600}= ~0.2. Cells fixation, preparation of slides and MicrobeJ phenotype analysis were made as described above.

2.4.2 Growth analysis under cell envelope stress in solid media

Overnight cultures of the selected strains were grown in 37ºC. The inoculum was adjusted to OD_{600}= 1 or OD_{600}= 2 and serial diluted (10^{-1} - 10^{-6}) in LB broth in a 96 well plate. A volume of 1.5 µL, 2.5 µL or 5 µL (as indicated in the figures legends) of each sample was inoculated on square Petri dishes with LB agar containing different cell envelope stress inducers. The stresses tested were osmolarity (0 mM and 500 mM NaCl), cell envelope targeting antibiotics (50 µg/mL and 100 µg/mL vancomycin), temperature (42ºC), detergents (4.8%, 3% and 1% SDS), metal chelators (0.125 mM, 0.25 mM, and 0.5 mM EDTA), and pH (4.8 and 5.2). The plates were incubated at 37°C and photographed after ~16 hours.

2.5 Genetic interaction

Genetic interaction assay was performed as described in Banzhaf, M. *et al.* (Banzhaf *et al.*, 2020). For each probed strain, a single source plate was generated and transferred to the genetic interaction plate using a pinning robot (Biomatrix 6). On each genetic interaction assay plate, the parental strain, the single deletion A, the single deletion B and the double deletion AB were arrayed, each in 96 copies per plate. Genetic interaction plates were incubated at 37°C for 12 h and imaged under controlled lighting conditions (spImager S&P Robotics) using an 18-megapixel Canon Rebel T3i (Canon). Colony integral opacity as fitness readout was quantified using the image analysis software Iris (Kritikos *et al*, 2017). Fitness ratios were calculated for all mutants by dividing their fitness values by the respective WT (wild-type) fitness value. The product of single mutant fitness ratios (expected) was compared to the double mutant fitness ratio (observed) across replicates. The probability that the two means (expected and observed) are equal across replicates is obtained by a Student's two-sample t-test. Dr Manuel Banzhaf and Dr George Kritikos performed Iris analyses.

2.6 Standard protein methods

2.6.1 DolP expression

The *dolP* gene was codon optimised and cloned into the pET-26b(+) plasmid vector at NdeI/ XhoI restriction sites (Bryant *et al.*, 2020). The construct has six

histidine residues followed by a cleavable Tobacco etch virus (TEV) site on the N-terminus of DolP. The plasmid was transformed into *E. coli* BL-21. The cells were grown in 2 L of LB broth at 37°C until OD_{600} =~0.5. The cultures were induced using 1 mM IPTG. After 4 hours of induction, cells were harvested by centrifugation at 6,900 x g for 15 minutes at 4°C. Pelleted cells were stored at -80°C until required for protein purification.

2.6.2 DolP purification

Cell pellets were resuspended in binding buffer (50 mM sodium phosphate or 50 mM tris HCl pH 7, 300 mM NaCl, 50 mM imidazole, 0.5 mM TCEP) and Roche cOmplete EDTA-free protease inhibitor cocktail tablets (1/1,000 dilution). Cells were lysed using a sonicator and C3 Emulsiflex Cell disruptor (Avastin). The lysate was centrifuged at 16,700 rpm for 1 hr at 4°C. The supernatant was recovered and incubated with 1 mL/L of Ni_2+ agarose beads (Jena Bioscience) pre-equilibrated with binding buffer for 1 h with mixing. The sample was applied to an elution column and washed with binding buffer before the protein was eluted with elution buffer (50 mM Sodium phosphate or 50 mM tris HCl pH 7, 300 mM NaCl, 500 mM imidazole, 0.5 mM TCEP). The protein DolP presence and purity was checked by running the sample on SDS-page gel.

2.6.3 Buffer dialysis

Serva dialysis tubing was left in contact to boiling dH_2O for 10 min and the process was repeated for three times before adding the protein elution. Elution fraction containing His-DolP was added to a dialysis tubing floating in 2 L dialysis buffer (150 mM NaCl, 50 mM Tris-HCl, 10% glycerol, pH=8) overnight with gentle stirring at 4°C.

2.6.4 Size exclusion chromatography

Dialyzed protein was concentrated and purified by size exclusion chromatography. Sample were dialysed in gel filtration buffer (50 mM sodium phosphate or 50 mM tris HCl pH 8, 300 mM NaCl, 0.5 mM TCEP), concentrated to 2 mL and injected into a pre-equilibrated S75 26 60 GE healthcare column. With a flow rate of 2 mL/min, 2 mL sample were collected and run on SDS-PAGE gels to assess purity. The protein was concentrated and stored at −80°C.

2.6.5 His-tag removal

For the removal of the His-tag, TEV protease (1:100 w/w) was added, and the sample was dialyzed in cleavage buffer (150 mM NaCl, 50 mM Tris-HCl pH 8, 10% glycerol). The protease was removed from the sample using an elution column.

2.6.6 Amidases purification

The *E. coli* amidases AmiA, AmiB, AmiC, and cognate regulators NlpD and EnvC were purified as previously described (Uehara *et al.*, 2010).

2.6.7 SDS-PAGE (Sodium dodecyl sulphate-polyacrylamide gel electrophoresis)

Proteins were separated according to their molecular weight using the method of discontinuous SDS-PAGE. Protein samples were mixed with sample buffer (2% w/v SDS, 2 mM ß-mercaptoethanol, 4% v/v glycerol, 0.04 M Tris-HCl, pH 6.8, 0.01% w/v bromophenolblue) and boiled for 10 minutes before being loaded in the gel. The gels utilised contained 10% or 12% of acrylamide, according to the table below.

Table 1. Reagents and concentrations for SDS-PAGE

1x Running Gel Solution		
	10%	12%
H_2O	12.3 mL	10.2 mL
1.5 M Tris-HCl, pH 8.8	7.5 mL	7.5 mL
20% (w/v) SDS	0.15 mL	0.15 mL
Acrylamide (30% w/v)	9.9 mL	12.0 mL
10% (w/v) ammonium persulfate (APS)	0.15 mL	0.15 mL
TEMED	0.02 mL	0.02 mL
Stacking Gel Solution (4% Acrylamide		
H_2O	3.075 mL	
0.5 M Tris-HCl, pH 6.8	1.25 mL	
20% (w/v) SDS	0.025 mL	
Acrylamide (30% w/v)	0.67 mL	
10% (w/v) ammonium persulfate (APS)	0.025 mL	
TEMED	0.005 mL	

The electrophoresis system was filled with running buffer (25 mM Tris-HCl, 200 mM glycine, 0.1% w/v SDS) at 100 V until passed the stacking layer, where they were run at 120-130 V, depending on the system utilised. A protein ladder (New England Biolabs Color Prestained Protein Standard, Broad Range (10-250 kDa)) was loaded in the gel to compare the molecular weight of the proteins analysed.

2.6.8 SDS-PAGE gel staining

Gels were stained using Coomassie dye (0.4 M citric acid, 20% isopropanol, 0.2% Coomassie R-250) and de-stained using 30% ethanol, 60% water, 10% acetic acid until the background was clear.

2.7 Protein interaction

2.7.1 MST

DolP was labelled with Monolith Protein Labeling Kit RED-NHS 2nd generation (Nanotemper) according to the manufacturer's instructions. Unlabelled ligands were titrated in the starting concentrations AmiA (200 µM), AmiB (148 µM) and AmiC (70 µM). Ligand proteins were two-fold serial diluted 16 times in MST buffer (150 mM NaCl, 10 mM MgCl2, 0.05% Tween 20, 50 mM Tris pH 7.4) and 100 nM of labelled DolP was added for interactions assay. The proteins were incubated for 1 hour at room temperature. The proteins were transferred to capillaries to be read on a Monolith

NT.115 10–40% MST power. Binding curves and kinetic parameters were plotted and analysed NT Analysis 1.5.41 and MO. Affinity Analysis (x64) software.

2.7.2 Ni^{2+} bead pulldown

His-tagged protein or natural binding protein (AmiA) was incubated with un-tagged protein in Ni-NTA agarose beads. Beads were pre-equilibrated before starting the assay. 40 µL of Ni^{2+} beads slurry were added in a 1.5 mL microcentrifuge tube and washed in 500 µL binding buffer (100 mM NaCl, 50 mM Tris-HCl, pH 8) by centrifugation for 2 minutes at 2500 rpm. The protein was added to each microcentrifuge tube, with 5 µL buffer added to those with only bait or target. The His-tagged proteins was incubated for five minutes before the un-tagged protein was added, upon which both were incubated together for 30 min at room temperature. The samples were washed with 250 µL washing buffer (300 mM NaCl, 50 mM tris, pH 8) and pelleted by centrifugation. Supernatant was discarded and the elution was incubated at 100°C in SDS-buffer (50 mM Tris–HCl pH 6.8, 2% SDS, 10% glycerol 0.02% bromophenol blue, 10% ßmercaptoethanol) and analysed by SDS-PAGE.

2.8 Peptidoglycan degradation assay

PG sacculi were isolated from *E. coli* Top10 and labelled with fluorescein isothiocyanate (FITC) as described previously (Gurnani Serrano *et al.*, 2021; Maeda, 1980). Master mix was prepared mixing FITC labelled PG sacculi (10 mg/mL) and 100

µL of buffer (150 mM NaCl + 50 mM Tris, pH 8.0) + 9 mL dH_2O. In microcentrifuge tubes 100 µL of master mix and the purified protein (2 µM) were added. The amount of protein was calculated as follows: X =Protein molarity/2. Protein µL = 100/X. Lysozyme (4 µM) was used as positive control and buffer with FITC-PG as negative control. The samples were incubated for 1 hour in heat-block at 37ºC in maximum speed shaker. The samples were transferred to a MultiScreen GV 96-well Filter Plate, 0.22 µm (Millipore). The plate was placed on top of a 96-well Black Flat Bottom Microplate. The reaction was stopped by filtration when the plates were centrifuged for 3 min, 2500 rpm. To each sample in the Black Flat Bottom Microplate were added 50 µL sodium hydroxide (0.5 M NaOH). The fluorescence of the soluble fraction was read (Ex. 495, Em, 519) was measured in Omega plate reader (BMG Labtech).

Chapter 3. Characterising the lipoprotein DolP

The results presented in this chapter are part of a published article in eLife journal (see Appendix) in collaboration with Dr Jack Bryant and Prof Ian Henderson (Bryant *et al.*, 2020). In addition to the figures presented here, I contributed to the Western blots of figures 2D and 4B of the article.

3.1 Introduction

The bacterial Gram-negative envelope is formed by three layers (IM, PG layer and OM) that gives shape to the cell and protects it against external perturbances to maintain homeostasis. The *E. coli* IM is composed of a phospholipid bilayer, while the OM is asymmetrically formed by LPS and integrated β-barrel proteins. Anchored to a portion of one of these membranes, the lipoproteins play important functions to bacterial physiology.

Recently, a study published by our group (Bryant *et al.*, 2020) revealed the structure of the *E. coli* lipoprotein DolP, (**d**ivision and **O**M stress-associated **l**ipid-binding **p**rotein – formerly YraP), a non-essential OM protein that is conserved among Gram-negative bacteria. DolP is composed of two BON (bacterial and OsmY nodulation) domains (BON1 and BON2). The C-terminal BON domain binds to anionic phospholipids by interaction of the protein to membrane, which facilitates interaction of the C-terminus with the membrane. This interaction is critical for function and is needed for sub-cellular localisation to the division site. It was also reported that DolP deletion promotes damages to the OM barrier function and therefore, increases the sensitivity to antibiotics and membrane disrupting agents.

Protein interactome studies showed an interaction of DolP and BAM (β-barrel assembly machinery) complex accessory components (Babu *et al.*, 2018; Carlson *et al.*, 2019). The BAM complex is composed of BamA, a β-barrel protein with an amino N-terminal periplasm domain consisted of five polypeptide transport-associated (POTRA) motifs (Kim *et al*, 2007; Wu *et al.*, 2005). These POTRA motifs scaffold four accessory lipoproteins (BamB, BamC, BamD and BamE). Altogether, the BAM complex folds and inserts β-barrel outer membrane proteins (OMPs) in the membrane (Knowles *et al.*, 2009; Ranava *et al*, 2018; Schiffrin *et al*, 2017; Tommassen, 2010). The interactome analysis suggested that DolP is a component of the BAM complex, linking DolP to OMP biogenesis. However, its specific function within the complex had not yet been clarified. Therefore, we aimed to study the impact of DolP for the BAM complex. In this study, we observed a decrease in cell fitness in *dolP* mutants when *bamB* or *bamE* were deleted, suggesting an indirect link of DolP to OMP biogenesis.

3.2 Results

3.2.1 Deletion of *bamB* and *bamE* in *dolP* mutant impacts cell fitness

DolP was reported to interact with the BAM complex, by protein interactome studies (Babu *et al.*, 2018; Carlson *et al.*, 2019). Therefore, we sought to investigate the role of DolP in the BAM complex.

We analysed if there was a genetic interaction with the unessential BAM complex genes and *dolP*. To do so, in a Δ*dolP* strain we deleted the non-essential components of the BAM complex, *bamB, bamC* and *bamE* and created a strain panel

consisting of single and newly created double mutants. We inoculated WT, the single mutants Δ*dolP*, Δ*bamB*, Δ*bamC,* Δ*bamE,* and the double mutants Δ*dolP*Δ*bamB,* Δ*dolP*Δ*bamC* and Δ*dolP*Δ*bamE* using a pinning robot (Biomatrix 6) onto solid LB agar plates. After 12 hours incubation at 37°C, an end-point picture was taken. Fitness of the strain panel was analysed by quantifying colony integral opacity using the image analysis software Iris as the opacity reflects the colony size and can be used as a proxy of fitness. We observed that deleting both *dolP* and *bamB* or *dolP* and *bamE* results in a negative genetic interaction (Figure 8). This means, that the double mutant had an observed fitness ratio that is smaller than the double expected fitness ratio and therefore, deleting both genes at once decreases the fitness (Material and methods 2.5). Our observations indicate that in a Δ*dolP* background, deleting *bamB* and *bamE* genes results in decreased cell fitness. This suggests that DolP might be needed for the BAM complex to fully function.

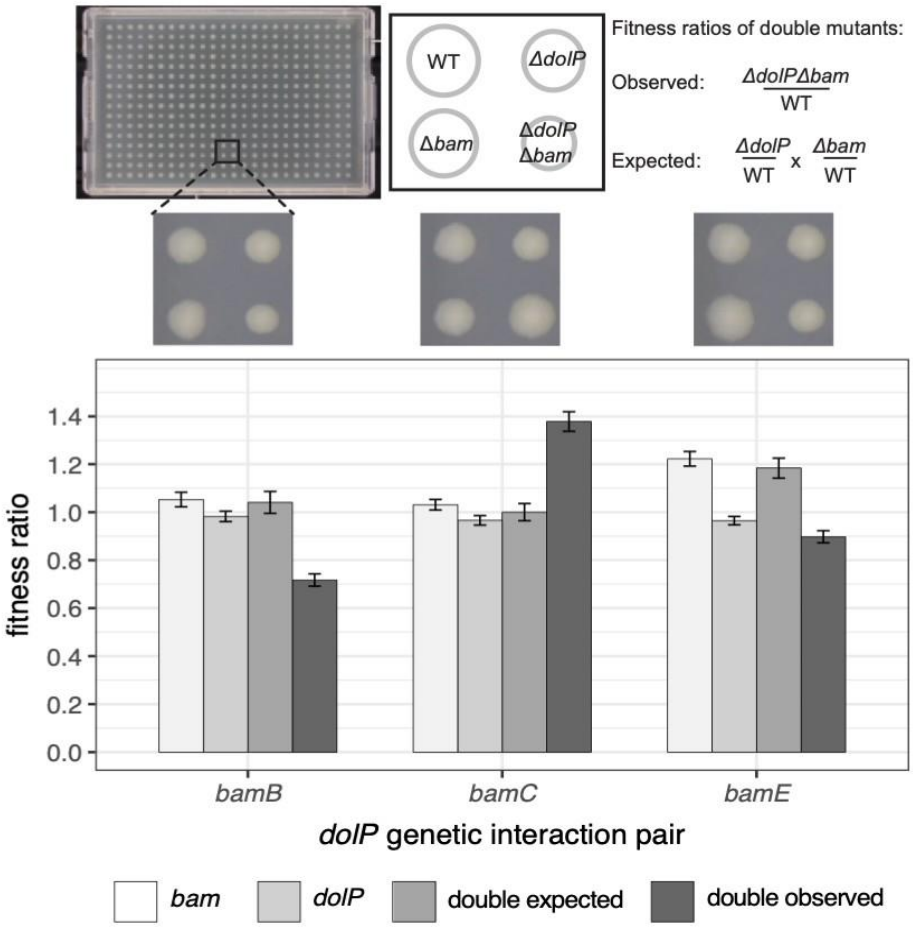

Figure 8. *dolP* genetically interacts with the genes encoding the non-essential Bam complex accessory lipoproteins.
Genetic interactions with *dolP* and *bamB, bamC*, and *bamE*. Strains were arrayed on LB agar plates using a Biomatrix 6 replicator. Genetic interaction plates were incubated at 37°C and imaged after 12h. An example of a 384-well plate is shown above the graph. Each plate contained a total of 384 colonies consisting of 96 wildtype, single, and double mutant clones. Fitness was measured by quantifying colony integral opacity using the image analysis software Iris.. Bar plots show the averaged values of 96 technical replicates. The error bars represent the average ± standard deviation showing a 95% confidence interval of Student's two-sample t-test.

3.2.2 Loss of *bamB* and *bamE* in Δ*dolP* causes cell lysis

To verify if the *bam*/*dolP* mutants strain panel present any morphological defects, we analysed their morphology by phase contrast microscopy. Cultures of the strains were grown in LB broth at 37°C to mid-exponential phase, inoculated on

agarose pads on slides and visualised using phase contrast optics. We observed that there were no significant changes in the morphology when analysing cell length and width (Table 2), however, we could observe an increase of lysed cells of Δ*dolP*Δ*bamB* (19.3%) and Δ*dolP*Δ*bamE* (13.6%) mutant strains (Figure 9). To confirm cell lysis, we live imaged Δ*dolP*Δ*bamB* cells for 185 min. The mother cell stopped dividing after 118 min and we observed phase light cells indicating cell death at 133 min (Figure 10). In contrast, WT cells completes lifespan after around 12 hours (Wang *et al*, 2010; Yang *et al*, 2019). Imaging of Δ*bamB,* Δ*dolP* and WT cells would be needed to fully understand the timing of cell lysis. Also, imaging of the strains Δ*dolP*Δ*bamE* and Δ*bamE* would be necessary to complete the panel of strains. However, due to time constraints during my PhD I could not complete such experiments. In accordance with our fitness data, this suggests that DolP may impact the BAM complex and in return this reduces fitness (increased lysis). However, we don't have enough evidence to describe a distinct mechanism to explain this observation yet.

Table 2. Phenotypes of *dolP* and *bam* mutants.

Relevant genotype	No. of cells[1]	Total length (μm)[2]	Avg length ± s.d. (μm)[3]	Total width (μm)[4]	Avg width ± s.d. (μm)[5]	Total no. of cells[6]	No. of lysed cells[7]	% of lysed cells[8]	*P*-value avg length[9]	*P*-value avg width[10]
WT	783	1554.2	2.0 ± 0.7	704.2	0.9 ± 0.1	783	0	0		
Δ*dolP*	869	1644.8	1.9 ± 0.7	765.3	0.9 ± 0.1	869	0	0	< 0.05	N.S.
Δ*bamB*	819	1591.0	1.9 ± 0.9	682.2	0.8 ± 0.2	819	0	0	< 0.05	< 0.05
Δ*bamC*	985	1940.1	2.0 ± 0.8	858.7	0.9 ± 0.1	985	0	0	N.S.	N.S.
Δ*bamE*	740	1489.6	2.0 ± 0.9	646.7	0.9 ± 0.2	740	0	0	N.S.	N.S.
Δ*dolP*Δ*bamB*	797	1387.9	1.7 ± 0.9	587.4	0.7 ± 0.2	988	191	19.3	< 0.05	< 0.05
Δ*dolP*Δ*bamC*	541	1082.4	2.0 ± 0.9	470.5	0.9 ± 0.2	541	0	0	N.S.	N.S.
Δ*dolP*Δ*bamE*	753	1304.7	1.7 ± 0.9	553.6	0.7 ± 0.2	872	119	13.6	< 0.05	< 0.05

[1] All cells were considered single cells.
[2] Total length means cumulative length of all cells measured.
[3] Refers to the total length/number of cells. S.d., standard deviation.
[4] Total width means cumulative width of all cells measured.
[5] Refers to the total width/number of cells. S.d., standard deviation.
[6] Total number of cells refers to the sum of viable cells and lysed cells.
[7] Phase light cells were considered as lysed cells.
[8] Percentage of lysed cells related to the total number of cells.

[9] *P*-values of Student t-test comparing the average length of WT cells with every mutant.
[10] *P*-values of Student t-test comparing the average width of WT cells with every mutant.
N.S., not significant (significance indicated by Student's t test)

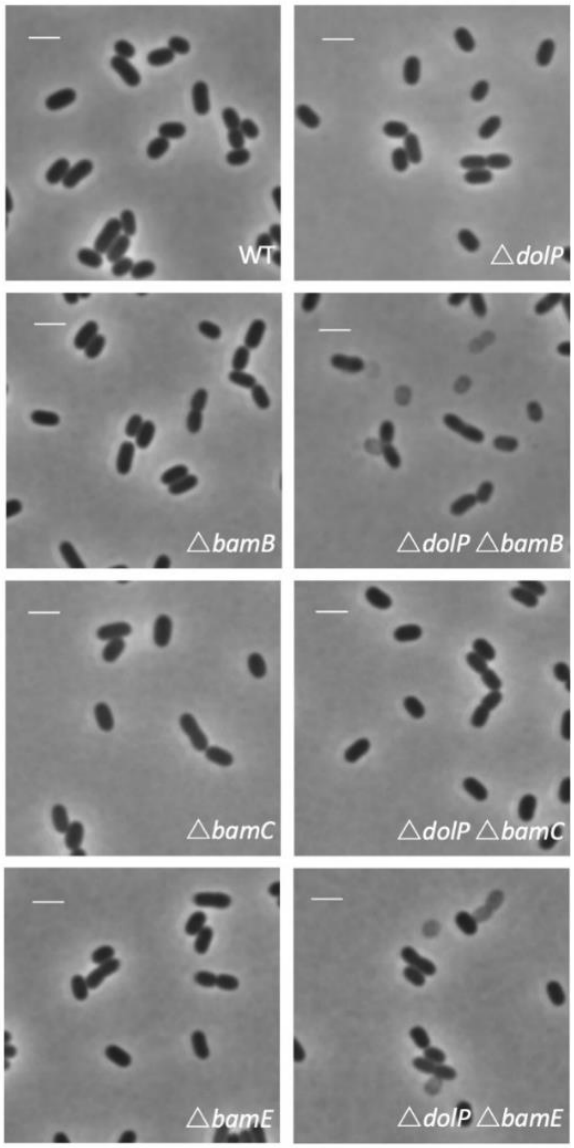

Figure 9. Phase contrast microscopy images showed no changes to cell morphology but an increase in number of lysed cells.
Phase contrast microscopy of WT, Δ*dolP*, Δ*bamB*, Δ*bamC,* Δ*bamE,* Δ*dolP* Δ*bamB,* Δ*dolP*Δ*bamC* and Δ*dolP*Δ*bamE.* Cells were grown to mid-exponential phase (OD600 ~0.4-0.8). Phase light cells can be observed for the Δ*dolP*Δ*bamB* and Δ*dolP*Δ*bamE* cells. Scale bar = 2 µm.

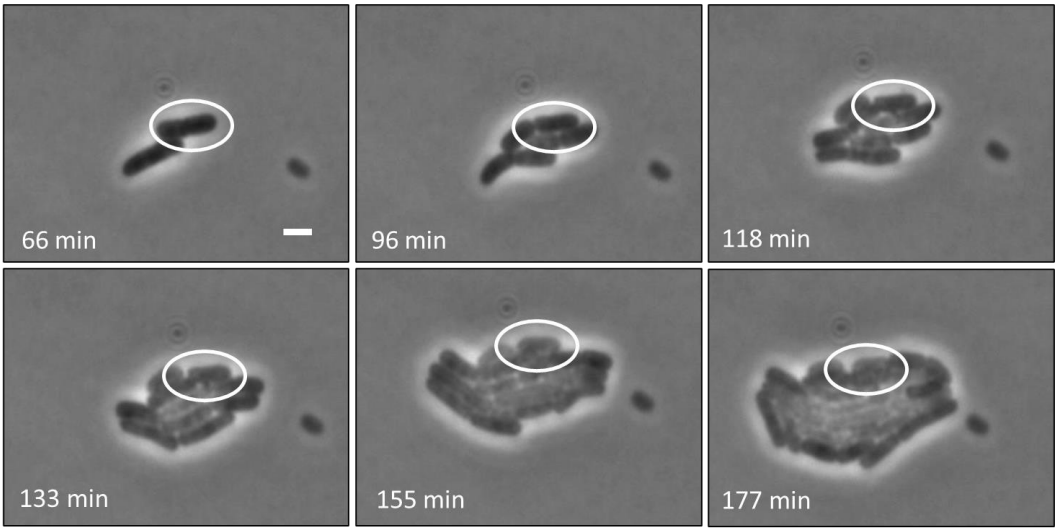

Figure 10. Live imaging of Δ*dolP*Δ*bamB* shows lysed cells.
Phase contrast microscopy time-lapse series of Δ*dolP*Δ*bamB.* Cells were grown for 185 min on agarose and LB pad. Timing is indicated in every frame. A white circle indicates the cells that stopped dividing and lysed. Scale bar = 2 µm.

3.2.3 Deletion of *bamB* and *bamC* does not affect *dolP* localisation to the division site

We showed that DolP binds anionic phospholipids and that this binding guides DolP localisation to the division site (Bryant *et al.*, 2020). After the observation that deletion of *bamB* and *bamE* in a Δ*dolP* background affects growth, we asked if this defect may be explained by a mislocalisation of DolP to the division site. To determine if loss of BAM complex non-essential components influence the localisation of DolP, we performed immuno-fluorescence microscopy. To do so, we used the DolP::mCherry construct to transform the Δ*bamB*, Δ*bamC*, or Δ*bamE* mutants in order to see if DolP::mCherry division site localisation was affected. Cells were grown to mid-exponential phase and visualised by fluorescence microscopy. Analysing the images, in Δ*bamB*, Δ*bamC*, or Δ*bamE* strains, no change to DolP division site localisation was

observed (Figure 11). This suggests that sub cellular localisation of DolP does not depend on the presence of the auxiliary BAM complex components.

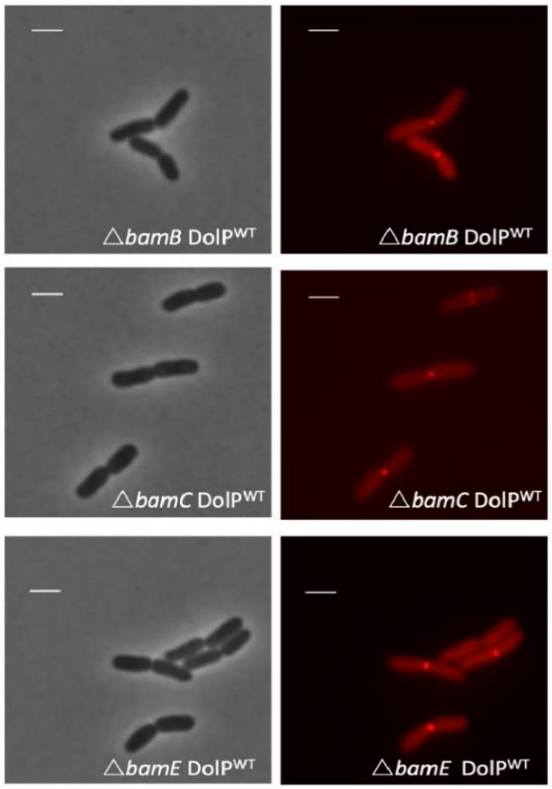

Figure 11. DolP localisation is unaffected by loss of the Bam complex non-essential components. Fluorescence microscopy of Δ*bamB,* Δ*bamC* or Δ*bamE* cells expressing DolP^{WT}::mCherry from the pET17b plasmid. Cells were grown to mid-exponential phase (OD600 ~0.4-0.8) in LB at 37°C. Left panel represents phase contrast and right panel the mCherry channel. Scale bar = 2 µm.

3.3 Discussion

DolP is a non-essential OM lipoprotein that has been placed as an important player in OM integrity, being crucial to maintain the integrity of the envelope under a series of cell envelope stresses (Bryant *et al.*, 2020; Morris *et al.*, 2018). It was also suggested to be involved in OMP biogenesis. In protein interactome studies, DolP was captured as an interactor of BamD and BamE (Babu *et al.*, 2018; Carlson *et al.*, 2019). In these studies, the authors developed a membrane mimetic scaffold to maintain

membrane proteins water-soluble, which they named “peptidisc”. This peptidisc was used to detect the cell envelope proteome of *E. coli.* Proteins of the peptidisc library across different fractions were detected by mass spectrometry. Having the proteome, an interaction score and probability were given to every interaction. For interaction between DolP and BamC/D/E the determined interaction score and probability were higher than 0.5 and 90% respectively. In addition, studies showed that a synthetic lethality is found in cells lacking both *dolP* and *surA,* that encodes a periplasmic chaperone involved in BAM complex pathway assembling ß-barrel proteins in the OM (Onufryk *et al.*, 2005; Typas *et al.*, 2008; Yan *et al.*, 2019). Therefore, to confirm a role of DolP for the BAM complex, we checked whether deleting the gene that encodes *dolP* and the BAM complex non-essential components would cause an impact on cell fitness.

The genetic interaction analysis revealed a reduction of fitness of the double mutants Δ*dolP*Δ*bamB* and Δ*dolP*Δ*bamE.* Furthermore, it was demonstrated that loss of DolP enhances membrane fluidity (Bryant *et al.*, 2020) and *bamB* mutants are sensitive to increased membrane fluidity (Storek *et al*, 2019) when tested with PDA (pyrenedecanoic acid), an intercalating dye which stains the membrane. Therefore, fitness reduction in Δ*dolP*Δ*bamB* and Δ*dolP*Δ*bamE* mutants might be due to this increase in fluidity of the membrane. Fluidity increase can be caused by changes on the length and composition of the fatty acids or phospholipids in the membrane. Despite this, no alteration in LPS or phospholipids composition in Δ*dolP* cells was found (Bryant *et al.*, 2020). However, it was shown that DolP binds to phospholipids which guides DolP to localise to the cell division site (Bryant *et al.*, 2020).

We demonstrated that deletion of any of the unessential *bam* genes does not change DolP localisation in the division site. In contrast, once *surA* is deleted, there is a decrease in the number of cells with GFP-DolP localisation (Ranava *et al.*, 2021). These results indicate that localisation of DolP to the division site is affected by certain envelope stresses, but it does not depend to the unessential component of the BAM complex.

Complementing our results, Ieva's group (Ranava *et al.*, 2018) has demonstrated that DolP is critical to maintain cell fitness, keeping BamA levels when there is a lack of BamB and when cells are under envelope stresses. The authors have also found that DolP assists BamA folding. It was suggested that DolP might be a transient chaperone to BamA, as OsmY, which is also a BON-domain protein, as chaperone to a group of autotransporters (Yan *et al.*, 2019). These findings support our indications that DolP has a role in OMP biogenesis.

In addition to the role of DolP in OMP biogenesis, it has been suggested that DolP might be involved in cell division at the step of daughter cells separation. Tsang and authors (Tsang *et al.*, 2017) speculated that DolP is a regulator of NlpD, an amidase activator itself, through a genetic screen. Moreover, Ranava and authors (Ranava *et al.*, 2021) performed a CRISPRi (Clustered Regularly Interspaced Short Palindromic Repeat interference) screen. With the screen, it was observed that silencing the genes *amiA, envC, ftsX* and *ftsE,* in Δ*dolP* cells, results in growth defects. To verify these findings experimentally, we sought to explore how DolP may impact cell division. The results can be found in the next chapter of this thesis.

Chapter 4. The lipoprotein DolP affects cell separation in *Escherichia coli*, but not as an upstream regulator of NlpD

The lipoprotein DolP affects cell separation in *Escherichia coli*, but not as an upstream regulator of NlpD

Published article

Gabriela Boelter[1,†], Jack A. Bryant[1,†], Hannah Doherty[1], Peter Wotherspoon[1], Dema Alodaini[1], Xuyu Ma[1], Micheal B. Alao[1], Patrick J. Moynihan[1], Danesh Moradigaravand[2], Monika Glinkowska[3], Timothy J. Knowles[1], Ian R. Henderson[1,4] and Manuel Banzhaf[1]

Microbiology. 2022 May 23;168(5):001197.

Acknowledgements
We want to thank all members and collaborators of the Banzhaf laboratory for their support and critical feedback for this manuscript.

Author contributions
Conceptualization, G.B., J.A.B., I.R.H. and M.B. Formal analysis, P.M. and D.M. Funding acquisition, M.B. Investigation, G.B., J.A.B., H.D., P.W., D.A., X.M. and M.B.A. Methodology, G.B., J.A.B. and M.B. Project administration, G.B., J.A.B. and M.B. Resources, T.K., I.R.H. and M.B. Supervision, M.B.; Validation, G.B., J.A.B., M.G., T.K. and M.B. Visualization, G.B., J.A.B. and M.B. Writing – original draft, G.B., J.A.B. and M.B. Writing – review and editing, G.B., J.A.B., H.D., P.W., D.A., X.M., M.B.A., P.M., D.M., M.G., T.K., I.R.H. and M.B.

[1]Institute of Microbiology and Infection, School of Biosciences, University of Birmingham, Birmingham, UK;
[2]Centre for Computational
Biology, Institute of Cancer and Genomic Sciences, University of Birmingham, Birmingham B15 2TT, UK;
[3]Department of Bacterial Molecular Genetics,
University of Gdansk, Gdańsk, Poland;
[4]Institute for Molecular Bioscience, University of Queensland, St. Lucia, Australia.
[†]These authors contributed equally to this work

This chapter includes the paper published in Microbiology journal (Boelter *et al*, 2022) which I am the first author. The Biosciences PGR lead Prof David Grainger and my supervisor Dr Manuel Banzhaf have agreed in including the paper in the body of my thesis as I wrote the original text.

4.1 Abstract

Most Gram-negative bacterial peptidoglycan amidases are essential to split the shared envelope of adjunct daughter cells to allow cell separation. Their activity needs to be precisely controlled to prevent cell lysis. In *Escherichia coli,* amidase activity is controlled by three regulatory proteins NlpD, EnvC and ActS. However, recent studies linked the outer membrane lipoprotein DolP (formerly YraP) as a potential upstream regulator of NlpD. In this study we explored this link in further detail. To our surprise DolP did not modulate amidase activity *in vitro* and was unable to interact with NlpD in pull-down and MST (MicroScale Thermophoresis) assays. Next, we excluded the hypothesis that Δ*dolP* phenocopied Δ*nlpD* in a range of envelope stresses. However, morphological analysis of double deletion mutants of amidases (AmiA, AmiB AmiC) and amidase regulators with *dolP* revealed that Δ*amiA*Δ*dolP* and Δ*envC*Δ*dolP* mutants display longer chain length compared to their parental strains indicating a role for DolP in cell division. Overall, we present evidence that DolP does not affect NlpD function *in vitro*, implying that DolP is not an upstream regulator of NlpD. However, DolP may impact daughter cell separation by interacting directly with AmiA or AmiC, or by a yet undiscovered mechanism.

4.2 Introduction

Gram-negative bacteria have a three-layered envelope: the inner membrane (IM), outer membrane (OM) and peptidoglycan (PG) cell wall. In order to grow and maintain their cell shape, Gram-negative bacteria enlarge their envelope using

dynamic and transient multiprotein complexes until they double in size (Graham *et al*, 2021). Subsequently, the envelope must be constricted by invagination of all three layers, in a process known as cell division, to separate the daughter cells while maintaining envelope integrity to prevent lysis (Egan *et al.*, 2020; Typas *et al.*, 2012).

At the final step of cell separation, the PG layer needs to be split by PG hydrolases. *E. coli* encodes three periplasmic amidases (AmiA, AmiB, AmiC) of which at least one is required for cell division (Heidrich *et al.*, 2001; Priyadarshini *et al.*, 2007; Tsang *et al.*, 2017). These amidases are auto inhibited and must be activated by two specific regulators (Tsang *et al.*, 2017; Uehara *et al.*, 2009; Uehara *et al.*, 2010; Yang *et al.*, 2011). AmiA and AmiB are activated by EnvC, which is anchored to the outer surface of the IM. For the activation of the amidases, EnvC needs to be recruited to the septal ring by an interaction between a periplasmic loop of the ATP-binding cassette (ABC) transporter-type membrane proteins FtsE-FtsX and the EnvC coiled-coil (CC) domain (Cook *et al.*, 2020; Pichoff *et al*, 2019; Yang *et al.*, 2011). In contrast, AmiC is activated by the OM-localized lipoprotein NlpD (Mesnage *et al*, 2014; Rocaboy *et al*, 2013).

In addition to EnvC and NlpD, *E. coli* has a further amidase activator, ActS (formerly YgeR) a lipoprotein that localizes peripherally oo the OM. ActS activates all three of the amidases but *in vitro* results suggest that it preferably activates AmiC (Gurnani Serrano *et al.*, 2021). However, in conditions of acidic pH, ActS preferentially activates AmiB, along with NlpD and EnvC, and to some extent activates AmiC (Mueller *et al.*, 2021).

Previously, aiming to identify additional proteins involved in cell separation, Tsang and collaborators (Tsang *et al.*, 2017) identified the OM lipoprotein DolP

(division and OM stress-associated lipid-binding protein - formerly YraP) as a potential upstream regulator of NlpD. Inactivation of DolP caused cell separation defects in an ∆*envC* background, in which the AmiA and AmiB amidases are lacking their activator, therefore suggesting that DolP may activate AmiC either directly or indirectly via activation of NlpD (Tsang *et al.*, 2017). DolP is a conserved OM anchored lipoprotein consisting of two BON (Bacterial OsmY and Nodulation) domains (Bryant *et al.*, 2020; Morris *et al.*, 2018), a protein domain that is broadly conserved across bacterial phyla and has been suggested to be required for phospholipid binding (Yeats & Bateman, 2003). Indeed, the C-terminal BON domain binds to anionic phospholipids and is essential for DolP localization to the division site (Bryant *et al.*, 2020). The detailed molecular function of DolP is yet to be completely resolved. To date, DolP is implicated in the function of the β-barrel-assembly machinery (BAM) complex (Ranava *et al.*, 2021) and cell division as an upstream regulator of NlpD (Tsang *et al.*, 2017).

In this study we explored the role of DolP as a potential upstream regulator of NlpD. DolP did not modulate the activity of any of the tested amidases in an *in vitro* PG degradation assay and was unable to interact with NlpD by pull-down and MST (MicroScale Thermophoresis) assays. In addition, our results show that Δ*dolP* and Δ*nlpD* mutants do not phenocopy each other when probed against envelope stresses. However, inactivation of *dolP* in combination with amidase encoding genes results in morphological changes and we provide some evidence that DolP interacts with AmiA and AmiC. These results suggest that DolP affects cell division, but likely not as a regulator of NlpD.

4.3 Materials and methods

Bacterial strains and growth conditions

E. coli BW25113 is the parental strain used in this study. *E. coli amiA*::*kan*, *amiB*::*kan, amiC*::*kan*, *envC*::*kan, nlpD*::*kan* mutants were obtained from the KEIO library (Baba *et al.*, 2006) and the mutations transduced into a clean parental strain. *E. coli* Δ*dolP* was created by resolving the Kan^R cassette (Datsenko & Wanner, 2000). Double mutants were created by P1 transduction as described previously (Thomason *et al.*, 2007). The chromosomal modification was confirmed by PCR when a Kan^R cassette was transduced. Strains were routinely cultured on LB agar (5 g l^{-1} NaCl, 5 g l^{-1} yeast extract, 10 g l^{-1} peptone, 1.5% agar) and LB broth (5 g l^{-1} NaCl, 5 g l^{-1} yeast extract, 10 g l^{-1} peptone).

Growth analysis under cell envelope stress in solid media

Overnight cultures of the selected strains were grown at 37 °C. The inoculum was adjusted to OD_{600}=1 or OD_{600}=2 and serial diluted (10^{-1} - 10^{-6}) in LB broth in a 96 well plate. A volume of 2.5 µL or 5 µL (as indicated in the figures legends) of each sample was inoculated on square Petri dishes with LB agar adjusted to different cell envelope stress inducers (0 mM, 500 mM NaCl, 50 µg ml^{-1} vancomycin, SDS, EDTA, and pH 4.8 and 5.2). The plates were incubated at 37°C and photographed after ~16 hours.

Microscopy

DolP and amidases/regulators fluorescence imaging: To visualise membrane and DNA compartmentalisation of the cells, FM1-43FX dye (Invitrogen) and DAPI (Stratech Scientific) were used, respectively. Overnight cultures were diluted to initial OD_{600}=0.01 in LB. The cells were incubated at 37°C until OD_{600}= ~0.4. A volume of 0.5 ml of the culture was stained with 5 µg ml^{-1} of FM1-43FX at room temperature for 10 min. The cells were adjusted to 33 mM sodium phosphate pH 7.4. Cells were fixed by addition of 2.4 % formaldehyde and 0.04 % glutaraldehyde to the cell suspension. Fixed cells were applied to agarose pads, which were prepared with 1.5 % agarose in PBS and set in Gene Frames (Thermo Scientific). Cells were imaged using a Zeiss AxioObserver equipped with a Plan-Apochromat 100x/Oil Ph3 objective and illumination from HXP 120V for phase contrast images. FM1-43FX images were captured using the Zeiss filter set 38 (Ex: 470/40 nm, beamsplitter 495 nm, Em: 525/50 nm). For DAPI images we used the Zeiss filter set 96 (Ex: 390/40 nm, beamsplitter 420, Em: 450/40 nm). For phenotype analysis in Table 3, 4 and 5 the MicrobeJ plugin for Fiji 600 was used (Ducret *et al.*, 2016).

Imaging of cells grown in acidic pH: An overnight culture in 37 °C was grown in LB media pH 6.9. Cells were subcultured in LB media pH 6.9 until the culture reached early exponential phase (OD_{600}= ~0.2). The cultures were back-diluted either in LB media with either pH 5.2 (containing MMT buffer (1:2:2 molar ratio of D,L-malic acid, MES, and Tris base) or pH 6.9. Cells were washed with pH 5.2 media before being transferred to a fresh flask containing pH 5.2 media. Cells were then incubated with aeration until OD_{600}= ~0.2. Preparation of slides was as described above. Phenotypic analysis was performed as described above.

Protein purification

The *dolP* gene was codon optimised and cloned into the pET-26b(+) plasmid vector at NdeI/ XhoI restriction sites (Bryant *et al.*, 2020). The construct has six histidine residues followed by a cleavable Tobacco etch virus (TEV) site on the N-terminus of DolP. The plasmid was transformed into *E. coli* BL-21. The cells were grown in 2 L of LB broth at 37 °C until OD_{600} =~0.5. The cultures were induced using 1 mM IPTG. After 4 hours of induction, cells were harvested by centrifugation at 6,900 x g for 15 minutes at 4 °C. Cell pellets were resuspended in binding buffer (50 mM sodium phosphate or 50 mM tris HCl pH 7, 300 mM NaCl, 50 mM imidazole, 0.5 mM TCEP) and Roche cOmplete EDTA-free protease inhibitor cocktail tablets (1/1,000 dilution). Cells were lysed using a sonicator and C3 Emulsiflex Cell disruptor (Avastin). The lysate was centrifuged at 31,400 x g for 1 hr at 4 °C. The supernatant was recovered and incubated with 1 ml L^{-1} of Ni2+ agarose beads (Jena Bioscience) pre-equilibrated with binding buffer for 1 hr with mixing. The sample was applied to an elution column and washed with binding buffer before the protein was eluted with elution buffer (50 mM Sodium phosphate or 50 mM tris HCl pH 7, 300 mM NaCl, 500 mM imidazole, 0.5 mM TCEP). Elution fraction containing His-DolP was dialyzed against 2 L dialysis buffer (150 mM NaCl, 50 mM Tris-HCl, 10% glycerol, pH=8) overnight at 4 °C. Dialyzed protein was concentrated and purified by size exclusion chromatography. Sample was dialysed in gel filtration buffer (50 mM sodium phosphate or 50 mM tris HCl pH 8, 300 mM NaCl, 0.5 mM TCEP), concentrated to 2 ml and injected into a pre-equilibrated S75 26 60 GE healthcare column. With a flow rate of 2 ml min^{-1}, 2 ml sample were collected and run on SDS-PAGE gels to assess purity. The protein was concentrated and stored at −80°C. For the removal of the His-

tag, TEV protease (1:100 w/w) was added, and the sample was dialyzed in cleavage buffer (150 mM NaCl, 50 mM Tris-HCl pH 8, 10% glycerol). The protease was removed from the sample using an elution column.

The *E. coli* amidases AmiA, AmiB, AmiC, and cognate regulators NlpD and EnvC were purified as previously described (Uehara *et al.*, 2010).

Ni^{2+} bead pulldown assay

His-tagged protein or natural binding protein (AmiA) was incubated with untagged protein in Ni^{2+}-NTA agarose beads. Beads were pre-equilibrated with binding buffer (100 mM NaCl, 50 mM Tris-HCl, pH 8) by centrifugation at 4,000 g, 4 min at 4°C. Samples were incubated for 30 min before being washed with washing buffer (300 mM NaCl, 50 mM tris, pH 8) and pelleted by centrifugation. Supernatant was discarded and the elution was incubated at 100°C in SDS-buffer (50 mM Tris–HCl pH 6.8, 2% SDS, 10% glycerol 0.02% bromophenol blue, 10% ß-mercaptoethanol) and analysed by SDS-PAGE.

MicroScale Thermophoresis (MST)

DolP was labelled with Monolith Protein Labeling Kit RED-NHS 2nd generation (Nanotemper) according to the manufacturer's instructions. Unlabelled ligands were titrated in the starting concentrations AmiA (200 µM), AmiB (148 µM) and AmiC (70 µM). Ligand proteins were two-fold serial diluted 16 times in MST buffer (150 nM NaCl, 10 mM $MgCl_2$, 0.05% Tween 20, 50 mM Tris pH 7.4) and 100 nM of labelled DolP was added for interactions assay. The proteins were transferred to capillaries to be read on a Monolith NT.115 10–40% MST power. Binding curves and kinetic parameters were

plotted and analysed using NT Analysis 1.5.41 and MO. Affinity Analysis (x64) software.

Peptidoglycan degradation assay

PG sacculi were isolated from *E. coli* Top10 and labelled with fluorescein isothiocyanate (FITC) as described in (Gurnani Serrano *et al.*, 2021; Maeda, 1980). To assess *in vitro* PG degradation, 2 µM of purified proteins were incubated with 10 mg ml^{-1} of FITC labelled PG sacculi (FITC-PG) in 100 µL of buffer (150mM NaCl + 50mM Tris, pH 8.0) for 1 hr at 37 °C with shaking. Lysozyme (4 µM) was used as positive control and FITC-PG, or buffer alone, as negative control. The reaction was stopped by filtration and the fluorescence of the soluble fraction was read (Ex: 495 nm, Em: 519 nm) in an Omega plate reader (BMG Labtech).

4.4 Results

4.4.1 DolP does not interact with NlpD or activate amidase activity in an *in vitro* peptidoglycan degradation assay

It was postulated that DolP could be an activator of NlpD, which in turn activates AmiC. Hence, we evaluated whether DolP is able to modulate amidase activity using PG degradation assays. To do this we modified an existing PG degradation assay protocol and used FITC labelled sacculi instead of RBB-dye labelled (Gurnani Serrano *et al.*, 2021; Maeda, 1980; Uehara *et al.*, 2010). We incubated DolP and FITC labelled

sacculi in combination with amidases alone or with their respective regulator. Next, we measured the absorbance of the fluorescence released when the PG is degraded, indicating amidase activity (Figure 12a). The amidases, activators, or DolP alone released very little fluorescence indicating very low enzyme activity. In contrast, amidase activity was high when incubated with their cognate regulators NlpD or EnvC. The addition of DolP did not activate any of the amidases, nor did it alter PG degradation when added in combination with the cognate regulators, suggesting that DolP likely is not an NlpD regulator.

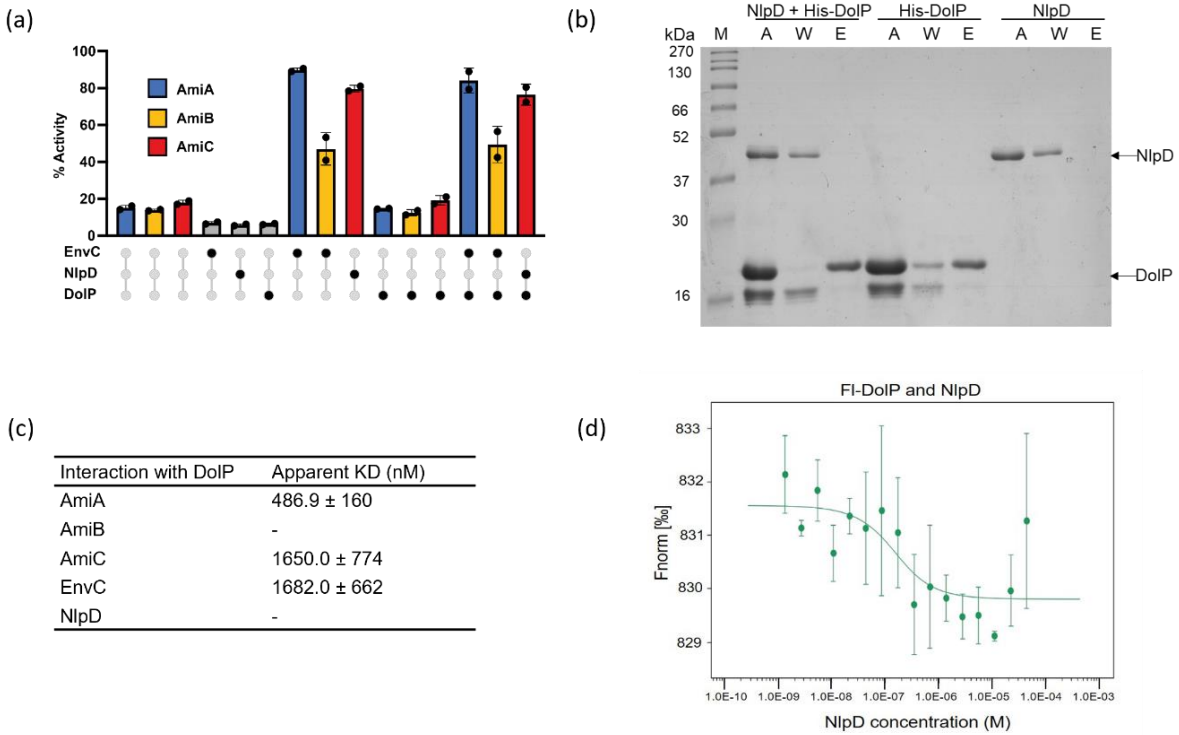

(c)

Interaction with DolP	Apparent KD (nM)
AmiA	486.9 ± 160
AmiB	-
AmiC	1650.0 ± 774
EnvC	1682.0 ± 662
NlpD	-

Figure 12. DolP does not activate amidases in an *in vitro* peptidoglycan degradation assay but interacts with two amidases in vitro.
(a) Relative degradation of FITC labelled sacculi by amidases and/or regulators normalized to a lysozyme control. The grey bars indicate EnvC, NlpD and DolP incubation alone. The dark dots in the x-axis represent addition of the respective enzyme. The % Activity is normalised to lysozyme control. The graph represents two replicates. (b) SDS–PAGE gel stained with Coomassie blue showing the pull-down of DolP and NlpD (see text for more information) to NiNi-NTA beads. (A) applied sample; (W) washed sample; (E) eluted sample; (M) marker. SDS-PAGE gel of AmiA, AmiB, AmiC and NlpD are shown in Fig. 13. (c) Dissociation constants for interactions between DolP with AmiA, AmiC and EnvC as determined by microscale thermophoresis (MST). The non-interaction of Fl-DolP with AmiB and NlpD is represented by a dash. The values are mean ± SD of three independent experiments. The corresponding MST binding curves are shown in Fig. 14 and 15. (d) MST binding curve for interaction

between fluorescently labelled DolP (Fl-DolP) with unlabelled NlpD MST curves plotted are the mean data of three independent experiments. (Fl) fluorescently labelled; (FNorm) normalized fluorescence. MST binding curves for Fl-DolP with unlabelled AmiA, AmiB, AmiC, and EnvC are shown in Fig. 14 and 15.

Next, we sought to investigate if DolP is able to interact with NlpD or any of the amidases to explore if protein-protein interaction could explain the role of DolP in cell division. To test this, we purified recombinant water-soluble DolP to test whether it is able to physically interact with amidases and regulators *in vitro*. To do so, we mixed DolP (untagged) or DolP-His-tagged with either AmiA, AmiB, AmiC, EnvC-His or NlpD. Subsequently, we performed pull-down assays using Ni-NTA agarose beads (Figure 12b and Figure 13). As AmiA has a natural affinity to the Ni-NTA beads and our EnvC construct did not allow for removal of the His-tag, we inverted bait and prey for both cases and used an untagged DolP, instead of the His-tagged DolP used for AmiB, AmiC and NlpD.

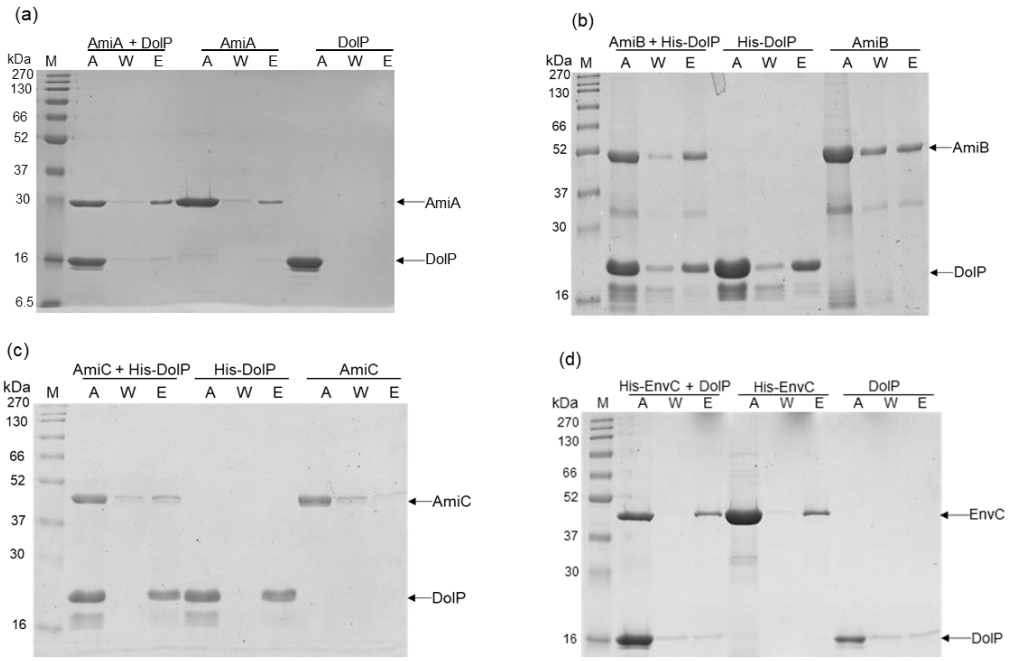

Figure 13. Representation of pull-down assay of DolP with amidases and regulators.
SDS-PAGE gels from Ni-NTA pull down assay of DolP and (a) AmiA, (b) AmiB, (c) AmiC or (d) EnvC. Proteins were incubated with Ni-NTA beads in combination or alone. Retention of untagged protein in

the presence of His-tagged protein indicates an interaction. (A) applied sample; (W) washed sample; (E) eluted sample; (M) marker.

His-DolP was unable to pull down NlpD, indicating that both proteins do not interact (Figure 12b). We also did not observe an interaction of EnvC-His with DolP (Figure 13). Interpreting the Amidase-DolP pull-downs is difficult as all amidases bound nonspecifically to the Ni-NTA agarose beads to varying degrees. We can observe that a portion of DolP was pulled down by AmiA, however, this interaction at best seems very weak. Nevertheless, it seems that more AmiC was retained by His-DolP when compared to their respective controls (Figure 13). For the AmiB-DolP pair we were unable to observe such a difference (Figure 13). These data suggest an interaction between DolP and AmiC, a potential weak interaction with AmiA, but no interaction with AmiB.

Double banding in His-DolP was observed (Figure 12b and Figure 13b and c). The second band could be a degradation product of DolP. To confirm the nature of both bands mass spectrometry would be necessary. The bands from a SDS-PAGE gel would be excised and reduced to be digested into peptides. Those peptides would be separated by liquid chromatography coupled to a mass spectrometer. Then, the peptides masses would be determined and through Tandem mass spectrometry the peptides sequence is confirmed. The sequence would be compared to a protein database to identify the nature of the peptides presented on the bands (Potel *et al*, 2018). However, due to time constraints during my PhD I could not do this experiment and the pull-down results were accepted for paper publication.

To confirm the observed pull-down assay interactions and to overcome the pitfall of amidases nonspecifically binding to Ni-NTA agarose beads we used a second

protein interaction technique, MST (MicroScale Thermophoresis). Fluorescently labelled DolP (Fl-DolP) (100 nM) was titrated against serial dilutions of unlabelled AmiA, AmiB, AmiC, NlpD and EnvC as ligands, and the thermophoresis of Fl-DolP was measured and quantified as normalized fluorescence (Fnorm). A change in Fnorm indicates binding with the ligand and can be plotted to determine the affinity of the protein-protein interaction. However, the affinity analysis (x64) software will fit by default the best possible binding curve, hence the determinator for a successful interaction is the signal to noise ratio reliability cut-off. Therefore, if the reliability cut-off is below 5.0 an interaction could not be determined.

Using MST, we could generate binding curves that indicate an interaction of DolP with AmiA (Kd 486.9 nM), AmiC (Kd 1650 nM) and EnvC (Kd 1682 nM). Although, the binding curve for AmiA and DolP interaction is inconclusive. The binding curve does not demonstrate a flat horizontal line at high concentrations, as is usually observed when saturation happens. In addition, the binding curves probing an interaction of DolP to NlpD and AmiB had a reliability cut-off below 5.0 suggesting that no interaction between these proteins occurred (Figure 12d and Figure 14 and Figure 15).

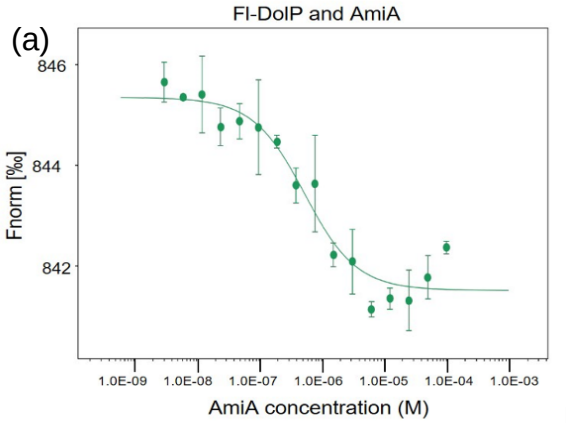

Name:	Experiment 1 (#01)
Graph Color:	●
Target Name:	Yrap
Target Concentration:	100 nM
Ligand Name:	AmiA
Ligand Concentration:	100 µM to 0.00305 µM
n:	3
Comments:	
Excitation Power:	20%
MST Power:	40%
Temperature:	25.0°C
Kd:	4.8696E-07
Kd Confidence:	± 1.6196E-07
Response Amplitude:	3.8264366
TargetConc:	1E-07[Fixed]
Unbound:	845.34
Bound:	841.52
Std. Error of Regression:	0.40303585
Reduced χ^2:	5.5404647
Signal to Noise:	10.19823

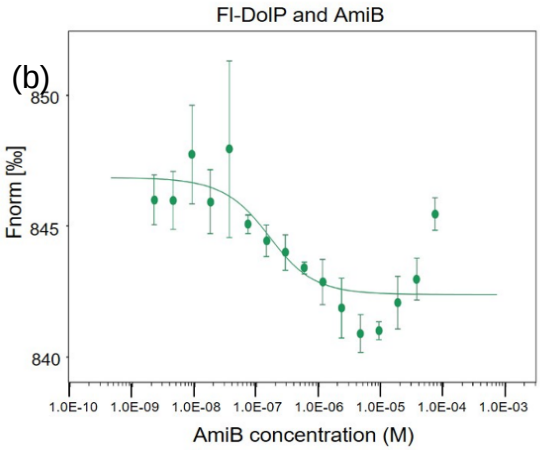

Name:	Experiment 1 (#01)
Graph Color:	●
Target Name:	Yrap
Target Concentration:	100 nM
Ligand Name:	AmiB
Ligand Concentration:	74.1 µM to 0.00226 µM
n:	3
Comments:	
Excitation Power:	60%
MST Power:	40%
Temperature:	23.6°C
Kd:	1.0703E-07
Kd Confidence:	± 1.1372E-07
Response Amplitude:	4.4612946
TargetConc:	1E-07[Fixed]
Unbound:	846.85
Bound:	842.39
Std. Error of Regression:	1.2792502
Reduced χ^2:	4.1834366
Signal to Noise:	3.7461

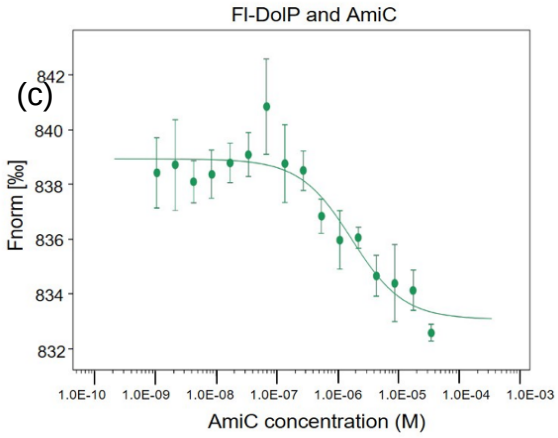

Name:	Experiment 1 (#01)
Graph Color:	●
Target Name:	YraP
Target Concentration:	100 nM
Ligand Name:	AmiC
Ligand Concentration:	34.9 µM to 0.00106 µM
n:	3
Comments:	
Excitation Power:	20%
MST Power:	40%
Temperature:	20.6°C
Kd:	1.6549E-06
Kd Confidence:	± 7.7505E-07
Response Amplitude:	5.8572717
TargetConc:	1E-07[Fixed]
Unbound:	838.93
Bound:	833.07
Std. Error of Regression:	0.79395322
Reduced χ^2:	1.0297817
Signal to Noise:	7.9245463

Figure 14. Representation of MST (Microscale thermophoresis) and dataset overview of DolP with amidases.

MST binding curves for interactions between fluorescently labelled DolP (Fl-DolP) with unlabelled (a) AmiA, (b) AmiB and (c) AmiC. MST curves plotted are the mean data of three independent experiments. (Fl) fluorescently labelled; (FNorm) normalized fluorescence. On the dataset overview, YraP refers to DolP.

(a)

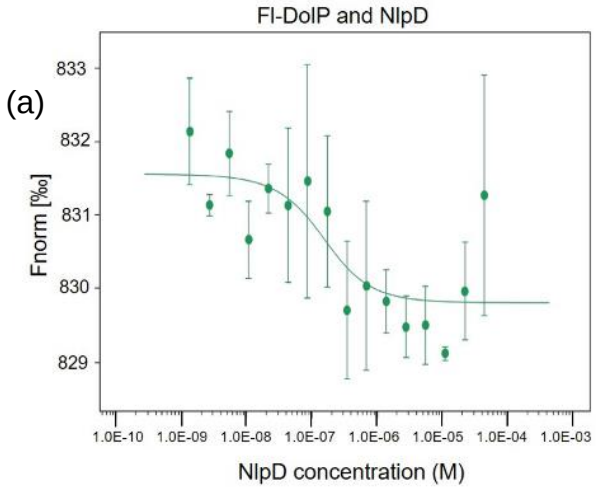

Name:	Experiment 2 (#02)
Graph Color:	•
Target Name:	YraP
Target Concentration:	100 nM
Ligand Name:	NlpD
Ligand Concentration:	44.1 µM to 0.00135 µM
n:	3
Comments:	
Excitation Power:	20%
MST Power:	40%
Temperature:	21.4°C
Kd:	1.0197E-07
Kd Confidence:	± 1.343E-07
Response Amplitude:	1.7485545
TargetConc:	1E-07[Fixed]
Unbound:	831.56
Bound:	829.81
Std. Error of Regression:	0.61675471
Reduced χ^2:	5.3430648
Signal to Noise:	3.0453741

(b)

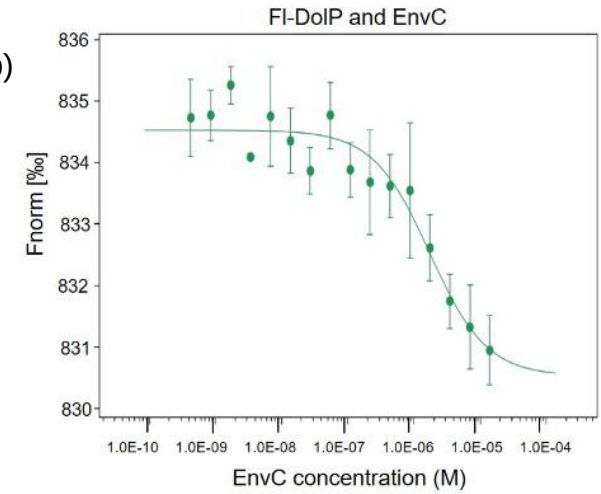

Name:	Experiment 1 (#01)
Graph Color:	•
Target Name:	YraP
Target Concentration:	100 nM
Ligand Name:	EnvC
Ligand Concentration:	14 µM to 0.000426 µM
n:	3
Comments:	
Excitation Power:	20%
MST Power:	40%
Temperature:	22.4°C
Kd:	1.682E-06
Kd Confidence:	± 6.6624E-07
Response Amplitude:	3.9957402
TargetConc:	1E-07[Fixed]
Unbound:	834.53
Bound:	830.53
Std. Error of Regression:	0.38115051
Reduced χ^2:	5.9896465
Signal to Noise:	11.260941

Figure 15. Representation of MST (Microscale thermophoresis) and dataset overview of DolP with amidase regulators.

MST binding curves for interactions between fluorescently labelled DolP (Fl-DolP) with unlabelled (a) NlpD and (b) EnvC. MST curves plotted are the mean data of three independent experiments. (Fl) fluorescently labelled; (FNorm) normalized fluorescence. On the dataset overview, YraP refers to DolP.

Taken together, the data supports the hypothesis that DolP does not interact with NlpD or activate amidase activity in an *in vitro* peptidoglycan degradation assay.

4.4.2 *dolP* and *nlpD* mutants do not phenocopy each other when grown under cell envelope stresses.

Knowing that DolP is not a regulator of NlpD we asked whether Δ*dolP* and Δ*nlpD* mutants phenocopy each other in various envelope stresses. By doing so, we hope to probe whether both genes are functionally connected. First, we created single mutants of amidases (Δ*amiA,* Δ*amiB,* Δ*amiC)* and cognate regulators (Δ*nlpD,* Δ*envC*) as a backbone for Δ*dolP* double mutants using P1 transduction in the *E. coli* BW25113 background (WT). Next, we grew the mutant panel on solid LB media supplemented with either the cell wall inhibitor vancomycin, the detergent sodium-dodecyl sulphate (SDS), the metal-chelating agent ethylene diamine tetra acetic acid (EDTA), a combination of SDS and EDTA, and LB with 0 mM or 500 mM NaCl. We then assessed their fitness (Figure 16 and Figure17).

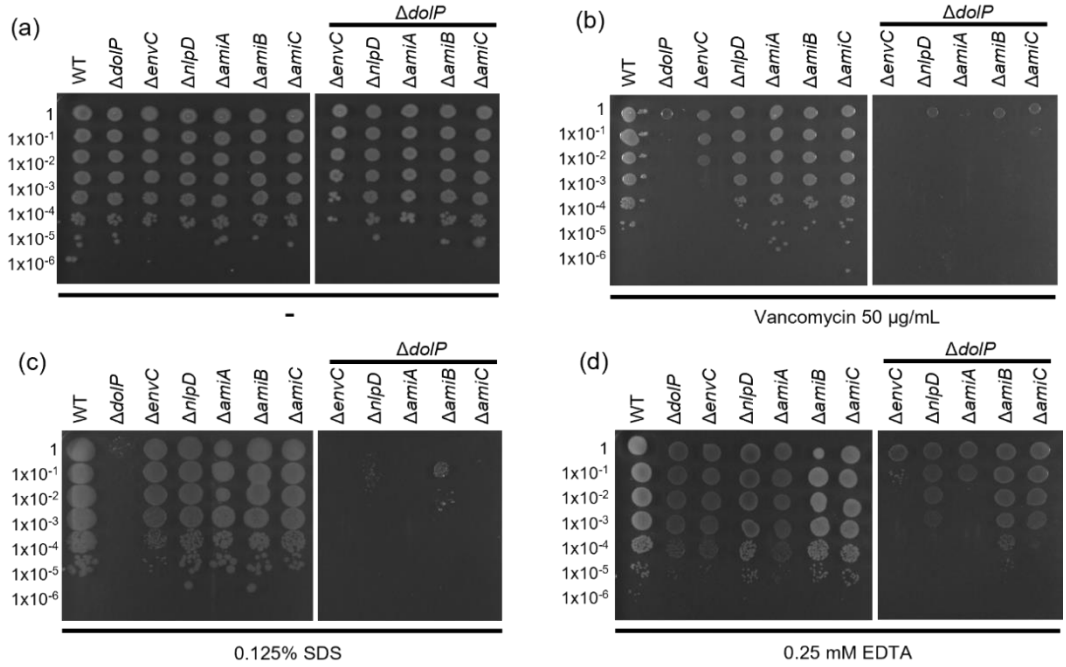

Figure 16. The mutant Δ*dolP* does not phenocopy Δ*nlpD* in most envelope stresses tested.
E. coli BW25113 WT, Δ*dolP,* Δ*amiA,* Δ*amiB,* Δ*amiC*, Δ*nlpD,* Δ*envC* and Δ*dolP* double mutants were grown overnight in LB at 37°C. After adjusting the cell density to OD_{600} = 1, the cultures were serially diluted (10^{-1} to 10^{-6}), and 5 µl of each dilution was spotted on (a) LB agar only or (b) supplemented with

vancomycin. Due to the surfactant effect of SDS, for the plates supplemented with (c) SDS and (d) EDTA the cultures were adjusted to cell density to OD600 = 2 and 2.5 µl of each dilution was spotted on the agar plates. The plates were incubated at 37°C and photographed after ~16 hours.

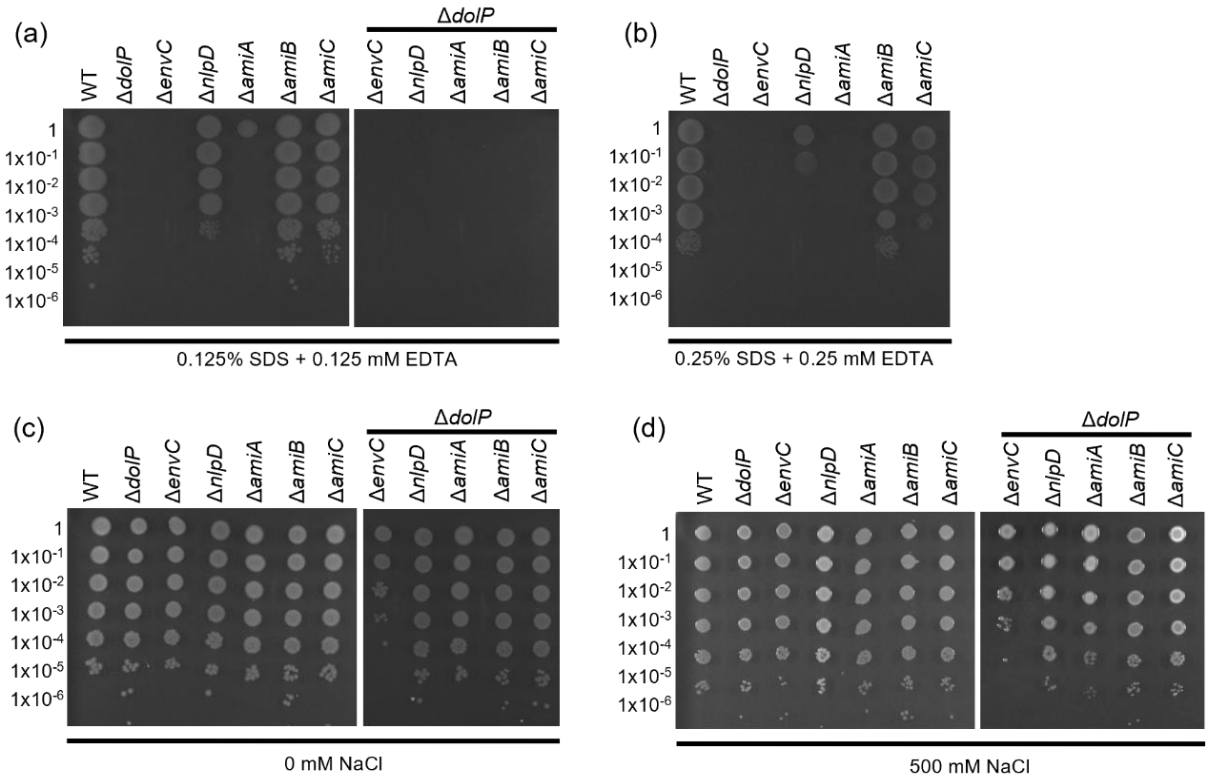

Figure 17 Exposure to SDS and EDTA leads to a fitness defect in Δ*dolP,* Δ*amiC*, Δ*envC* and Δ*amiA,* but change in osmolarity has no effect.
(a-b) The WT, Δ*dolP,* Δ*amiA,* Δ*amiB,* Δ*amiC*, Δ*nlpD,* Δ*envC,* and Δ*dolP* double mutant strains were grown overnight in LB at 37°C. After adjusting the cell density to OD_{600} = 2, cultures were serially diluted (10^{-1} to 10^{-6}), and 2.5 µl of each dilution was spotted on the agar plates supplemented with the indicated SDS and EDTA concentrations. The plates were incubated at 37°C and photographed after ~16 hours. (c-d) The WT, Δ*dolP,* Δ*amiA,* Δ*amiB,* Δ*amiC*, Δ*nlpD,* Δ*envC,* and Δ*dolP* double mutant strains were grown overnight in LB at 37°C. After adjusting the cell density to OD_{600} = 1, cultures were serially diluted (10^{-1} to 10^{-6}), and 5 µl of each dilution was spotted on LB agar plates adjusted to the indicated NaCl concentration. The plates were incubated at 37°C and photographed after ~16 hours.

None of the mutants had significant fitness differences when grown on LB agar plates (Figure 16a). However, under most stress conditions the single Δ*dolP* and Δ*envC* mutants showed severe growth defects, which was in contrast to Δ*nlpD* (Figure 16 and Figure 17). All *dolP* double deletion mutants phenocopied the Δ*dolP* single mutant in most conditions indicating that loss of DolP impairs their fitness (Figure 16 and Figure 17a and b). An exception to this trend was the EDTA condition in which

Δ*dolP* fitness was less affected than on SDS and vancomycin, leaving fitness space to assess the *dolP* double mutants (Figure 16d). When grown with 0.25 mM EDTA, the double mutants Δ*dolP*Δ*amiA* and Δ*dolP*Δ*envC* had decreased fitness compared to the Δ*dolP* single mutant, which was also observed for the Δ*dolP*Δ*nlpD* double mutant (Figure 16d). In addition, the Δ*dolP*Δ*envC* strain was the only double deletion mutant that had reduced fitness in both salt stresses (Figure 17c and d).

Therefore, our fitness data indicates that Δ*dolP* and Δ*nlpD* mutants do not phenocopy each other, which can be seen as evidence that both genes are not necessarily functionally connected.

4.4.3 Deletion of *dolP* induces chaining in Δ*amiA*, Δ*envC* and Δ*ftsEX* mutants.

As amidases are essential for cell separation, amidase mutants can display characteristic chaining and filamentation morphology. In fact, this morphological analysis largely contributed to our current knowledge of amidases and their cognate regulators in *E. coli* (Tsang *et al.*, 2017; Uehara *et al.*, 2009; Uehara *et al.*, 2010). Hence, we decided to analyse the morphology of the mutant panel lacking DolP and the amidases using the same method (Uehara *et al.*, 2009). To do so, cultures of the mutants were grown in LB at 37°C to mid-exponential phase, stained with a membrane dye (FM1-43FX), fixed, and stained with DAPI. Images of the cells were captured by using both phase contrast and fluorescence optics. For a complete morphological analysis, we measured cell length and detected septa using the MicrobeJ plugin of Fiji 600 software (Ducret *et al.*, 2016; Tsang *et al.*, 2017). To analyse elongated cells that could not be visualised in one image we applied a stitching plugin of Fiji 600 software (Preibisch *et al.*, 2009) to provide a complete view.

All single deletion mutants showed wild-type like morphology with the exception of Δ*envC*, which had 60.7% of cells chaining (Figure 18, Figure 19 and Table 3). The *dolP* double deletion mutant in combination with *envC* (Δ*dolP*Δ*envC*) exacerbated the *envC* single deletion mutant defect and had 100% of cells chaining. All other double deletion mutants displayed wild-type like morphology except for Δ*dolP*Δ*amiA,* which had 36.3% of chaining cells. The observation that Δ*dolP*Δ*envC* grows as chain was described previously and led to the hypothesis that DolP might be an upstream regulator of NlpD as it phenocopies the filamentous growth of an Δ*nlpD*Δ*envC* mutant (Tsang *et al.*, 2017). However, as Δ*dolP* and Δ*nlpD* mutants have different fitness profiles against a number of stress conditions tested in this study this assumption is unlikely to be true (Figure 16 and Figure 17). We also note that the Δ*dolP*Δ*amiB* mutant did not demonstrate a chaining phenotype, unlike the Δ*dolP*Δ*amiA* mutant, implying that the majority of the cell separation defect caused by the loss of EnvC in the Δ*dolP*Δ*envC* mutant is likely due to a lack of AmiA activation.

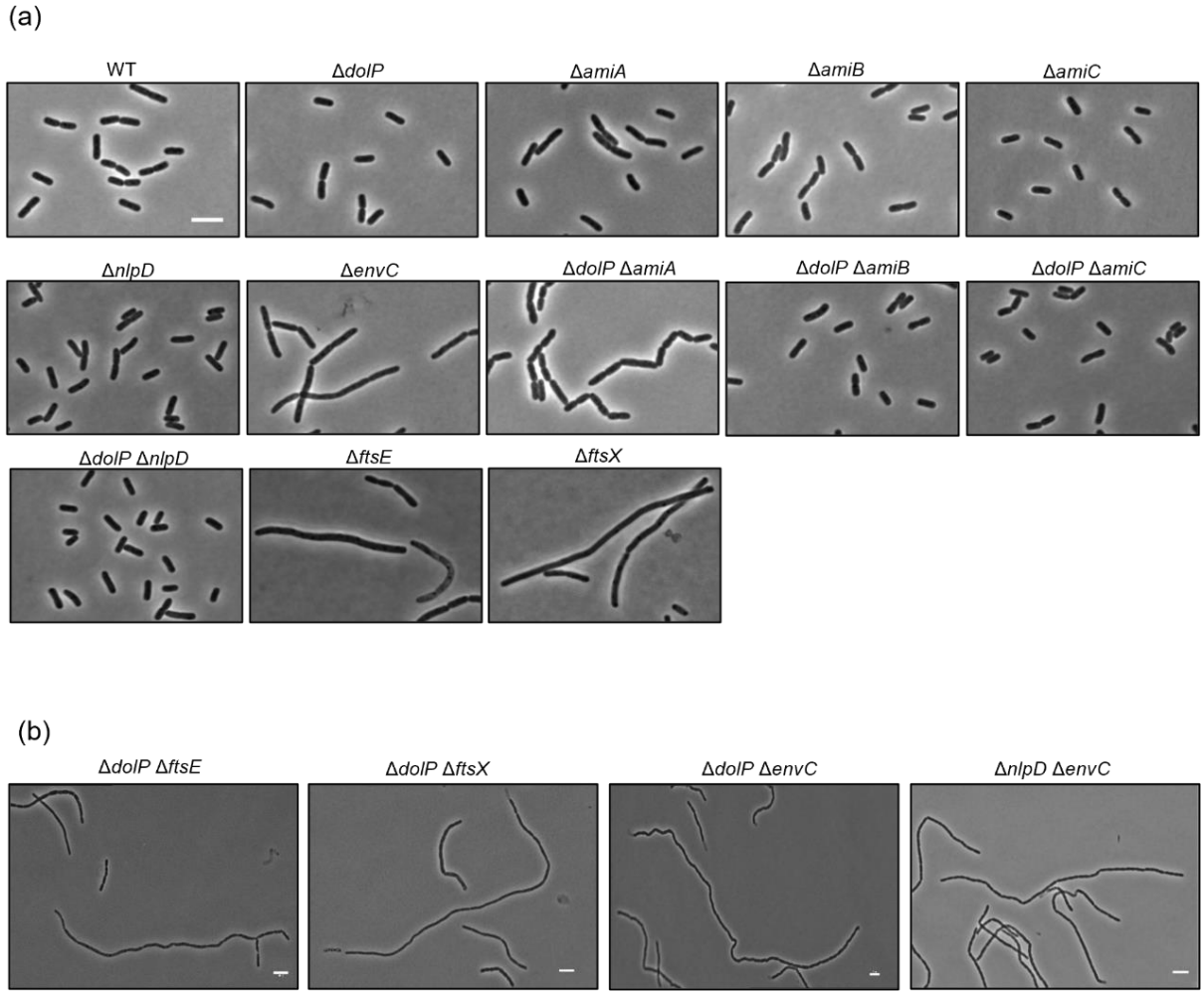

Figure 18. DolP deletion causes chain formation in Δ*amiA,* Δ*envC and* Δ*ftsEX* mutants.
Phase contrast microscopy of (a) WT, Δ*dolP,* Δ*nlpD,* Δ*envC,* Δ*amiA,* Δ*amiB,* Δ*amiC*, Δ*ftsE,* Δ*ftsX,* Δ*dolP*Δ*nlpD,* Δ*dolP*Δ*amiA,* Δ*dolP*Δ*amiB,* Δ*dolP*Δ*amiC,* (b) Δ*dolP*Δ*ftsE,* Δ*dolP*Δ*ftsX,* Δ*dolP*Δ*envC* and Δ*nlpD*Δ*envC* cells in mid-exponential phase growth (OD_{600} = 0.4) in LB medium at 37°C. Images of fluorescence microscopy are shown in Fig. 19. Scale Bar = 5 μm. Images of Δ*dolP*Δ*ftsE,* Δ*dolP*Δ*ftsX,* Δ*dolP*Δ*envC* and Δ*nlpD*Δ*envC* have been stitched from multiple fields of view to enable total cell length visualisation. Scale bar = 5 μm. In a Student's t-test, the length of WT cells was significantly different than the mutants tested ($P < 0.05$), except for Δ*dolP* and Δ*amiB*. In a Chi-square test the number of septa/cell of WT cells was significantly different than most of the mutants tested ($P < 0.05$) (Table 3).

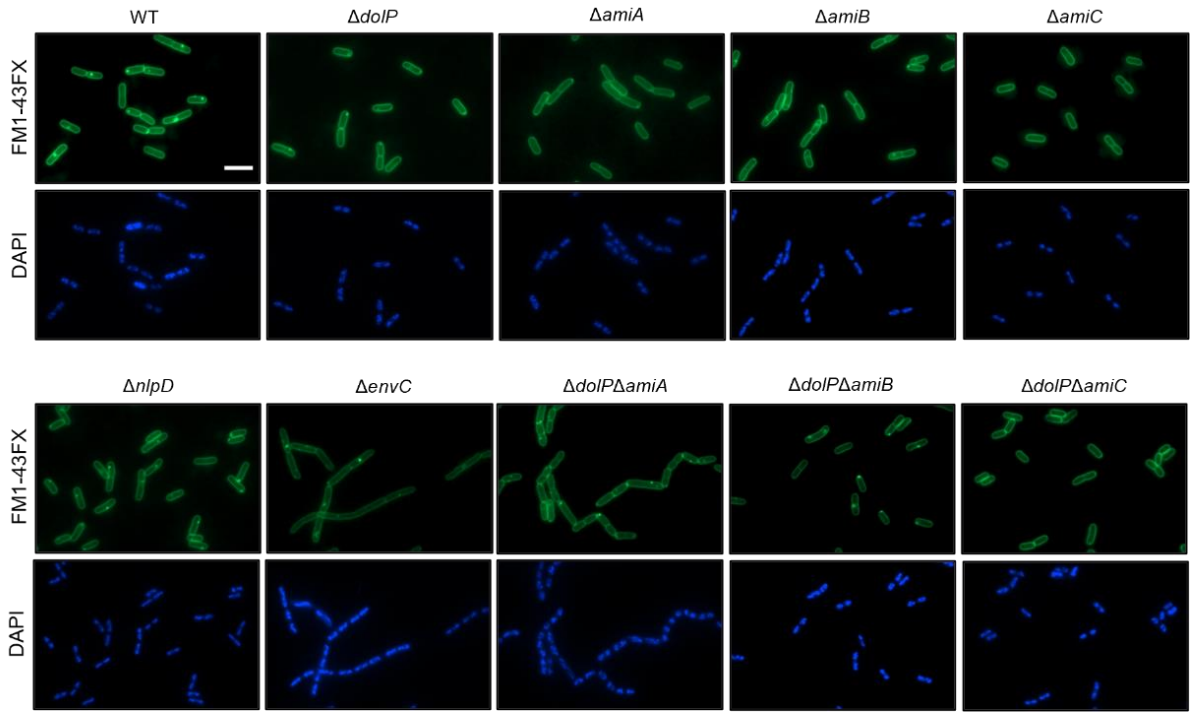

Figure 19. Fluorescence microscopy of the WT, Δ*dolP*, Δ*amiA*, Δ*amiB*, Δ*amiC*, Δ*nlpD*, Δ*envC*, Δ*dolP*Δ*amiA*, Δ*dolP*Δ*amiB* and Δ*dolP*Δ*amiC* strains.
Cells were grown to mid-exponential phase (OD_{600} = 0.4) in LB at 37°C, stained with the membrane dye FM1-43-FX, fixed, and stained with DAPI. The cells were visualised by fluorescence microscopy. Scale bar = 5 µm.

Table 3. Phenotypes of *dolP*, amidases and regulators mutants

Strain	Relevant genotype	No. of cells[1]	Total length (μm)[2]	Avg length ± s.d.(μm)[3]	Total no. of septa[4]	Length/ septum (μm)[5]	Length/ segment (μm)[6]	No. of septa/cell	No. of chaining cells[7]	% of chaining cells[8]	*P*-value avg. length[9]	*P*-value no. of septa/cell[10]
MB01064	WT	610	2257.4	3.7 ± 0.8	274	8.2	2.6	0.4	2	0.3		
MB01065	Δ*dolP*	431	1594.8	3.7 ± 0.9	197	8.1	2.5	0.5	1	0.2	N.S.	N.S.
MB01119	Δ*amiA*	436	1980.1	4.5 ± 1.2	246	8.0	2.9	0.6	2	0.5	< 0.05	< 0.05
MB01120	Δ*amiB*	372	1416.4	3.8 ± 1.0	136	10.4	2.8	0.4	2	0.5	N.S.	N.S.
MB01121	Δ*amiC*	258	838.5	3.2 ± 0.7	113	7.4	2.3	0.4	1	0.4	< 0.05	N.S.
MB01122	ΔenvC	229	2651.9	11.6 ± 4.1	526	5.0	3.5	2.3	145	63.3	< 0.05	< 0.05
MB01051	Δ*nlpD*	285	1124.0	3.9 ± 1.1	121	9.3	2.8	0.4	0	0.0	< 0.05	N.S.
MB01123	Δ*ftsE*	207	2386.8	11.5 ± 9.3	450	5.3	3.6	2.2	93	44.9	< 0.05	< 0.05
MB01124	Δ*ftsX*	263	3034.2	11.5 ± 11.3	544	5.6	3.8	2.1	145	55.1	< 0.05	< 0.05
MB01125	Δ*dolP*Δ*amiA*	281	2002.2	7.1 ± 5.3	489	4.1	2.6	1.7	102	36.3	< 0.05	< 0.05
MB01126	Δ*dolP*Δ*amiB*	418	1654.4	4.0 ± 1.2	151	11.0	2.9	0.4	4	1.0	< 0.05	N.S.
MB01127	Δ*dolP*Δ*amiC*	423	1309.9	3.1 ± 0.8	142	9.2	2.3	0.3	1	0.2	< 0.05	< 0.05
MB01128	Δ*dolP*Δ*envC*	28	1985.3	70.9 ± 28.8	759	2.6	2.5	27.1	28	100.0	< 0.05	< 0.05
MB01052	Δ*dolP*Δ*nlpD*	287	1103.4	3.8 ± 1.0	121	9.1	2.7	0.4	1	0.3	< 0.05	N.S.
MB01129	Δ*dolP*Δ*ftsE*	35	2207.6	63.1 ± 36.7	493	4.5	4.2	14.1	34	97.1	< 0.05	< 0.05
MB01130	Δ*dolP*Δ*ftsX*	20	1424.6	71.2 ± 19.8	426	3.3	3.2	21.3	20	100.0	< 0.05	< 0.05
MB01152	Δ*nlpD*Δ*amiA*	372	2659.8	7.2 ± 2.7	388	6.9	3.0	1.0	51.0	13.7	< 0.05	< 0.05
MB01153	Δ*nlpD*Δ*envC*	30	2005.6	66.9 ± 19.6	1043	1.9	2.3	34.8	30	100.0	< 0.05	< 0.05

[1] All cells were considered single cells independent of the number of segments.

[2] Total length means cumulative length of all cells measured.

[3] Refers to the total length/number of cells. S.d., standard deviation. Some of the strains have a great s.d. because of the severe growth defect caused by the deleted genes.

[4] Septa are considered as any membrane constrictions or completed membrane septa in cell chains.

[5] Length/septum indicates the total length/total number of septa. It shows the frequency at which septa are detected. The number is much lower in chaining cells because septa persist for an abnormally long time.

[6] The number of cell segments refers to the number of cells plus the number of septa. The “length/segment” is the total length/total number of segments. In normal (nonchaining) cells, this measurement is similar to the average cell length (pole-pole distance), but the value is smaller because predivisional cells contain two segments and are counted as two

cells instead of one (i.e., some pole-to-septa measurements are taken into account, as well as pole-pole measurements). In chaining cells, the length/segment measurement refers mainly to the distance between adjacent septa.

[7] Cells with more than one septum are considered chaining cells.

[8] Percentage of chaining cells related to the total no. of cells.

[9] *P*-values of Student t-test comparing the average length of WT cells with every mutant.

[10] *P*-values of Chi-square test comparing number of septa/cell of WT cells with every mutant.

N.S., not significant (significance indicated by Student's t test or Chi-square test *P* value)

The amidase activator EnvC is itself activated by FtsEX (Cook *et al.*, 2020; Pichoff *et al.*, 2019; Yang *et al.*, 2011) hence we explored whether loss of DolP might affect the morphology of *ftsEX* mutants. Indeed, all tested double mutants grew as elongated chains (Figure 18, Figure 19, Figure 20 and Table 3). We further observed that loss of DolP exacerbated the Δ*ftsE* or Δ*ftsX* elongation phenotype and that the Δ*dolP*Δ*ftsE and* Δ*dolP*Δ*ftsX* mutants had longer segments (4.2 µm and 3.2 µm) when compared to Δ*dolP*Δ*envC* and Δ*nlpD*Δ*envC* (2.5 µm and 2.3 µm). This indicates that DolP, like NlpD and EnvC, is needed for successful cell separation in *ΔftsEX* mutants.

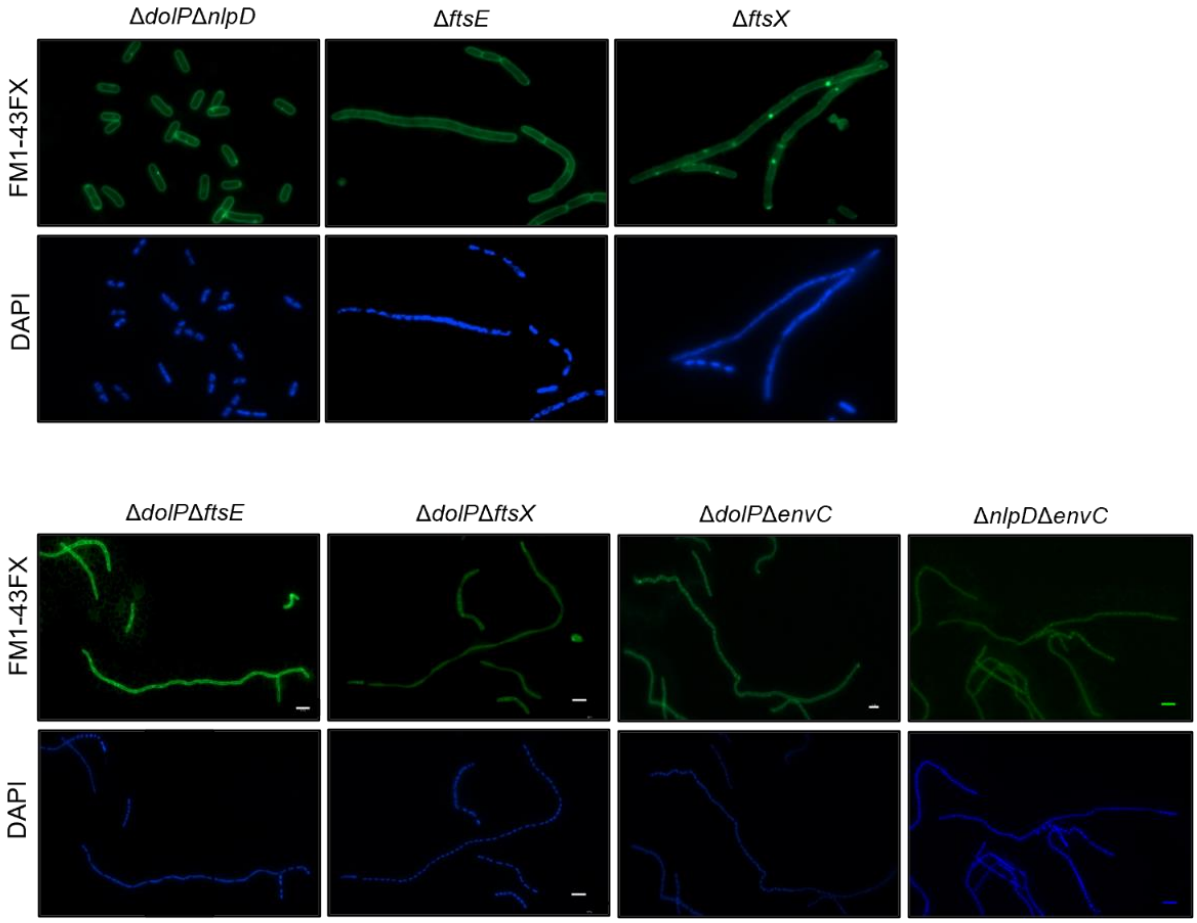

Figure 20. Fluorescence microscopy of the Δ*dolP*Δ*nlpD*, Δ*ftsE*, Δ*ftsX*, Δ*dolP*Δ*ftsE*, Δ*dolP*Δ*ftsX*, Δ*dolP*Δ*envC* and Δ*nlpD*Δ*envC* strains.
Cells were grown to mid-exponential phase (OD_{600} = 0.4) in LB at 37°C, stained with the membrane dye FM1-43-FX, fixed, and stained with DAPI. The cells were visualised by fluorescence microscopy. Scale bar = 5 µm

4.4.4 Δ*dolP*Δ*amiA* grows in distinct chains with small segments.

We noted that 36.3% of Δ*dolP*Δ*amiA* grew as chains whereas the Δ*nlpD*Δ*amiA* chaining phenotype was less severe with 13.3% chaining cells. As this mutant combination allows us to directly compare *dolP* and *nlpD* in a mutant background that causes a phenotype, we imaged both strains to compare the morphological features (Figure 21a, Figure 22 and Table 3). The Δ*nlpD*Δ*amiA* and Δ*dolP*Δ*amiA* mutants had a similar average chain length of 7.0 and 7.1 μm respectively (Student's t-test, $P > 0.05$). However, we detected less septa in Δ*nlpD*Δ*amiA* compared to Δ*dolP*Δ*amiA* chains (Chi-square test, $P < 0.05$) leading to longer, more filamentous segments for Δ*nlpD*Δ*amiA*. This indicates that in the Δ*amiA* background DolP is needed for the full function of AmiB or AmiC despite the presence of NlpD and EnvC. In addition, it seems that, unlike loss of NlpD, DolP deletion does not affect formation of septa in Δ*amiA* mutants.

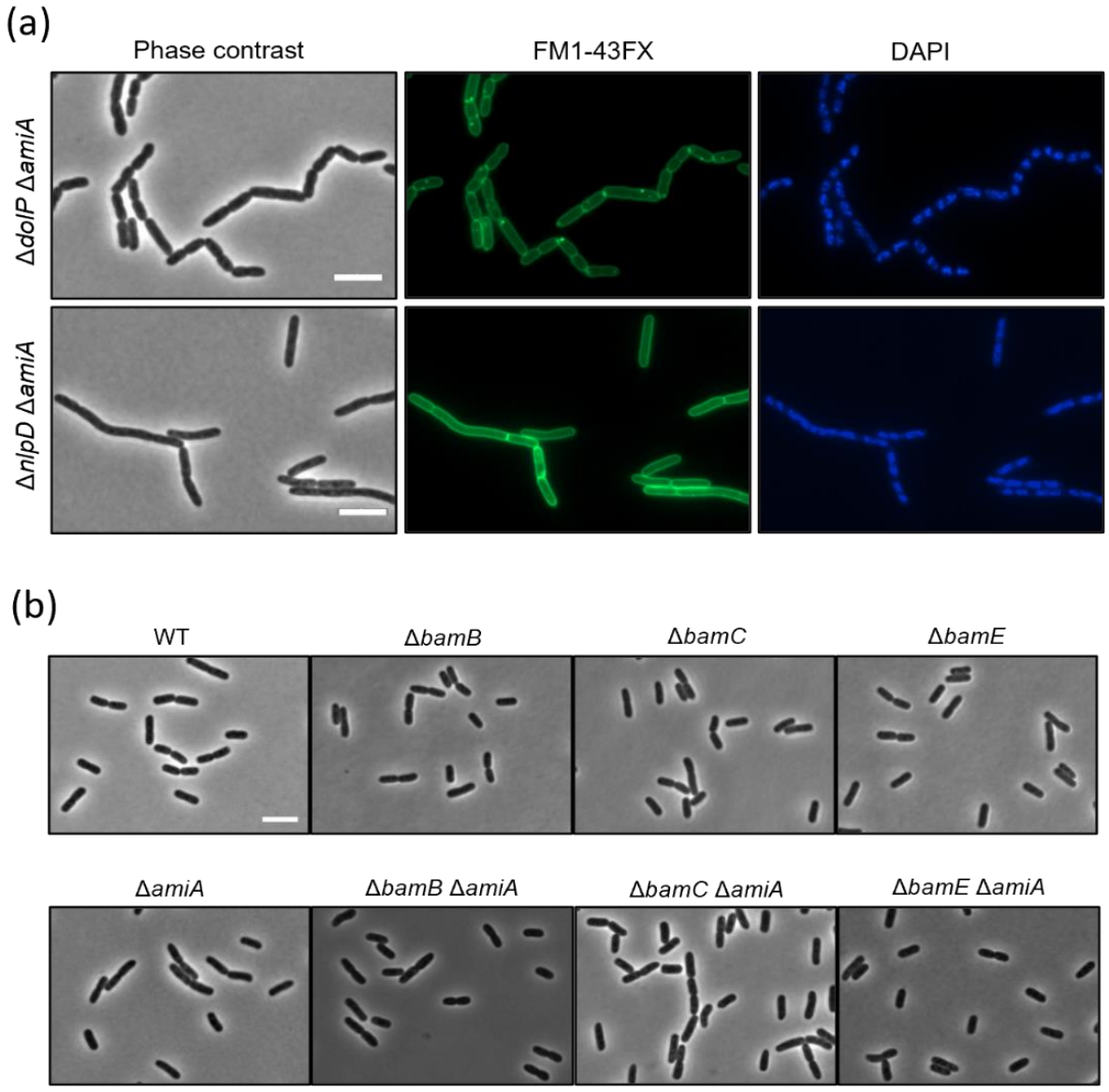

Figure 21. The Δ*dolP*Δ*amiA* mutant demonstrates different chain morphology to the Δ*nlpD*Δ*amiA* and Δ*bam*Δ*amiA* cells.
(a) Microscopy of Δ*dolP*Δ*amiA* and Δ*nlpD*Δ*amiA* cells. Cells were grown to mid-exponential phase (OD_{600} = 0.4) in LB at 37°C, stained with the membrane dye FM1-43FX, fixed, and stained with DAPI. The cells were visualised by phase contrast microscopy and fluorescence microscopy. In a Student's t-test, the length of Δ*dolP*Δ*amiA* cells was not significantly different to that of Δ*nlpD*Δ*amiA* cells ($P > 0.05$). In a Chi-square test the number of septa/cell of Δ*dolP*Δ*amiA* cells was significantly different from that of Δ*nlpD*Δ*amiA* ($P < 0.05$) (Table 4). (b) Imaging of Δ*bamB,* Δ*bamC,* Δ*bamE,* Δ*bamB*Δ*amiA,* Δ*bamC*Δ*amiA* and Δ*bamE*Δ*amiA* cells. Cells were grown to mid-exponential phase (OD_{600} = 0.4) in LB at 37°C, fixed and visualised by phase contrast microscopy. Images of fluorescence microscopy are shown in Fig. 22. Scale bar = 5 μm. In a Student's t-test, the length of WT cells was significantly different than the mutants tested ($P < 0.05$), except Δ*dolP* and Δ*bamC*. In a Chi-square test the number of septa/cell of WT cells was significantly different than the mutants tested ($P < 0.05$) (Table 4).

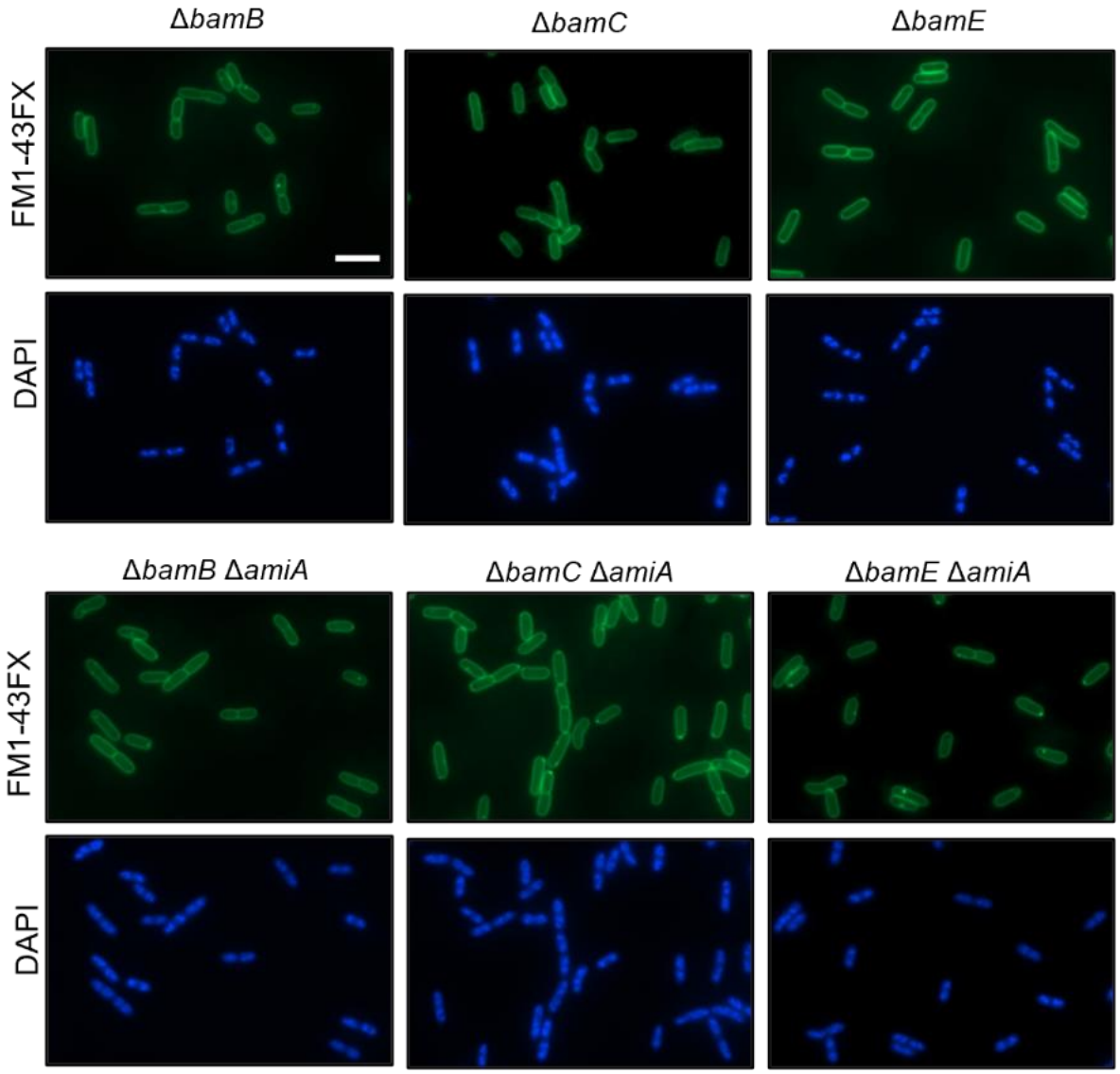

Figure 22. Fluorescence microscopy imaging of the Δ*bamB*, Δ*bamC*, Δ*bamE*, Δ*bamB*Δ*amiA*, Δ*bamC*Δ*amiA* and Δ*bamE*Δ*amiA* strains.
Cells were grown to mid-exponential phase (OD_{600} = 0.4) in LB at 37°C, stained with the membrane dye FM1-43-FX, fixed, and stained with DAPI. The cells were visualised by fluorescence microscopy. Scale bar = 5 µm

Previous studies indicate that DolP interacts with the BAM complex and Δ*dolP*Δ*bamB* and Δ*dolP*Δ*bamE* double mutants are growth impaired through increasing cell lysis events (Bryant *et al.*, 2020; Ranava *et al.*, 2021). As we have gathered some evidence for an interaction between DolP and AmiA, we questioned whether DolP could mediate a link, through AmiA, between the cell division machinery and the BAM complex. Therefore, we tested whether deleting the non-essential

components of the BAM complex (*bamB, bamC*, and *bamE*) in an *amiA* mutant would have the same phenotype as Δ*dolP*Δ*amiA*. We observed that the three Δ*amiA*Δ*bam* double mutants showed a minor number of chaining cells (3.9% – 6.4% compared to 36.7% of Δ*dolP*Δ*amiA*) (Figure 21b and Figure 22 and Table 4). The results suggest that the chaining phenotype of Δ*dolP*Δ*amiA* is not related to the presence/function of the BAM complex.

Table 4. Phenotypes of *dolP*, *amiA* and *bamBCE* mutants

Strain	Relevant genotype	No. of cells[1]	Total length (μm)[2]	Avg length ± s.d (μm)[3]	Total no. of septa[4]	Length/ septum (μm)[5]	Length/segment (μm)[6]	No. of septa/cell	No. of chaining cells[7]	% of chaining cells[8]	*P*-value avg. length[9]	*P*-value no. of septa/cell[10]
MB01064	WT	610	2257.4	3.7 ± 0.8	274	8.2	2.6	0.4	2	0.3		
MB01065	*ΔdolP*	431	1594.8	3.7 ± 0.9	197	8.1	2.5	0.5	1	0.2	N.S.	
MB01105	*ΔbamB*	270	977.8	3.6 ± 1.0	101	9.7	1.1	0.4	3	1.1	< 0.05	
MB0107	*ΔbamC*	263	975.2	3.7 ± 1.0	112	8.7	1.1	0.4	2	0.8	N.S.	
MB0109	*ΔbamE*	261	993.4	3.8 ± 0.9	126	7.9	1.1	0.5	3	1.1	< 0.05	
MB0119	*ΔamiA*	436	1980.1	4.5 ± 1.2	246	8.0	2.9	0.6	2	0.5	< 0.05	
MB0125	*ΔdolPΔamiA*	281	2002.2	7.1 ± 5.3	489	4.1	2.6	1.7	103	36.7	< 0.05	
MB01110	*ΔbamBΔamiA*	317	1323.0	4.2 ± 2.0	166	8.0	1.5	0.5	16.0	5.0	< 0.05	< 0.05
MB01111	*ΔbamCΔamiA*	452	1989.5	4.4 ± 1.7	266	7.5	2.3	0.6	29.0	6.4	< 0.05	< 0.05
MB01112	*ΔbamEΔamiA*	258	1005.91	3.9 ± 1.4	123	8.2	1.1	0.5	10	3.9	< 0.05	< 0.05

[1] All cells were considered single cells independent of the number of segments.

[2] Total length means cumulative length of all cells measured.

[3] Refers to the total length/number of cells. S.d., standard deviation.

[4] Septa are considered as any membrane constrictions or completed membrane septa in cell chains.

[5] Length/septum indicates the total length/total number of septa. It shows the frequency at which septa are detected. The number is much lower in chaining cells because septa persist for an abnormally long time.

[6] The number of cell segments refers to the number of cells plus the number of septa. The “length/segment” is the total length/total number of segments. In normal (nonchaining) cells, this measurement is similar to the average cell length (pole-pole distance), but the value is smaller because predivisional cells contain two segments and are counted as two cells instead of one (i.e., some pole-to-septa measurements are taken into account, as well as pole-pole measurements). In chaining cells, the length/segment measurement refers mainly to the distance between adjacent septa.

[7] Cells with more than one septum are considered chaining cells.

[8] Percentage of chaining cells related to the total no. of cells.

[9] *P*-values of Student t-test comparing the average length of WT cells with every mutant.

[10] *P*-values of Chi-squared test comparing number of septa/cell of WT cells with Δ*bamB*Δ*amiA, ΔbamCΔamiA* and Δ*bamE*Δ*amiA*.

N.S., not significant (significance indicated by Student's t or Chi-square test test *P* value)

4.4.5 The function of DolP is unrelated to ActS and pH

Next, we tested whether DolP could have a conditional role as an amidase activator in low pH, as the activity of certain PG enzymes differs according to physiochemical properties of the growth medium (Mueller *et al*, 2019). In addition to this analysis, we added *ΔactS* to the mutant panel. ActS was recently described as an activator of AmiA, AmiB, and AmiC (Gurnani Serrano *et al.*, 2021), and interestingly has a conditional role in which it preferentially activates AmiB at pH 5.2 (Mueller *et al.*, 2021). Therefore, we tested the fitness of the mutant panel under acidic pH conditions (Figure 23a to c).

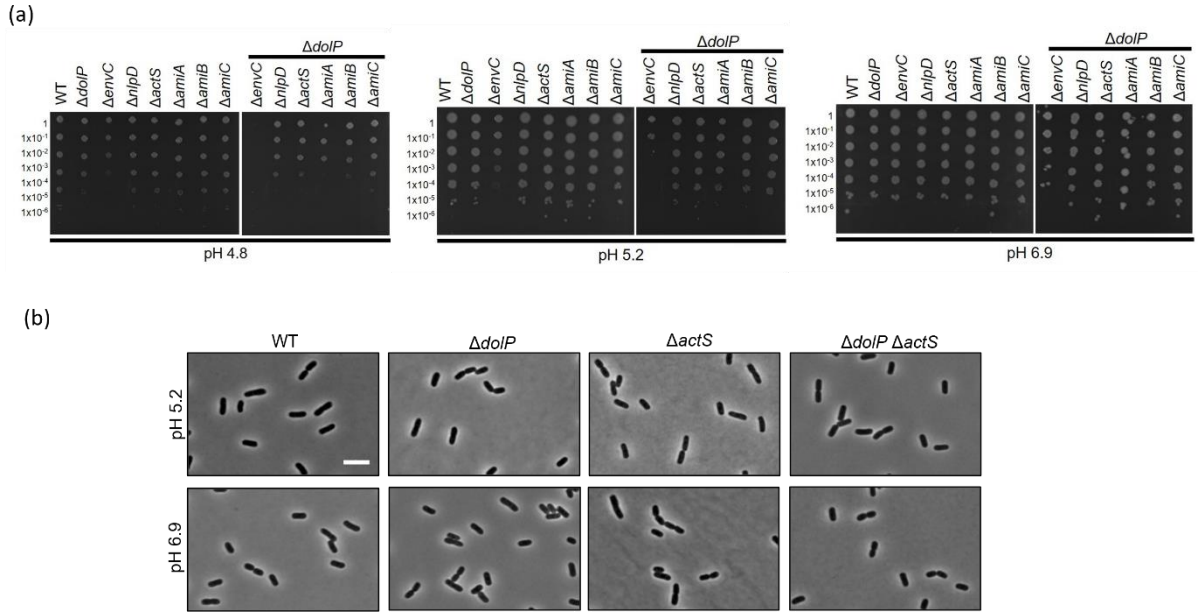

Figure 23. DolP is likely not linked to the ActS pathway.
(a to c) The WT, Δ*dolP,* Δ*amiA,* Δ*amiB,* Δ*amiC*, Δ*nlpD,* Δ*envC,* Δ*actS* and Δ*dolP* double mutants were grown overnight in LB at 37°C. After adjusting the cell density to OD_{600} = 1, cultures were serially diluted (10^{-1} to 10^{-6}), and 5 µl of each dilution was spotted on LB agar plates adjusted to the indicated pH 4.8, 5.2 or 6.9. The plates were incubated at 37°C and photographed after ~16 hours. (d) The WT, Δ*dolP,* Δ*actS* and Δ*dolP*Δ*actS* mutants were grown at 37°C in LB medium to early exponential phase (OD_{600}= ~0.2), back-diluted to either media buffered to pH 5.2 or pH 6.9 and grown until OD_{600}= ~0.2. The samples were stained and fixed for microscopy as described in the legend to Fig. 19. Images of fluorescence microscopy are shown in Fig. 24. Scale bar = 5 µm. In a Student's t-test, the length of cells grown in pH 5.2 was significantly different than most of the cells grown in pH 6.9 ($P < 0.05$). In a Chi-square test the number of septa/cell of cells grown in pH 5.2 was significantly different than the cells grown in pH 6.9 ($P < 0.05$) (Table 5).

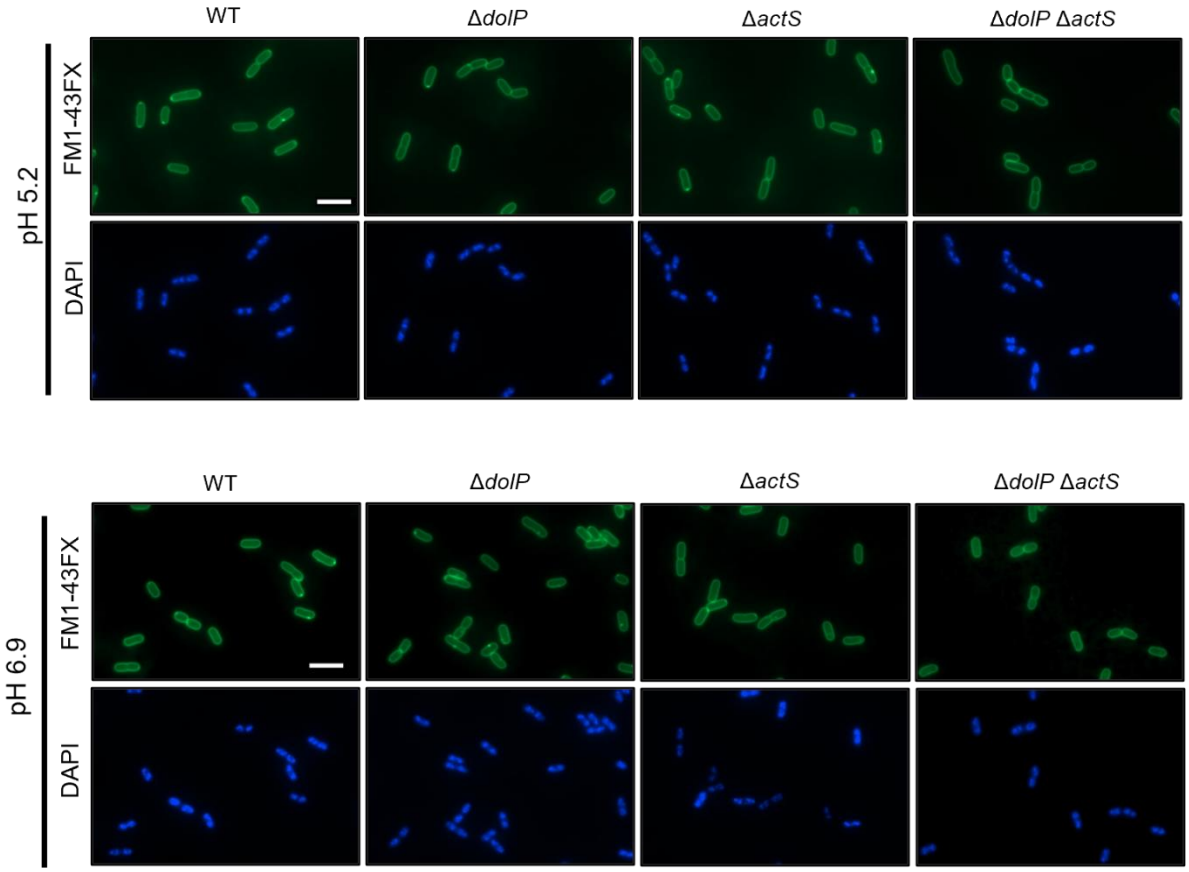

Figure 24. Fluorescence images of the WT, Δ*dolP*, Δ*actS* and Δ*dolP*Δ*actS* strains.
Cells were grown at 37°C in LB medium to early exponential phase (OD_{600}= ~0.2), back-diluted to either media buffered to pH 5.2 or pH 6.9 and grown until OD_{600}= ~0.2. The samples were stained with the membrane dye FM1-43FX, fixed, and stained with DAPI. Scale bar = 5 µm.

We observed reduced fitness for all mutants grown on LB pH 4.8 and 5.2, with the exception of the *ΔdolPΔenvC* mutant, which was unable to grow in LB pH 4.8. However, this result is not surprising as *ΔenvC* had a low starting fitness in LB pH 4.8 and overall *ΔdolPΔenvC* shows reduced fitness in several of the envelope stress conditions we tested (Figure 16). As we did not identify a genetic interaction between *dolP* and *actS* we tested whether *ΔdolPΔactS* mutants show any morphological abnormalities. Microscopic analyses reveal none of the single or double mutations of *dolP* and *actS* showed morphological differences when grown in media buffered to pH

5.2 or pH 6.9 (Figure 23b and c and Figure 24 and Table 5). These results indicate that ActS is likely not important for the function of DolP and vice versa.

Table 5. Phenotypes of *dolP* and *actS* mutants in pH 5.2 and pH 6.9

Strain	Relevant genotype	pH	No. of cells[1]	Total length (µm)[2]	Avg length ± s.d. (µm)[3]	Total no. of septa[4]	Length/ septum (µm)[5]	Length/ segment (µm)[6]	No. of septa/cell	No. of chaining cells[7]	% of chaining cells[8]	*P*-value avg. length[9]	P-value no. of septa/cell[10]
MB01064	WT	5.2	317	1069.7	3.4 ± 0.9	115	9.3	1.2	0.4	12.0	3.8	< 0.05	< 0.05
MB01065	Δ*dolP*	5.2	327	1105.4	3.4 ± 0.9	109	10.1	1.3	0.3	5.0	1.5	< 0.05	< 0.05
MB01116	Δ*actS*	5.2	343	1183.6	3.4 ± 0.8	124	9.5	1.3	0.4	4.0	1.2	N.S.	< 0.05
MB01117	Δ*dolP*Δ*actS*	5.2	430	1599.6	3.7 ± 1.3	215	7.4	1.8	0.5	23.0	5.3	< 0.05	< 0.05
MB01064	WT	6.9	610	2257.4	3.7 ± 0.8	274	8.2	2.6	0.4	2	0.3		
MB01065	Δ*dolP*	6.9	431	1594.8	3.7 ± 0.9	197	8.1	2.5	0.5	1	0.2		
MB01116	Δ*actS*	6.9	259	869.4	3.4 ± 0.8	70	12.4	1.0	0.3	1.0	0.4		
MB01117	Δ*dolP*Δ*actS*	6.9	255	722.6	2.8 ± 0.6	88	8.2	0.8	0.3	1.0	0.4		

[1] All cells were considered single cells independent of the number of segments.

[2] Total length means cumulative length of all cells measured.

[3] Refers to the total length/number of cells. S.d., standard deviation.

[4] Septa are considered as any membrane constrictions or completed membrane septa in cell chains.

[5] Length/septum indicates the total length/total number of septa. It shows the frequency at which septa are detected. The number is much lower in chaining cells because septa persist for an abnormally long time.

[6] The number of cell segments refers to the number of cells plus the number of septa. The “length/segment” is the total length/total number of segments. In normal (nonchaining) cells, this measurement is similar to the average cell length (pole-pole distance), but the value is smaller because predivisional cells contain two segments and are counted as two cells instead of one (i.e., some pole-to-septa measurements are taken into account, as well as pole-pole measurements). In chaining cells, the length/segment measurement refers mainly to the distance between adjacent septa.

[7] Cells with more than one septum are considered chaining cells.

[8] Percentage of chaining cells related to the total no. of cells.

[9] *P*-values of Student t-test comparing the average length of cells in pH 5.2 compared with the same strain in pH 6.9.

[10] *P*-values of Chi-squared test comparing number of septa/cell of cells in pH 5.2 with cells in pH 6.9.

N.S., not significant (significance indicated by Student's t or Chi-square test test *P* value

4.5 Discussion

Bacterial amidases must be tightly regulated to separate daughter cells while maintaining envelope integrity and to prevent lysis. In this study we explored the possibility that the lipoprotein DolP acts as an upstream regulator of the amidase regulator NlpD.

4.5.1 DolP is not an upstream regulator of NlpD

In a previous study it was reported that the double deletion mutants Δ*dolP*Δ*envC* and Δ*nlpD*Δ*envC* share the same chaining phenotype (Tsang *et al.*, 2017). This finding is intriguing as similar to the amidase activator EnvC, which needs FtsEX to activate AmiA and AmiB (Cook *et al.*, 2020), this result could place DolP to perform a similar function for NlpD in order to activate AmiC. Inspired by this initial observation, we tested this hypothesis using various assays.

First, we tested the ability of DolP to modulate amidase activity *in vitro* using a PG degradation assay. However, the presence or absence of DolP did not alter the activity of the tested amidases/regulators (Figure 12a). In addition, we were unable to detect a protein-protein interaction between DolP and NlpD using pulldown and MST assays. The lack of interaction between both proteins makes it unlikely that DolP acts as a regulator of NlpD.

When probed against an array of envelope stresses, the *dolP* and *nlpD* mutants did not always phenocopy each other. This is not surprising as it was reported that

Δ*dolP* mutants have a weakened envelope integrity, allowing harmful substances to breach the outer membrane (Bryant *et al.*, 2020; Onufryk *et al.*, 2005). This is evidenced by the higher susceptibility of Δ*dolP* to vancomycin and SDS (Figure 16b and c). The collective evidence presented above suggest that it is rather unlikely that DolP is an upstream regulator of NlpD.

4.5.2 DolP affects cell separation by a yet undiscovered mechanism

DolP likely does not directly regulate NlpD or amidase activity, however we and others demonstrated that DolP has a profound impact on cell division (Bryant *et al.*, 2020; Ranava *et al.*, 2021; Tsang *et al.*, 2017). DolP is sub-cellularly localized to the division site by interaction of its BON domain with anionic phospholipids (Bryant *et al.*, 2020). This localisation makes it an ideal candidate to play a role within the divisome. In addition, DolP helps BamA folding and therefore supports BAM-complex function, which is crucial for providing OMPs to maintain envelope integrity during cell division (Ranava *et al.*, 2021).

The most prominent phenotypes we observed are that Δ*dolP*Δ*amiA* and Δ*dolP*Δ*envC* mutants grow as chains and have fitness defects. These fitness defects have also been observed when Δ*dolP* was probed using a Clustered Regularly Interspaced Short Palindromic Repeat interference (CRISPRi) approach (Ranava *et al.*, 2021). This screen revealed that silencing *amiA, envC, ftsX* and *ftsE* in Δ*dolP* results in growth defects. These findings are in accordance with our results and indicate that NlpD-AmiC cannot sufficiently function without the presence of DolP. However, as DolP likely does not regulate NlpD or AmiC activity (Figure 12a) its

function may be indirect and outside of amidase activity. Analysing the morphology of ΔdolP amidase double mutants revealed that the ΔdolPΔamiA strain forms shorter chains when compared to an ΔnlpDΔamiA mutant, which forms short filaments containing an overall lower number of septa per cell length (Figure 21). This suggests that NlpD may be more important for septa formation when AmiA is missing. However, DolP is still needed for completion of cell separation.

In this study we present evidence that DolP interacts weakly with AmiC and potentially with AmiA (Figure 12b to d, Figure 13 and Figure 14). Frequently, transient bonds occur in regulative protein:protein interactions within multiprotein complexes where proteins associate and disassociate depending on the stimuli (Miura, 2018; Peters *et al*, 2013). Such a transient protein:protein interaction of DolP and AmiC could be important for recruiting the cognate amidase to the divisome. However, AmiC localisation to the division site is unperturbed in a Δ*dolP* mutant (Tsang *et al.*, 2017). In contrast, AmiA is peripherally distributed without septal localisation (Bernhardt & de Boer, 2003), therefore making it unlikely to be dependent on DolP to localise to the division site. As we excluded that the observed Δ*dolP*Δ*amiA* phenotype is related to the association of DolP with the BAM-complex (Figure 21b) or that DolP has importance in pH stress (Figure 23) we conclude that the effect of DolP on cell separation may be related to its ability to interact with AmiA or AmiC or by a yet undiscovered mechanism.

4.6 References

Graham CLB, Newman H, Gillett FN, Smart K, Briggs N *et al.* A dynamic network of proteins facilitates cell envelope biogenesis in gram-negative bacteria. *Int J Mol Sci* 2021; 22:23

Typas A, Banzhaf M, Gross CA, Vollmer W. From the regulation of peptidoglycan synthesis to bacterial growth and morphology. *Nat Rev Microbiol* 2011; 10:123–136

Egan AJF, Errington J, Vollmer W. Regulation of peptidoglycan synthesis and remodelling. *Nat Rev Microbiol* 2020; 18:446–460

Tsang MJ, Yakhnina AA, Bernhardt TG. NlpD links cell wall remodeling and outer membrane invagination during cytokinesis in *Escherichia coli*. *PLoS Genet* 2017; 13:e1006888

Heidrich C, Templin MF, Ursinus A, Merdanovic M, Berger J *et al.* Involvement of N-acetylmuramyl-L-alanine amidases in cell separation and antibiotic-induced autolysis of *Escherichia coli*. *Mol Microbiol* 2001; 41:167–178

Priyadarshini R, de Pedro MA, Young KD. Role of peptidoglycan amidases in the development and morphology of the division septum in *Escherichia coli*. *J Bacteriol* 2007; 189:5334–5347

Uehara T, Dinh T, Bernhardt TG. LytM-domain factors are required for daughter cell separation and rapid ampicillin-induced lysis in *Escherichia coli*. *J Bacteriol* 2009; 191:5094–5107

Uehara T, Parzych KR, Dinh T, Bernhardt TG. Daughter cell separation is controlled by cytokinetic ring-activated cell wall hydrolysis. *EMBO J* 2010; 29:1412–1422

Yang DC, Peters NT, Parzych KR, Uehara T, Markovski M *et al.* An ATP-binding cassette transporter-like complex governs cell-wall hydrolysis at the bacterial cytokinetic ring. *Proc Natl Acad Sci U S A* 2011; 108:E1052–60

Pichoff S, Du S, Lutkenhaus J. Roles of FtsEX in cell division. *Res Microbiol* 2019; 170:374–380

Cook J, Baverstock TC, McAndrew MBL, Stansfeld PJ, Roper DI *et al.* Insights into bacterial cell division from a structure of EnvC bound to the FtsX periplasmic domain. *Proc Natl Acad Sci U S A* 2020; 117:28355–28365

Rocaboy M, Herman R, Sauvage E, Remaut H, Moonens K *et al.* The crystal structure of the cell division amidase AmiC reveals the fold of the AMIN domain, a new peptidoglycan binding domain. *Mol Microbiol* 2013; 90:267–277

Mesnage S, Dellarole M, Baxter NJ, Rouget J-B, Dimitrov JD *et al.* Molecular basis for bacterial peptidoglycan recognition by LysM domains. *Nat Commun* 2014; 5:4269

Gurnani Serrano CK, Winkle M, Martorana AM, Biboy J, Morè N *et al.* ActS activates peptidoglycan amidases during outer membrane stress in *Escherichia coli*. *Mol Microbiol* 2021; 116:329–342

Mueller EA, Iken AG, Ali Öztürk M, Winkle M, Schmitz M *et al.* The active repertoire of *Escherichia coli* peptidoglycan amidases varies with physiochemical environment. *Mol Microbiol* 2021; 116:311–328

Bryant JA, Morris FC, Knowles TJ, Maderbocus R, Heinz E *et al.* Structure of dual BON-domain protein DolP identifies phospholipid binding as a new mechanism for protein localisation. *Elife* 2020; 9:e62614

Morris FC, Wells TJ, Bryant JA, Schager AE, Sevastsyanovich YR *et al.* YraP contributes to cell envelope integrity and virulence of *Salmonella enterica* Serovar Typhimurium. *Infect Immun* 2018; 86:11

Yeats C, Bateman A. The BON domain: a putative membrane-binding domain. *Trends Biochem Sci* 2003; 28:352–355

Ranava D, Yang Y, Orenday-Tapia L, Rousset F, Turlan C *et al.* Lipoprotein DolP supports proper folding of BamA in the bacterial outer membrane promoting fitness upon envelope stress. *Elife* 2021; 10:e67817

Baba T, Ara T, Hasegawa M, Takai Y, Okumura Y *et al.* Construction of *Escherichia coli* K-12 in-frame, single-gene knockout mutants: the Keio collection. *Mol Syst Biol* 2006; 2:0008

Datsenko KA, Wanner BL. One-step inactivation of chromosomal genes in *Escherichia coli* K-12 using PCR products. *Proc Natl Acad Sci U S A* 2000; 97:6640–6645

Thomason LC, Costantino N, Court DL. *E. coli* genome manipulation by P1 transduction. *Curr Protoc Mol Biol* 2007; Chapter 1:1

Ducret A, Quardokus EM, Brun YV. MicrobeJ, a tool for high throughput bacterial cell detection and quantitative analysis. *Nat Microbiol* 2016; 1:16077

Preibisch S, Saalfeld S, Tomancak P. Globally optimal stitching of tiled 3D microscopic image acquisitions. *Bioinformatics* 2009; 25:1463–1465

Mueller EA, Egan AJ, Breukink E, Vollmer W, Levin PA. Plasticity of *Escherichia coli* cell wall metabolism promotes fitness and antibiotic resistance across environmental conditions. *Elife* 2019; 8:e40754

Onufryk C, Crouch ML, Fang FC, Gross CA. Characterization of six lipoproteins in the sigmaE regulon. *J Bacteriol* 2005; 187:4552–4561

Peters NT, Morlot C, Yang DC, Uehara T, Vernet T *et al.* Structure-function analysis of the LytM domain of EnvC, an activator of cell wall remodelling at the *Escherichia coli* division site. *Mol Microbiol* 2013; 89:690–701

Miura K. An overview of current methods to confirm protein-protein interactions. *Protein Pept Lett* 2018; 25:728–733

Bernhardt TG, de Boer PAJ. The *Escherichia coli* amidase AmiC is a periplasmic septal ring component exported via the twin-arginine transport pathway. *Mol Microbiol* 2003; 48:1171–1182

5. General discussion

The bacterial cell envelope is a three-layered barrier that protects the cell from environmental threats. Its integrity during cell life cycle until its separation into daughter cells is essential. Several protein complexes or individual proteins via its interaction with others must be well coordinated to avoid cell lysis. In this thesis, we described a lipoprotein crucial for OM integrity, DolP, and tried to elucidate its function.

DolP is an important player in OM biogenesis. Studies have demonstrated that deletion of *dolP* in combination with *surA*, a gene involved in OM integrity, leads to cell death (Onufryk *et al.*, 2005; Typas *et al.*, 2008; Yan *et al.*, 2019). Moreover, cells lacking *dolP* shows perturbance in the membrane, becoming sensitive to detergents and antibiotics (Bryant *et al.*, 2020; Morris *et al.*, 2018; Tsang *et al.*, 2017).

Contributing to the study of the role of DolP in OM biogenesis, protein interactome studies have suggested that DolP is a component of the BAM complex (Babu *et al.*, 2018; Carlson *et al.*, 2019). In this study we tried to validate this model. We showed that there was an increase in the number of lysed cells visualised by microscopy of Δ*dolP*Δ*bamB* and Δ*dolP*Δ*bamE.* Furthermore, genetic interaction between those genes revealed a negative interaction, showing that deletion of *dolP* impacts cell fitness of *bamB* and *bamE* mutants. The impact in cell fitness can be due to alteration of membrane fluidity. Our previous study (Bryant *et al.*, 2020) showed an increase in membrane fluidity when DolP was deleted and others showed that *bamB* mutants are sensitive to membrane fluidity (Storek *et al.*, 2019), partially explaining the interaction. Therefore, this data suggests that DolP influences the function of outer membrane assembly and, more broadly, OM biogenesis.

However, our obtained results could not ultimately show how DolP may affect the BAM complex. Results published by the group of Ieva (Ranava *et al.*, 2021)

demonstrated that DolP is important for BamA folding, suggesting that DolP might not affect the complex mainly via BamB/C/E. These findings and ours support the hypothesis that DolP impacts BAM complex function.

The structure of DolP was recently revealed as a dual BON domain protein (BON1 and BON2). Specifically via BON2:α1 portion, DolP interacts with anionic phospholipids localising to the division site (Bryant *et al.*, 2020). Its localisation makes DolP an ideal protein to be part of the division process. Corroborating this theory, after genetic screenings, Tsang and group (Tsang *et al.*, 2017) identified DolP as a potential NlpD (amidase activator) regulator. Using PG degradation assay we have shown that it might not be the case. As evidence, we showed that the contact of DolP with amidases did not promote PG degradation. We also showed that DolP does not interact with NlpD, a feature expected for an activator (as AmiA/B/C interact with their cognate activators (Cook *et al.*, 2020; Uehara *et al.*, 2010)). In addition, Δ*dolP* does not phenocopy Δ*nlpD* under cell envelope stress conditions. If both proteins had connected functions, it would be expected to see the same phenotype in the conditions tested. These data indicate that DolP might not be a NlpD regulator. This information is relevant to the field, as future studies will take in consideration that the NlpD-AmiC pathway is regulated by a different mechanism and not via DolP.

Despite that DolP may not be an amidase activator, we identified that DolP is indeed involved in cell division. This link might be by interaction with the amidases AmiA and AmiC. Our *in vitro* interaction assays showed that DolP may interact with AmiA and interacts weakly with AmiC. AmiA is a promiscuous protein which interacts with multiple proteins. For example, aside its cognate regulator EnvC (Uehara *et al.*, 2010) it also interacts with the hydrolase scaffold protein NlpI (unpublished data), but

does not participate in the same pathway. Trying to elucidate these interactions we used a program, AlphaFold 2 Colab, to give us another indication if such interactions are likely. AlphaFold (Jumper *et al*, 2021) is a program that using a given amino acid sequence can predict 3D models of protein structure and protein:protein interaction. After structure analysis of intermolecular contact in ChimeraX 1.4 (Pettersen *et al*, 2021), a few bonds were revealed for DolP and AmiA, indicating a possible interaction (Figure 25). The closest predicted binding was a tyrosine (Y81) in AmiA and a tryptophan (W104) in DolP (atom distance 2.28 Å). Importantly, this same tryptophan was found to be determinant to DolP binding to anionic phospholipid, which guides DolP to cell division site localisation (Bryant *et al.*, 2020). Therefore, this tryptophan might be important for both binding AmiA and anionic phospholipids. This weak interaction might play a role in momentaneous recruitment of AmiA to the division site along with DolP for PG cleavage. As it will be discussed later, AmiA localises peripherally during cell division, so this recruitment can be sporadic. For the interaction between DolP and AmiC, we observed a link between AmiC tyrosine (Y263) and DolP threonine (T26) (atom distance 2.91 Å) (Figure 26).

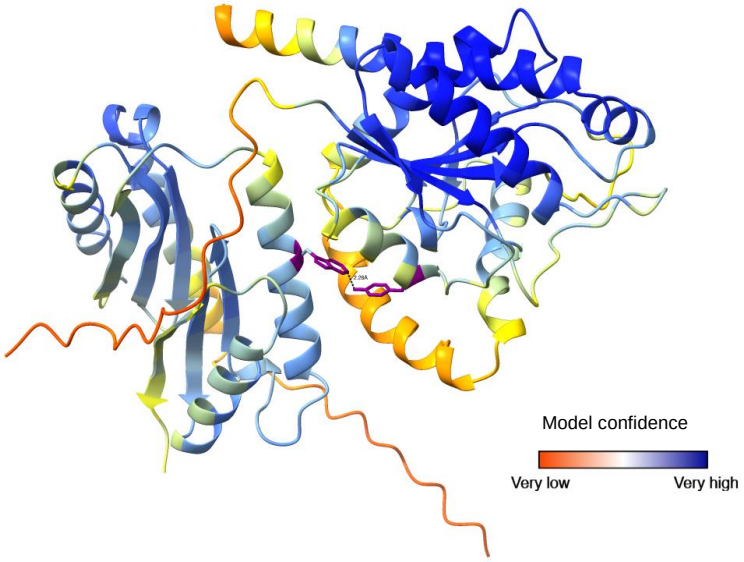

Figure 25 Prediction of protein interaction of DolP and AmiA. Prediction run by AlphaFold2 Colab.
The interacted residues (AmiA Y81 and DolP W104) are highlighted in purple. The distance between atoms is 2.28 Å indicated by dashed lines. Colour code indicates the model of confidence per-residue from very high (pLDDT > 90) to very low (pLDDT < 50). pLDDT = local distance difference test. Figure generated by ChimeraX 1.4.

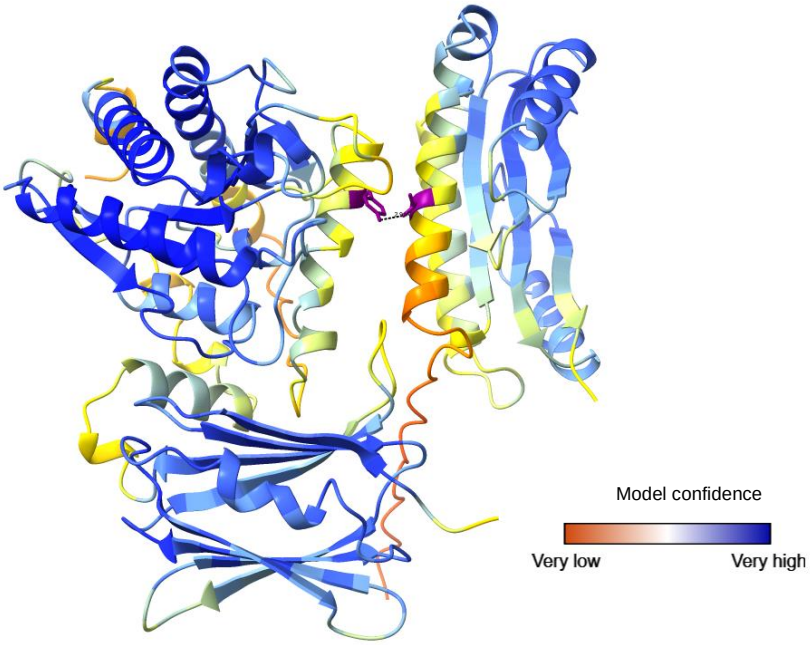

Figure 26 Prediction of protein interaction of DolP and AmiC. Prediction run by AlphaFold2 Colab.
The interacted residues (AmiC Y263 and DolP T26) are highlighted in purple. The distance between atoms is 2.91 Å indicated by dashed lines. Colour code indicates the model of confidence per-residue from very high (pLDDT > 90) to very low (pLDDT < 50). pLDDT = local distance difference test. Figure generated by ChimeraX 1.4.

The short distance between the atoms (less than 6 Å) can be considered as a reliable interaction (Yan *et al*, 2008). However, comparing with EnvC-FtsX, which are proteins with proved interaction and functionality, the complex presents more closer intermolecular contacts compared to DolP-amidases (Cook *et al.*, 2020). Besides, comparing the Kd showed in our MST data (AmiA Kd =486.9 nM ± 160 and AmiC 1650.0 nM ± 774) with other proven protein interaction, the Kd is higher. An example is NlpI and MepS (Kd =145 nM ± 52) where NlpI regulates the levels of MepS in cell to keep envelope integrity (Banzhaf *et al.*, 2020).

As we did not observe an interaction of DolP with AmiB by pull-down or MST, we also tested a prediction in AlphaFold to observe how a non-interaction is presented. Surprisingly, it detected an interaction of a glutamate (E278) in AmiB and a threonine (T103) in DolP (atom distance 3.04 Å) (Figure 27). It might present a very weak transient interaction that was not possible to detect by the *in vitro* methods used. In contrast, there was no interaction detected between DolP and EnvC (Figure 28), confirming the pull-down assay results. Nevertheless, to confirm predicted interface of DolP and amidases, we would have to test it experimentally. One way to test it is mutating single residues and verify if the proteins interaction would be disrupted. We would select, for example, the tryptophan (W104) in DolP that showed binding with AmiA. To detect which residue to be replaced with, we could do a coevolutionary analysis using Gremlin, a model that after sequencing alignment, it ranks inter protein residue pairs (Cook *et al.*, 2020; Ovchinnikov *et al*, 2014). After the point mutation, we would check the presence of interaction by pull-down. If there is no interaction detected, it means that the residue mutated is essential for protein interaction.

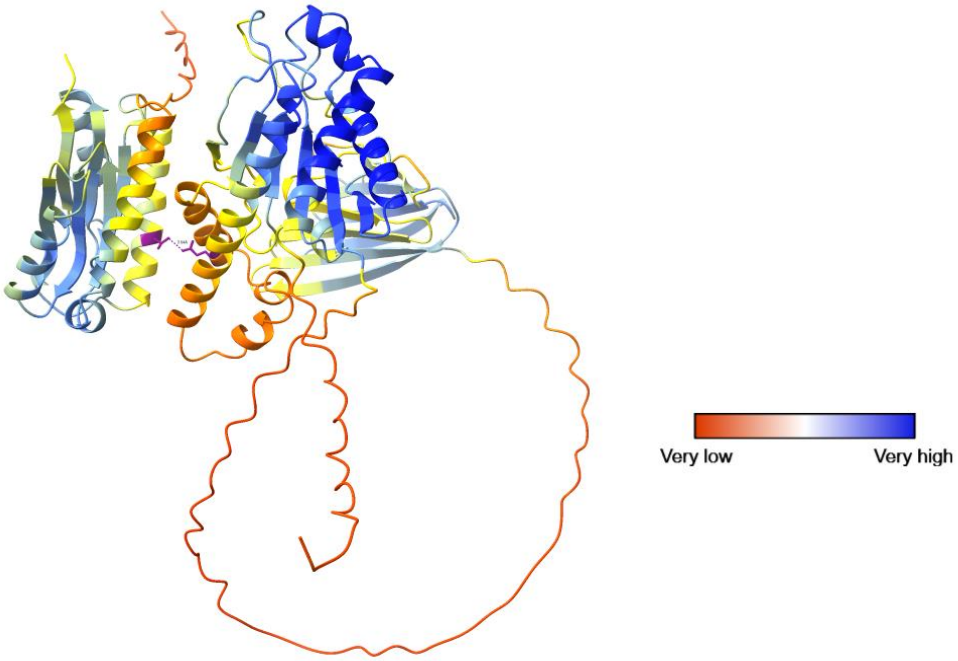

Figure 27. Prediction of protein interaction of DolP and AmiB. Prediction run by AlphaFold2 Colab.
The interacted residues (AmiB E278 and DolP T103) are highlighted in purple. The distance between atoms is 3.04 Å indicated by dashed lines. Colour code indicates the model of confidence per-residue from very high (pLDDT > 90) to very low (pLDDT < 50). pLDDT = local distance difference test. Figure generated by ChimeraX 1.4.

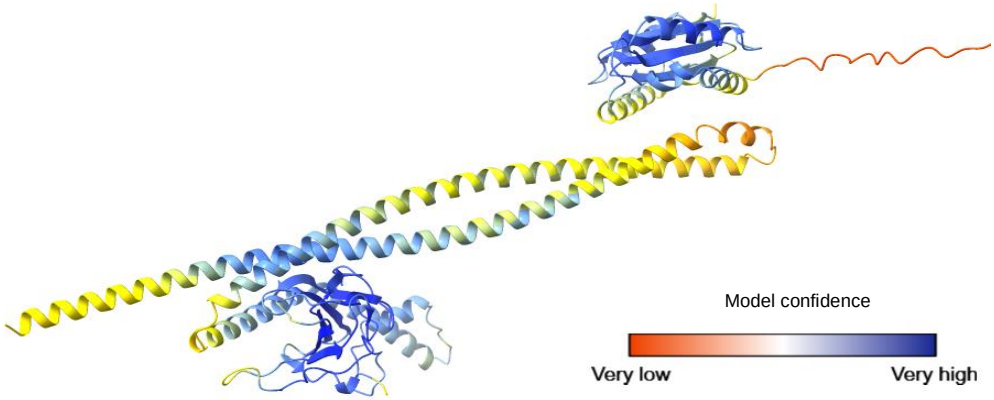

Figure 28 Prediction of protein interaction of DolP and EnvC. Prediction run by AlphaFold2 Colab.
There was no interaction detected. Colour code indicates the model of confidence per-residue from very high (pLDDT > 90) to very low (pLDDT < 50). pLDDT = local distance difference test. Figure generated by ChimeraX 1.4.

Overall, the interaction of DolP and the amidases might be transient, not forming strong binding affinity. The complex formation may be variable and dynamic as the multi-protein complex of PG synthases during cell elongation (Pazos *et al*, 2017). DolP might be part of such dynamic interaction with amidases and its regulator during cell division, assembling and disassembling to complete the PG hydrolysis.

Even though the interactions of DolP with AmiA and AmiC are weak, we showed other evidence of relation of DolP to division. We spotted new phenotypes when a panel of double mutants were analysed. Deletion of both *dolP* and *amiA* resulted in a mild chaining phenotype, indicating a defect in cleavage of the PG layer, which is not observed in its single mutation. Severe chaining was observed when the genes *envC, ftsX* or *ftsE* were deleted in cells lacking *dolP*. Seeing the same phenotype in absence of *dolP* and one of these three genes, agrees with their connected function of FtsEX regulating the activity of PG amidases via its interaction with EnvC. In this background, not having the FtsEX-EnvC-AmiA,B pathway available in absence of DolP, the remaining NlpD-AmiC is not enough to separate the cells. This data suggests that DolP may play a role in the NlpD-AmiC part of the PG hydrolysis.

Interestingly, when we deleted both *nlpD* and *amiA,* it was observed a filamentous phenotype, in contrast to the chaining in Δ*dolP*Δ*amiA.* This can indicate the importance of NlpD in septation opposed to DolP. To further investigate Δ*dolP*Δ*amiA* chaining phenotype, we excluded the hypothesis that it was caused by a link to the BAM complex or to ActS pathway. We failed in detecting a distinct phenotype when deleting these genes. Then, we raised the hypothesis that DolP involvement in cell division could be the amidases recruitment and localisation. However, we could not test this approach as AmiA localises peripherally (Bernhardt & de Boer, 2003) and

it has been published that AmiC localises to the division site independently of DolP (Tsang *et al.*, 2017).

The fact that DolP may interact with AmiA and AmiC strengthen the idea that DolP has an impact in cell separation. However, the exact mechanism is still unknown, and more studies are needed to clarify this role. An *in vivo* interaction between DolP and amidases could provide more insights on how and how strong these proteins stablish interaction. It was my plan to visit the University of Amsterdam to learn FRET (Förster Resonance Energy Transfer) technique during the period of my PhD, however, it was not possible due to the COVID-19 pandemic. FRET (Miura, 2018; Sun *et al*, 2013) would be a suitable option, as it demonstrates if the proteins physically interact. This technique depends on tagging the two proteins of interest, one with an acceptor chromophore which absorbs the donor fluorophore energy. If there is an interaction, just the acceptor fluorescence, usually yellow, will be detected by light microscopy. With these data, we could find that, for example, DolP physically interacts with AmiC during the cell division. As we know that deletion of *dolP* and *amiA* causes cell separation defect, the main remaining amidase available to complete the PG cleavage, AmiC, cannot function alone with NlpD. Just *in vitro* interactions do not show the proper possibility of interaction during the cell processes. FRET can indicate if the proteins are in close contact, as it could be the case for DolP and amidases at the division site.

We could not explicitly confirm the function of DolP and it is possibly related to a cellular process other than amidase or BAM complex regulation. Previous work in our lab (data not published) detected potential genetic interaction partners with *dolP* by TraDIS (Transposon Directed Insertion Site Sequencing). TraDIS is a high-

throughput genetics screen in which a library of random transposon insertion mutants are analysed by using DNA sequencing to identify transposon insertion sites. Essential genes are detected by the absence of transposon insertion sites and conditionally essential genes are identified by the comparison of the wild-type parent library to that of the knockout strain (Langridge *et al*, 2009). In our unpublished study we detected conditionally essential genes (genes that become essential) in a Δ*dolP* transposon mutant library after outgrowth. The data confirms the link to the amidases as *envC* and *ftsE* are detected as conditionally essential in the *dolP* strain (Figure 29a). The data also demonstrates that the gene *tolA* became essential (Figure 29b), indicating that the Tol-Pal system, especially TolA, could be a close interactor. Tol-Pal is a suitable pathway to relate to DolP, as both are involved in OM biogenesis. Tol-Pal is responsible for invaginating the OM and cleaving glycans during cell division (Gerding *et al.*, 2007; Yakhnina & Bernhardt, 2020). And DolP, as we now know, is involved in cell division and integrity of the OM. Further support for an interaction between *dolP* and *tol-pal* comes from a protein interactome study which revealed interaction between DolP and the proteins TolB/Q/R detecting an interaction score and probability higher than 0.6 and 90% respectively (Carlson *et al.*, 2019).

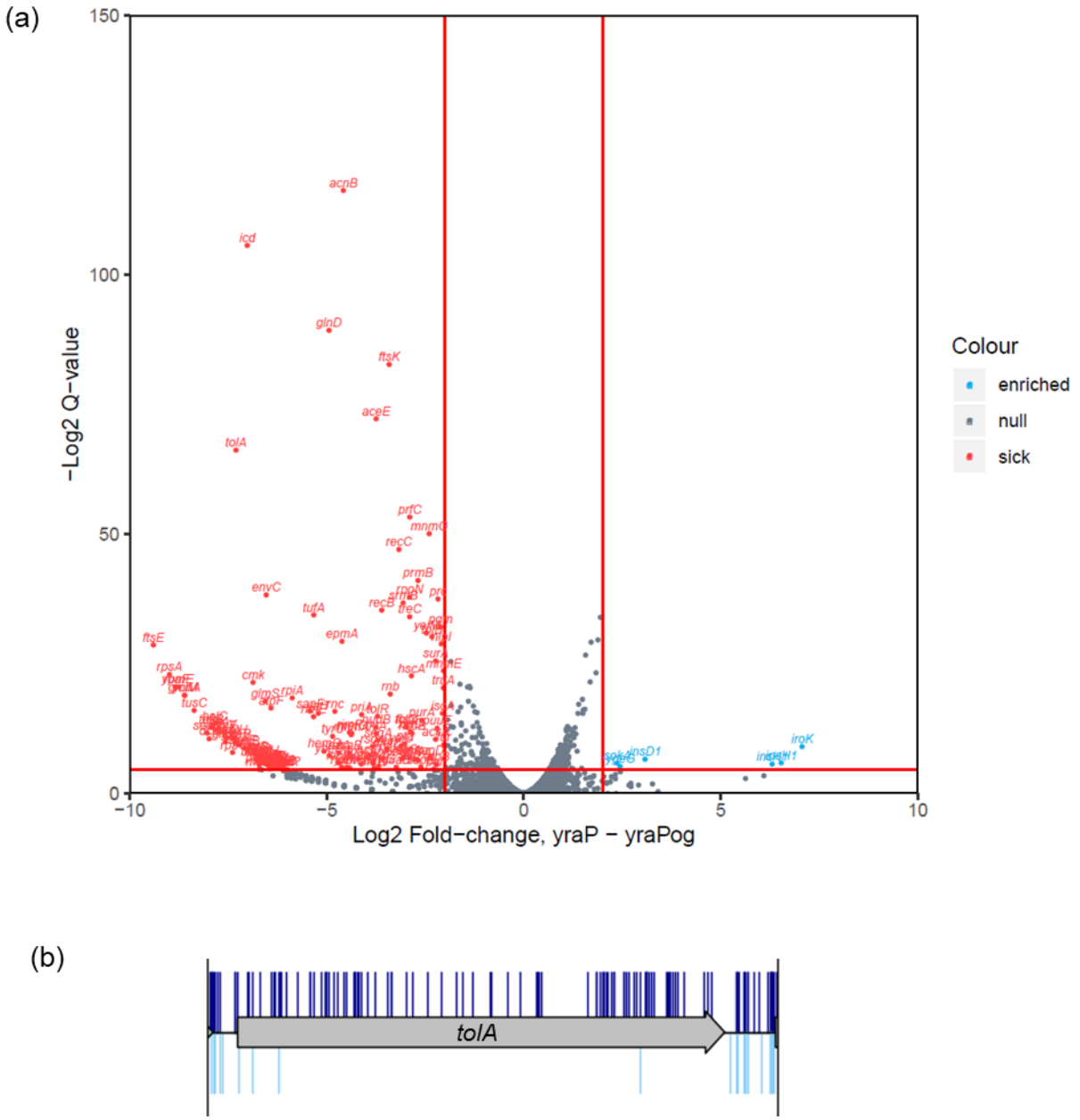

Figure 29 TraDIS data shows *tolA, envC* and *ftsE* as conditionally essential genes in a Δ*dolP* transposon mutant library after outgrowth in LB.
(a) Volcano plot of the fold-change in mapped reads between conditions, calculated using BioTraDIS. Datapoints in red correspond with genes with >2-fold decrease in reads in the Δ*dolP* dataset relative to the Δ*dolP* outgrowth dataset, and with a Q-value >0.01 (red horizontal line). (b) Representation of the *tolA* insertion data following Δ*dolP* dataset (dark blue, above) or in Δ*dolP* outgrowth (light blue, below). The transposon insertion position along the gene is marked by a vertical line.

To validate this model, microscopy of a panel of single and double mutants lacking *dolP* and *tol-pal* genes could speculate if DolP is indeed involved with this

system. The deletion of *tolA* and *pal* alone or the entire *tol-pal* system (*tolQRA-tolB-pal*) form long chains with PG splitting defect (Yakhnina & Bernhardt, 2020). If DolP is involved in this complex, it would be expected that deletion of *dolP* would worsen the chaining phenotype. Pal is the main substrate of the system due to its abundance (Szczepaniak *et al.*, 2020), therefore, deletion of *dolP* and specially *pal* would result in long cells. In addition, protein interaction *in vitro* (MST and pull-down) and *in vivo* (FRET) would inform if DolP and Tol-Pal can form complexes, as for example, TolA interacts with TolQ, TolR and Pal. With these results in hand, still it is quite complicated to find the exact function within the complex as we are dealing with promiscuous proteins.

Besides, as part of my PhD, originally, I would use another approach to detect hits of genes involved in cell envelope biogenesis, a CPRG (Chlorophenol red-beta-D-galactopyranoside) assay. The assay consists in incubating single gene deletion cells with CPRG. When the envelope is intact, this molecule cannot pass through. However, when the cell envelope is disrupted, the yellow CPRG crosses the envelope and reaches the cytoplasm. CPRG, a substrate of the β-galactosidase enzyme, is subsequently processed by this enzyme to the red chromophore CPR. This turnover indicates that the cell envelope is damaged. The project would involve analysing the KEIO collection under stress conditions to detect hits of genes involved in cell envelope biogenesis, and later focusing on other Gram-negative bacteria species. The data would contribute to detecting and describing other lipoproteins besides DolP. However, due to the COVID-19 pandemic, I could not complete this part of the project.

In summary, this thesis contributed to the lipoproteins field, indicating that lipoproteins are not involved just in synthesis and are not activators or need to be

activated. We showed evidence that DolP is indeed involved in cell division. Speculation of its exact mechanism still needs to be pondered. We also better described the role of DolP in the OM biogenesis, showing its link with the outer membrane protein assembly.

6. References

Baba T, Ara T, Hasegawa M, Takai Y, Okumura Y, Baba M, Datsenko KA, Tomita M, Wanner BL, Mori H (2006) Construction of *Escherichia coli* K-12 in-frame, single-gene knockout mutants: the Keio collection. *Mol Syst Biol* 2: 2006 0008

Babu M, Bundalovic-Torma C, Calmettes C, Phanse S, Zhang Q, Jiang Y, Minic Z, Kim S, Mehla J, Gagarinova A *et al* (2018) Global landscape of cell envelope protein complexes in *Escherichia coli*. *Nat Biotechnol* 36: 103-112

Bakelar J, Buchanan SK, Noinaj N (2016) The structure of the beta-barrel assembly machinery complex. *Science* 351: 180-186

Banzhaf M, Yau HC, Verheul J, Lodge A, Kritikos G, Mateus A, Cordier B, Hov AK, Stein F, Wartel M *et al* (2020) Outer membrane lipoprotein NlpI scaffolds peptidoglycan hydrolases within multi-enzyme complexes in *Escherichia coli*. *EMBO J* 39: e102246

Barreteau H, Kovac A, Boniface A, Sova M, Gobec S, Blanot D (2008) Cytoplasmic steps of peptidoglycan biosynthesis. *FEMS Microbiol Rev* 32: 168-207

Bernhardt TG, de Boer PA (2003) The *Escherichia coli* amidase AmiC is a periplasmic septal ring component exported via the twin-arginine transport pathway. *Mol Microbiol* 48: 1171-1182

Bernstein HD (2011) The double life of a bacterial lipoprotein. *Mol Microbiol* 79: 1128-1131

Bi EF, Lutkenhaus J (1991) FtsZ ring structure associated with division in *Escherichia coli*. *Nature* 354: 161-164

Boelter G, Bryant JA, Doherty H, Wotherspoon P, Alodaini D, Ma X, Alao MB, Moynihan PJ, Moradigaravand D, Glinkowska M *et al* (2022) The lipoprotein DolP affects cell separation in *Escherichia coli*, but not as an upstream regulator of NlpD. *Microbiology (Reading)* 168

Botta GA, Park JT (1981) Evidence for involvement of penicillin-binding protein 3 in murein synthesis during septation but not during cell elongation. *J Bacteriol* 145: 333-340

Bouhss A, Trunkfield AE, Bugg TD, Mengin-Lecreulx D (2008) The biosynthesis of peptidoglycan lipid-linked intermediates. *FEMS Microbiol Rev* 32: 208-233

Braun V, Hantke K (2019) Lipoproteins: Structure, Function, Biosynthesis. *Subcell Biochem* 92: 39-77

Braun V, Rehn K (1969) Chemical characterization, spatial distribution and function of a lipoprotein (murein-lipoprotein) of the *E. coli* cell wall. The specific effect of trypsin on the membrane structure. *Eur J Biochem* 10: 426-438

Bryant JA, Morris FC, Knowles TJ, Maderbocus R, Heinz E, Boelter G, Alodaini D, Colyer A, Wotherspoon PJ, Staunton KA *et al* (2020) Structure of dual BON-domain protein DolP identifies phospholipid binding as a new mechanism for protein localisation. *Elife* 9

Burman LG, Park JT (1984) Molecular model for elongation of the murein sacculus of *Escherichia coli*. *Proc Natl Acad Sci U S A* 81: 1844-1848

Carlson ML, Stacey RG, Young JW, Wason IS, Zhao Z, Rattray DG, Scott N, Kerr CH, Babu M, Foster LJ *et al* (2019) Profiling the *Escherichia coli* membrane protein interactome captured in Peptidisc libraries. *Elife* 8

Chimalakonda G, Ruiz N, Chng SS, Garner RA, Kahne D, Silhavy TJ (2011) Lipoprotein LptE is required for the assembly of LptD by the beta-barrel assembly machine in the outer membrane of *Escherichia coli*. *Proc Natl Acad Sci U S A* 108: 2492-2497

Chodisetti PK, Reddy M (2019) Peptidoglycan hydrolase of an unusual cross-link cleavage specificity contributes to bacterial cell wall synthesis. *Proc Natl Acad Sci U S A* 116: 7825-7830

Choi DS, Yamada H, Mizuno T, Mizushima S (1986) Trimeric structure and localization of the major lipoprotein in the cell surface of *Escherichia coli*. *J Biol Chem* 261: 8953-8957

Chung HS, Yao Z, Goehring NW, Kishony R, Beckwith J, Kahne D (2009) Rapid beta-lactam-induced lysis requires successful assembly of the cell division machinery. *Proc Natl Acad Sci U S A* 106: 21872-21877

Cook J, Baverstock TC, McAndrew MBL, Stansfeld PJ, Roper DI, Crow A (2020) Insights into bacterial cell division from a structure of EnvC bound to the FtsX periplasmic domain. *Proc Natl Acad Sci U S A* 117: 28355-28365

Dartigalongue C, Missiakas D, Raina S (2001) Characterization of the *Escherichia coli* sigma E regulon. *J Biol Chem* 276: 20866-20875

Datsenko KA, Wanner BL (2000) One-step inactivation of chromosomal genes in *Escherichia coli* K-12 using PCR products. *Proc Natl Acad Sci U S A* 97: 6640-6645

de Boer PA (2010) Advances in understanding *E. coli* cell fission. *Curr Opin Microbiol* 13: 730-737

de Boer PA, Crossley RE, Hand AR, Rothfield LI (1991) The MinD protein is a membrane ATPase required for the correct placement of the *Escherichia coli* division site. *EMBO J* 10: 4371-4380

de Boer PA, Crossley RE, Rothfield LI (1989) A division inhibitor and a topological specificity factor coded for by the minicell locus determine proper placement of the division septum in *E. coli*. *Cell* 56: 641-649

de Jong IG, Beilharz K, Kuipers OP, Veening JW (2011) Live Cell Imaging of Bacillus subtilis and *Streptococcus pneumoniae* using Automated Time-lapse Microscopy. *J Vis Exp*

Delcour AH (2009) Outer membrane permeability and antibiotic resistance. *Biochim Biophys Acta* 1794: 808-816

den Blaauwen T, Luirink J (2019) Checks and Balances in Bacterial Cell Division. *mBio* 10

Dominguez-Escobar J, Chastanet A, Crevenna AH, Fromion V, Wedlich-Soldner R, Carballido-Lopez R (2011) Processive movement of MreB-associated cell wall biosynthetic complexes in bacteria. *Science* 333: 225-228

Dramsi S, Magnet S, Davison S, Arthur M (2008) Covalent attachment of proteins to peptidoglycan. *FEMS Microbiol Rev* 32: 307-320

Du S, Lutkenhaus J (2017) Assembly and activation of the *Escherichia coli* divisome. *Mol Microbiol* 105: 177-187

Dubuisson JF, Vianney A, Hugouvieux-Cotte-Pattat N, Lazzaroni JC (2005) Tol-Pal proteins are critical cell envelope components of *Erwinia chrysanthemi* affecting cell morphology and virulence. *Microbiology* 151: 3337-3347

Ducret A, Quardokus EM, Brun YV (2016) MicrobeJ, a tool for high throughput bacterial cell detection and quantitative analysis. *Nat Microbiol* 1: 16077

Ebbensgaard A, Mordhorst H, Aarestrup FM, Hansen EB (2018) The Role of Outer Membrane Proteins and Lipopolysaccharides for the Sensitivity of *Escherichia coli* to Antimicrobial Peptides. *Front Microbiol* 9: 2153

Egan AJF (2018) Bacterial outer membrane constriction. *Mol Microbiol* 107: 676-687

Egan AJF, Errington J, Vollmer W (2020) Regulation of peptidoglycan synthesis and remodelling. *Nat Rev Microbiol*

Ehlert K, Holtje JV (1996) Role of precursor translocation in coordination of murein and phospholipid synthesis in *Escherichia coli*. *J Bacteriol* 178: 6766-6771

Erridge C, Bennett-Guerrero E, Poxton IR (2002) Structure and function of lipopolysaccharides. *Microbes Infect* 4: 837-851

Garner EC, Bernard R, Wang W, Zhuang X, Rudner DZ, Mitchison T (2011) Coupled, circumferential motions of the cell wall synthesis machinery and MreB filaments in *B. subtilis*. *Science* 333: 222-225

Gerding MA, Ogata Y, Pecora ND, Niki H, de Boer PA (2007) The trans-envelope Tol-Pal complex is part of the cell division machinery and required for proper outer-membrane invagination during cell constriction in *E. coli*. *Mol Microbiol* 63: 1008-1025

Goodall ECA, Robinson A, Johnston IG, Jabbari S, Turner KA, Cunningham AF, Lund PA, Cole JA, Henderson IR (2018) The Essential Genome of *Escherichia coli* K-12. *mBio* 9

Graham CLB, Newman H, Gillett FN, Smart K, Briggs N, Banzhaf M, Roper DI (2021) A Dynamic Network of Proteins Facilitate Cell Envelope Biogenesis in Gram-Negative Bacteria. *International Journal of Molecular Science* 22(23): 12831

Gray AN, Egan AJ, Van't Veer IL, Verheul J, Colavin A, Koumoutsi A, Biboy J, Altelaar AF, Damen MJ, Huang KC *et al* (2015) Coordination of peptidoglycan synthesis and outer membrane constriction during *Escherichia coli* cell division. *Elife* 4

Gu Y, Li H, Dong H, Zeng Y, Zhang Z, Paterson NG, Stansfeld PJ, Wang Z, Zhang Y, Wang W *et al* (2016) Structural basis of outer membrane protein insertion by the BAM complex. *Nature* 531: 64-69

Gurnani Serrano CK, Winkle M, Martorana AM, Biboy J, More N, Moynihan P, Banzhaf M, Vollmer W, Polissi A (2021) ActS activates peptidoglycan amidases during outer membrane stress in *Escherichia coli*. *Mol Microbiol*

Hagan CL, Kahne D (2011) The reconstituted *Escherichia coli* Bam complex catalyzes multiple rounds of beta-barrel assembly. *Biochemistry* 50: 7444-7446

Hantke K, Braun V (1973) Covalent binding of lipid to protein. Diglyceride and amide-linked fatty acid at the N-terminal end of the murein-lipoprotein of the *Escherichia coli* outer membrane. *Eur J Biochem* 34: 284-296

Hayashi S, Wu HC (1990) Lipoproteins in bacteria. *J Bioenerg Biomembr* 22: 451-471

Heidrich C, Templin MF, Ursinus A, Merdanovic M, Berger J, Schwarz H, de Pedro MA, Holtje JV (2001) Involvement of N-acetylmuramyl-L-alanine amidases in cell

separation and antibiotic-induced autolysis of *Escherichia coli*. *Mol Microbiol* 41: 167-178

Ikeda M, Sato T, Wachi M, Jung HK, Ishino F, Kobayashi Y, Matsuhashi M (1989) Structural similarity among *Escherichia coli* FtsW and RodA proteins and *Bacillus subtilis* SpoVE protein, which function in cell division, cell elongation, and spore formation, respectively. *J Bacteriol* 171: 6375-6378

Jumper J, Evans R, Pritzel A, Green T, Figurnov M, Ronneberger O, Tunyasuvunakool K, Bates R, Zidek A, Potapenko A *et al* (2021) Highly accurate protein structure prediction with AlphaFold. *Nature* 596: 583-589

Kim S, Malinverni JC, Sliz P, Silhavy TJ, Harrison SC, Kahne D (2007) Structure and function of an essential component of the outer membrane protein assembly machine. *Science* 317: 961-964

Knowles TJ, Scott-Tucker A, Overduin M, Henderson IR (2009) Membrane protein architects: the role of the BAM complex in outer membrane protein assembly. *Nat Rev Microbiol* 7: 206-214

Kritikos G, Banzhaf M, Herrera-Dominguez L, Koumoutsi A, Wartel M, Zietek M, Typas A (2017) A tool named Iris for versatile high-throughput phenotyping in microorganisms. *Nat Microbiol* 2: 17014

Langridge GC, Phan MD, Turner DJ, Perkins TT, Parts L, Haase J, Charles I, Maskell DJ, Peters SE, Dougan G *et al* (2009) Simultaneous assay of every *Salmonella* Typhi gene using one million transposon mutants. *Genome Res* 19: 2308-2316

Loose M, Kruse K, Schwille P (2011) Protein self-organization: lessons from the min system. *Annu Rev Biophys* 40: 315-336

Maeda H (1980) A new lysozyme assay based on fluorescence polarization or fluorescence intensity utilizing a fluorescent peptidoglycan substrate. *J Biochem* 88: 1185-1191

Magnet S, Bellais S, Dubost L, Fourgeaud M, Mainardi JL, Petit-Frere S, Marie A, Mengin-Lecreulx D, Arthur M, Gutmann L (2007) Identification of the L,D-transpeptidases responsible for attachment of the Braun lipoprotein to *Escherichia coli* peptidoglycan. *J Bacteriol* 189: 3927-3931

Maldonado RF, Sa-Correia I, Valvano MA (2016) Lipopolysaccharide modification in Gram-negative bacteria during chronic infection. *FEMS Microbiol Rev* 40: 480-493

Malinverni JC, Werner J, Kim S, Sklar JG, Kahne D, Misra R, Silhavy TJ (2006) YfiO stabilizes the YaeT complex and is essential for outer membrane protein assembly in *Escherichia coli*. *Mol Microbiol* 61: 151-164

Mamou G, Corona F, Cohen-Khait R, Housden NG, Yeung V, Sun D, Sridhar P, Pazos M, Knowles TJ, Kleanthous C *et al* (2022) Peptidoglycan maturation controls outer membrane protein assembly. *Nature* 606: 953-959

Meeske AJ, Riley EP, Robins WP, Uehara T, Mekalanos JJ, Kahne D, Walker S, Kruse AC, Bernhardt TG, Rudner DZ (2016) SEDS proteins are a widespread family of bacterial cell wall polymerases. *Nature* 537: 634-638

Mesnage S, Dellarole M, Baxter NJ, Rouget JB, Dimitrov JD, Wang N, Fujimoto Y, Hounslow AM, Lacroix-Desmazes S, Fukase K *et al* (2014) Molecular basis for bacterial peptidoglycan recognition by LysM domains. *Nat Commun* 5: 4269

Miura K (2018) An Overview of Current Methods to Confirm Protein-Protein Interactions. *Protein Pept Lett* 25: 728-733

Mohammadi T, van Dam V, Sijbrandi R, Vernet T, Zapun A, Bouhss A, Diepeveen-de Bruin M, Nguyen-Disteche M, de Kruijff B, Breukink E (2011) Identification of FtsW as a transporter of lipid-linked cell wall precursors across the membrane. *EMBO J* 30: 1425-1432

Morris FC, Wells TJ, Bryant JA, Schager AE, Sevastsyanovich YR, Squire DJP, Marshall J, Isom GL, Rooke J, Maderbocus R *et al* (2018) YraP Contributes to Cell Envelope Integrity and Virulence of *Salmonella enterica* Serovar Typhimurium. *Infect Immun* 86

Mueller EA, Egan AJ, Breukink E, Vollmer W, Levin PA (2019) Plasticity of *Escherichia coli* cell wall metabolism promotes fitness and antibiotic resistance across environmental conditions. *Elife* 8

Mueller EA, Iken AG, Ali Ozturk M, Winkle M, Schmitz M, Vollmer W, Di Ventura B, Levin PA (2021) The active repertoire of *Escherichia coli* peptidoglycan amidases varies with physiochemical environment. *Mol Microbiol*

Nakayama H, Kurokawa K, Lee BL (2012) Lipoproteins in bacteria: structures and biosynthetic pathways. *FEBS J* 279: 4247-4268

Nierhaus T, McLaughlin SH, Burmann F, Kureisaite-Ciziene D, Maslen SL, Skehel JM, Yu CWH, Freund SMV, Funke LFH, Chin JW *et al* (2022) Bacterial divisome protein FtsA forms curved antiparallel double filaments when binding to FtsN. *Nat Microbiol* 7: 1686-1701

O'Neil PK, Rollauer SE, Noinaj N, Buchanan SK (2015) Fitting the Pieces of the beta-Barrel Assembly Machinery Complex. *Biochemistry* 54: 6303-6311

Ohara M, Wu HC, Sankaran K, Rick PD (1999) Identification and characterization of a new lipoprotein, NlpI, in *Escherichia coli* K-12. *J Bacteriol* 181: 4318-4325

Okuda S, Tokuda H (2011) Lipoprotein sorting in bacteria. *Annu Rev Microbiol* 65: 239-259

Onufryk C, Crouch ML, Fang FC, Gross CA (2005) Characterization of six lipoproteins in the sigmaE regulon. *J Bacteriol* 187: 4552-4561

Ovchinnikov S, Kamisetty H, Baker D (2014) Robust and accurate prediction of residue-residue interactions across protein interfaces using evolutionary information. *Elife* 3: e02030

Papanastasiou M, Orfanoudaki G, Koukaki M, Kountourakis N, Sardis MF, Aivaliotis M, Karamanou S, Economou A (2013) The *Escherichia coli* peripheral inner membrane proteome. *Mol Cell Proteomics* 12: 599-610

Paradis-Bleau C, Markovski M, Uehara T, Lupoli TJ, Walker S, Kahne DE, Bernhardt TG (2010) Lipoprotein cofactors located in the outer membrane activate bacterial cell wall polymerases. *Cell* 143: 1110-1120

Patrick GL (2013) An Introduction to Medicinal Chemistry. *Oxford* 5th edition

Pazos M, Peters K, Casanova M, Palacios P, VanNieuwenhze M, Breukink E, Vicente M, Vollmer W (2018) Z-ring membrane anchors associate with cell wall synthases to initiate bacterial cell division. *Nat Commun* 9: 5090

Pazos M, Peters K, Vollmer W (2017) Robust peptidoglycan growth by dynamic and variable multi-protein complexes. *Curr Opin Microbiol* 36: 55-61

Peters NT, Morlot C, Yang DC, Uehara T, Vernet T, Bernhardt TG (2013) Structure-function analysis of the LytM domain of EnvC, an activator of cell wall remodelling at the *Escherichia coli* division site. *Mol Microbiol* 89: 690-701

Pettersen EF, Goddard TD, Huang CC, Meng EC, Couch GS, Croll TI, Morris JH, Ferrin TE (2021) UCSF ChimeraX: Structure visualization for researchers, educators, and developers. *Protein Sci* 30: 70-82

Pichoff S, Du S, Lutkenhaus J (2019) Roles of FtsEX in cell division. *Res Microbiol* 170: 374-380

Potel CM, Lin MH, Heck AJR, Lemeer S (2018) Widespread bacterial protein histidine phosphorylation revealed by mass spectrometry-based proteomics. *Nat Methods* 15: 187-190

Preibisch S, Saalfeld S, Tomancak P (2009) Globally optimal stitching of tiled 3D microscopic image acquisitions. *Bioinformatics* 25: 1463-1465

Priyadarshini R, de Pedro MA, Young KD (2007) Role of peptidoglycan amidases in the development and morphology of the division septum in *Escherichia coli*. *J Bacteriol* 189: 5334-5347

Qiao Y, Srisuknimit V, Rubino F, Schaefer K, Ruiz N, Walker S, Kahne D (2017) Lipid II overproduction allows direct assay of transpeptidase inhibition by beta-lactams. *Nat Chem Biol* 13: 793-798

Raetz CR, Dowhan W (1990) Biosynthesis and function of phospholipids in *Escherichia coli*. *J Biol Chem* 265: 1235-1238

Ranava D, Caumont-Sarcos A, Albenne C, Ieva R (2018) Bacterial machineries for the assembly of membrane-embedded beta-barrel proteins. *FEMS Microbiol Lett* 365

Ranava D, Yang Y, Orenday-Tapia L, Rousset F, Turlan C, Morales V, Cui L, Moulin C, Froment C, Munoz G *et al* (2021) Lipoprotein DolP supports proper folding of BamA in the bacterial outer membrane promoting fitness upon envelope stress. *Elife* 10

Rietschel ET, Kirikae T, Schade FU, Mamat U, Schmidt G, Loppnow H, Ulmer AJ, Zahringer U, Seydel U, Di Padova F *et al* (1994) Bacterial endotoxin: molecular relationships of structure to activity and function. *FASEB J* 8: 217-225

Rocaboy M, Herman R, Sauvage E, Remaut H, Moonens K, Terrak M, Charlier P, Kerff F (2013) The crystal structure of the cell division amidase AmiC reveals the fold of the AMIN domain, a new peptidoglycan binding domain. *Mol Microbiol* 90: 267-277

Rojas ER, Billings G, Odermatt PD, Auer GK, Zhu L, Miguel A, Chang F, Weibel DB, Theriot JA, Huang KC (2018) The outer membrane is an essential load-bearing element in Gram-negative bacteria. *Nature* 559: 617-621

Ruiz N (2008) Bioinformatics identification of MurJ (MviN) as the peptidoglycan lipid II flippase in *Escherichia coli*. *Proc Natl Acad Sci U S A* 105: 15553-15557

Ruiz N, Kahne D, Silhavy TJ (2009) Transport of lipopolysaccharide across the cell envelope: the long road of discovery. *Nat Rev Microbiol* 7: 677-683

Salje J, van den Ent F, de Boer P, Lowe J (2011) Direct membrane binding by bacterial actin MreB. *Mol Cell* 43: 478-487

Sanchez-Pulido L, Devos D, Genevrois S, Vicente M, Valencia A (2003) POTRA: a conserved domain in the FtsQ family and a class of beta-barrel outer membrane proteins. *Trends Biochem Sci* 28: 523-526

Schiffrin B, Brockwell DJ, Radford SE (2017) Outer membrane protein folding from an energy landscape perspective. *BMC Biol* 15: 123

Shrivastava R, Jiang X, Chng SS (2017) Outer membrane lipid homeostasis via retrograde phospholipid transport in *Escherichia coli*. *Mol Microbiol* 106: 395-408

Silhavy TJ, Kahne D, Walker S (2010) The bacterial cell envelope. *Cold Spring Harb Perspect Biol* 2: a000414

Singh SK, Parveen S, SaiSree L, Reddy M (2015) Regulated proteolysis of a cross-link-specific peptidoglycan hydrolase contributes to bacterial morphogenesis. *Proc Natl Acad Sci U S A* 112: 10956-10961

Singh SK, SaiSree L, Amrutha RN, Reddy M (2012) Three redundant murein endopeptidases catalyse an essential cleavage step in peptidoglycan synthesis of *Escherichia coli* K12. *Mol Microbiol* 86: 1036-1051

Sklar JG, Wu T, Gronenberg LS, Malinverni JC, Kahne D, Silhavy TJ (2007) Lipoprotein SmpA is a component of the YaeT complex that assembles outer membrane proteins in *Escherichia coli*. *Proc Natl Acad Sci U S A* 104: 6400-6405

Skovierova H, Rowley G, Rezuchova B, Homerova D, Lewis C, Roberts M, Kormanec J (2006) Identification of the sigmaE regulon of *Salmonella enterica* serovar Typhimurium. *Microbiology (Reading)* 152: 1347-1359

Storek KM, Vij R, Sun D, Smith PA, Koerber JT, Rutherford ST (2019) The *Escherichia coli* beta-Barrel Assembly Machinery Is Sensitized to Perturbations under High Membrane Fluidity. *J Bacteriol* 201

Sturgis JN (2001) Organisation and evolution of the *tol-pal* gene cluster. *J Mol Microbiol Biotechnol* 3: 113-122

Sun Y, Rombola C, Jyothikumar V, Periasamy A (2013) Forster resonance energy transfer microscopy and spectroscopy for localizing protein-protein interactions in living cells. *Cytometry A* 83: 780-793

Szczepaniak J, Holmes P, Rajasekar K, Kaminska R, Samsudin F, Inns PG, Rassam P, Khalid S, Murray SM, Redfield C *et al* (2020) The lipoprotein Pal stabilises the bacterial outer membrane during constriction by a mobilisation-and-capture mechanism. *Nat Commun* 11: 1305

Szewczyk J, Collet JF (2016) The Journey of Lipoproteins Through the Cell: One Birthplace, Multiple Destinations. *Adv Microb Physiol* 69: 1-50

Terrak M, Sauvage E, Derouaux A, Dehareng D, Bouhss A, Breukink E, Jeanjean S, Nguyen-Disteche M (2008) Importance of the conserved residues in the peptidoglycan glycosyltransferase module of the class A penicillin-binding protein 1b of *Escherichia coli*. *J Biol Chem* 283: 28464-28470

Thomason LC, Costantino N, Court DL (2007) *E. coli* genome manipulation by P1 transduction. *Curr Protoc Mol Biol* Chapter 1: Unit 1 17

Tommassen J (2010) Assembly of outer-membrane proteins in bacteria and mitochondria. *Microbiology* 156: 2587-2596

Tsang MJ, Bernhardt TG (2015a) Guiding divisome assembly and controlling its activity. *Curr Opin Microbiol* 24: 60-65

Tsang MJ, Bernhardt TG (2015b) A role for the FtsQLB complex in cytokinetic ring activation revealed by an ftsL allele that accelerates division. *Mol Microbiol* 95: 925-944

Tsang MJ, Yakhnina AA, Bernhardt TG (2017) NlpD links cell wall remodeling and outer membrane invagination during cytokinesis in *Escherichia coli*. *PLoS Genet* 13: e1006888

Typas A, Banzhaf M, Gross CA, Vollmer W (2012) From the regulation of peptidoglycan synthesis to bacterial growth and morphology. *Nat Rev Microbiol* 10: 123-136

Typas A, Nichols RJ, Siegele DA, Shales M, Collins SR, Lim B, Braberg H, Yamamoto N, Takeuchi R, Wanner BL *et al* (2008) High-throughput, quantitative analyses of genetic interactions in *E. coli*. *Nat Methods* 5: 781-787

Uehara T, Bernhardt T.G. (2011) More than just lysins: peptidoglycan hydrolases tailor the cell wall. *Current Opinion in Microbiology*

Uehara T, Dinh T, Bernhardt TG (2009) LytM-domain factors are required for daughter cell separation and rapid ampicillin-induced lysis in *Escherichia coli*. *J Bacteriol* 191: 5094-5107

Uehara T, Parzych KR, Dinh T, Bernhardt TG (2010) Daughter cell separation is controlled by cytokinetic ring-activated cell wall hydrolysis. *EMBO J* 29: 1412-1422

van den Ent F, Johnson CM, Persons L, de Boer P, Lowe J (2010) Bacterial actin MreB assembles in complex with cell shape protein RodZ. *EMBO J* 29: 1081-1090

van Teeffelen S, Wang S, Furchtgott L, Huang KC, Wingreen NS, Shaevitz JW, Gitai Z (2011) The bacterial actin MreB rotates, and rotation depends on cell-wall assembly. *Proc Natl Acad Sci U S A* 108: 15822-15827

Vollmer W, Bertsche U (2008) Murein (peptidoglycan) structure, architecture and biosynthesis in *Escherichia coli*. *Biochim Biophys Acta* 1778: 1714-1734

Vollmer W, Blanot D, de Pedro MA (2008) Peptidoglycan structure and architecture. *FEMS Microbiol Rev* 32: 149-167

Vollmer W, Seligman SJ (2010) Architecture of peptidoglycan: more data and more models. *Trends Microbiol* 18: 59-66

Voulhoux R, Bos MP, Geurtsen J, Mols M, Tommassen J (2003) Role of a highly conserved bacterial protein in outer membrane protein assembly. *Science* 299: 262-265

Wang P, Robert L, Pelletier J, Dang WL, Taddei F, Wright A, Jun S (2010) Robust growth of *Escherichia coli*. *Curr Biol* 20: 1099-1103

Widmalm JSG (2019) Lipopolysaccharides of Gram-Negative Bacteria: Biosynthesis and Structural Aspects. *Trends in Glycoscience and Glycotechnology*

Wu EL, Fleming PJ, Yeom MS, Widmalm G, Klauda JB, Fleming KG, Im W (2014) *E. coli* outer membrane and interactions with OmpLA. *Biophys J* 106: 2493-2502

Wu HC, Lai JS, Hayashi S, Giam CZ (1982) Biogenesis of membrane lipoproteins in *Escherichia coli*. *Biophys J* 37: 307-315

Wu T, Malinverni J, Ruiz N, Kim S, Silhavy TJ, Kahne D (2005) Identification of a multicomponent complex required for outer membrane biogenesis in *Escherichia coli*. *Cell* 121: 235-245

Xiao J, Goley ED (2016) Redefining the roles of the FtsZ-ring in bacterial cytokinesis. *Curr Opin Microbiol* 34: 90-96

Yakhnina AA, Bernhardt TG (2020) The Tol-Pal system is required for peptidoglycan-cleaving enzymes to complete bacterial cell division. *Proc Natl Acad Sci U S A* 117: 6777-6783

Yan C, Wu F, Jernigan RL, Dobbs D, Honavar V (2008) Characterization of protein-protein interfaces. *Protein J* 27: 59-70

Yan Z, Hussain S, Wang X, Bernstein HD, Bardwell JCA (2019) Chaperone OsmY facilitates the biogenesis of a major family of autotransporters. *Mol Microbiol* 112: 1373-1387

Yang DC, Peters NT, Parzych KR, Uehara T, Markovski M, Bernhardt TG (2011) An ATP-binding cassette transporter-like complex governs cell-wall hydrolysis at the bacterial cytokinetic ring. *Proc Natl Acad Sci U S A* 108: E1052-1060

Yang Y, Santos AL, Xu L, Lotton C, Taddei F, Lindner AB (2019) Temporal scaling of aging as an adaptive strategy of *Escherichia coli*. *Science Advances* 5: eaaw2069

Yeats C, Bateman A (2003) The BON domain: a putative membrane-binding domain. *Trends Biochem Sci* 28: 352-355

Yousif SY, Broome-Smith JK, Spratt BG (1985) Lysis of *Escherichia coli* by beta-lactam antibiotics: deletion analysis of the role of penicillin-binding proteins 1A and 1B. *J Gen Microbiol* 131: 2839-2845

7. Appendix

Oligonucleotides

Name	Sequence 5’ - 3’
envC fw	CCGCTGATTTACGTTGGTGA
envC rv	CGTGCGGTGAATCGGGTAAT
nlpD fw	CCGTGCGCTTTGTCCCTTTAG
nlpD rv	CAAATCGTTATCACTGGGTTCC
amiA fw	GCGTGAACGGTCGAATTAGC
amiA rv	TCTTCGACAAATTCTGCGCC
amiB fw	CCACTTATACGCTGGTCGAA
amiB rv	AAAGCCCAGGCTGATAATGG
amiC fw	GCTAAAGTTTCCGGTCAAAT
amiC rv	GGTCGTCGGTTCAAATCCGG
actS fw	AGTTCGATACCTCTACAGCG
actS rv	ATCGAACCCTCGTATAGAGC
bamB fw	GCGCGTAGTGCATGGGAAGC
bamB rv	CAACGCACGCTATATTCGCG
bamC fw	GGTCTTGTGGCGACCGATAC
bamC rv	CCTTATCCGAACTACGTCCG
bamE fw	GCTTCACGGTCAGAGTAAAC
bamE rv	GAGCTTCGCAGGCAACGAGC

Plasmids

Plasmid	Properties	Source
pET17b *dolP*::mCherry	codon optimised mCherry gene at the 3’ end of the *dolP* gene	(Bryant *et al.*, 2020)
pET-26b(+)	plasmid vector at NdeI/ XhoI restriction sites	(Bryant *et al.*, 2020)

Bacterial strains

Strain ID	Genotype	Source
MB01064	BW25113	(Datsenko & Wanner, 2000)
MB01065	BW25113 Δ*dolP*	(Bryant *et al.*, 2020)
MB01086	BW25113 *ΔdolP ΔbamB::cm*	This study
MB01083	BW25113 *ΔdolPΔbamC::kan*	This study
MB01081	BW25113 *ΔdolPΔbamE::kan*	This study
MB01119	BW25113 Δ*amiA::kan*	This study
MB01120	BW25113 Δ*amiB::kan*	This study
MB01121	BW25113 Δ*amiC::kan*	This study
MB01122	BW25113 Δ*envC::kan*	This study
MB01051	BW25113 Δ*nlpD::kan*	This study
MB01123	BW25113 Δ*ftsE::kan*	This study
MB01124	BW25113 Δ*ftsX::kan*	This study
MB01125	BW25113 Δ*dolP*Δ*amiA::kan*	This study
MB01126	BW25113 Δ*dolP*Δ*amiB::kan*	This study
MB01127	BW25113 Δ*dolP*Δ*amiC::kan*	This study
MB01128	BW25113 Δ*dolP*Δ*envC::kan*	This study
MB01052	BW25113 Δ*dolP*Δ*nlpD::kan*	This study
MB01129	BW25113 Δ*dolP*Δ*ftsE::kan*	This study
MB01130	BW25113 Δ*dolP*Δ*ftsX::kan*	This study
MB01152	BW25113 *ΔnlpDΔamiA::kan*	This study
MB01153	BW25113 *ΔnlpDΔenvC::kan*	This study
MB01105	BW25113 *ΔbamB::cm*	This study
MB01107	BW25113 *ΔbamC::cm*	This study
MB01109	BW25113 *ΔbamE::cm*	This study
MB01110	BW25113 *ΔbamB::cmΔamiA::kan*	This study
MB01111	BW25113 *ΔbamC::cmΔamiA::kan*	This study
MB01112	BW25113 *ΔbamE::cmΔamiA::kan*	This study
MB01116	BW25113 Δ*actS::kan*	This study
MB01117	BW25113 Δ*dolP*Δ*actS::kan*	This study

Design of novel Zn-Ag-Zr alloy with enhanced strength as a potential biodegradable implant material

Maria Watroba, Wiktor Bednarczyk, Jakub Kawałko, Krzysztof Mech, Marianna Marciszko, **Gabriela Boelter**, Manuel Banzhaf, Piotr Bała

Materials & Design. 2019 Dec 5;183:108154.
DOI: 10.1016/j.matdes.2019.108154

In this article, the authors developed an alloy with biodegradable property, not being necessary to remove the implant from the body. To validate this possibility, the implant had to be tested against microorganisms' growth to evaluate its antimicrobial property. With this purpose, in our lab, we performed an antimicrobial activity test of the material for Gram-positive (*S. aureus)* and Gram-negative (*E. coli*) bacteria. The results showed that the metal alloys containing Ag (silver) were the most successful in terms of antibacterial effects.

My contribution was the antimicrobial activity assay (Figure 8). I prepared cultures of *E. coli* and *S. aureus* to be inoculated and spread on LB agar plates. I sterilised and autoclaved the metal alloys to remove any contaminant. The alloys were placed on the agar plates containing a lawn of bacteria and the plates were incubated overnight at 37°C. After the incubation time, I took pictures of the plates and observed the formation of halo around the alloys, measuring the inhibition zone of bacterial growth. Presence of inhibition zone meant that the metal, especially Ag, ions were released on the media, avoiding the growth of microorganisms tested.

Biofilm Inhibitor Taurolithocholic Acid Alters Colony Morphology, Specialized Metabolism, and Virulence of *Pseudomonas aeruginosa*

Alanna R. Condren, Lisa Juliane Kahl, **Gabriela Boelter**, George Kritikos, Manuel Banzhaf, Lars E. P. Dietrich, and Laura M. Sanchez

ACS infectious diseases. 2019 Dec 18;6(4):603-12.
DOI: 10.1021/acsinfecdis.9b00424

The paper's aim was to test the biofilm inhibitor Taurolithocholic Acid (TLCA) against *P. aeruginosa.* To test the virulence effects of TLCA we used *Galleria mellonella* as model organism. A previously reported biofilm-dispersing agent, sodium nitroprusside (SNP), was also included in the study to compare its effects with TLCA. TLCA and SNP were injected in larvae infected and non-infected with *P. aeruginosa.* These two groups were compared with larvae infected with bacteria but no TLCA. The main conclusion was the treatment with TLCA increases virulence of *P. aeruginosa,* showing a lower survival rate for this group of larvae.

My contribution to the study was the experimental part of virulence assay with *Galleria mellonella*. I performed the preliminary tests to find the right concentration of the chemicals tested and the best OD of bacteria for injection in the larvae. After injection, I recorded the number of living larvae checking it by external stimuli (poking) and took pictures of the organisms tested at every time point of one hour after 8 hours of infection. Once the preliminary tests were satisfactory, I did several repeats to gather the final results which are shown in the paper (Figure 3).

Structure of dual BON-domain protein DolP identifies phospholipid binding as a new mechanism for protein localisation

Jack A Bryant, Faye C Morris, Timothy J Knowles, Riyaz Maderbocus, Eva Heinz, **Gabriela Boelter**, Dema Alodaini, Adam Colyer, Peter J Wotherspoon, Kara A Staunton, Mark Jeeves, Douglas F Browning, Yanina R Sevastsyanovich, Timothy J Wells, Amanda E Rossiter, Vassiliy N Bavro, Pooja Sridhar, Douglas G Ward, Zhi-Soon Chong, Emily CA Goodall, Christopher Icke, Alvin CK Teo, Shu-Sin Chng, David I Roper, Trevor Lithgow, Adam F Cunningham, Manuel Banzhaf, Michael Overduin, Ian R Henderson

Elife. 2020 Dec 14;9:e62614.
DOI: 10.7554/eLife.62614

In this paper the authors solved the structure of the lipoprotein DolP (formerly YraP) in *E. coli* and gave contributions on its function in cell envelope biogenesis and folding of ß-barrel proteins. DolP is localised in the bacterial outer membrane, and it is composed of two BON-domains. It was found that the C-terminal of BON domains bind anionic phospholipids. This link is important for DolP localisation to the division site. Besides the structural discoveries, it was described that cells lacking *dolP* gene presents increase in membrane fluidity and become sensitive to stresses such as vancomycin and SDS, linking it to envelope biogenesis. Also, a suggestion that DolP contributes to the BAM complex was raised. The study showed that bacterial growth is affected when *dolP* gene is deleted in cells lacking *bamB* and *bamE* genes.

My contribution to the work was regarding genetic interactions and microscopy of DolP and the non-essential components of the BAM complex, BamB, BamC and BamE (Figure supplement 1). As described in Chapter 3 of this thesis, I did the microscope experiments and genetic interaction with Δ*dolP,* Δ*bamB,* Δ*bamC,* Δ*bamE,* Δ*dolP*Δ*bamB,* Δ*dolP*Δ*bamC* and Δ*dolP*Δ*bamE.* The genetic interaction results indicated that Δ*dolP*Δ*bamB* and Δ*dolP*Δ*bamE* shows negative interaction when compared to WT, and single *dolP* and *bamB* knockouts. The microscopy revealed that Δ*dolP*Δ*bamB* and Δ*dolP*Δ*bamE* show a high number of lysing cells. In conclusion, DolP might impact the BAM complex function.

Structure-Function Characterization of the Conserved Regulatory Mechanism of the *Escherichia coli* M48 Metalloprotease BepA

Jack A. Bryant, Ian T. Cadby, Zhi-Soon Chong, **Gabriela Boelter**, Yanina R. Sevastsyanovich, Faye C. Morris, Adam F. Cunningham, George Kritikos, Richard W. Meek, Manuel Banzhaf, Shu-Sin Chng, Andrew L. Lovering, Ian R. Henderson

Journal of bacteriology. 2020 Dec 18;203(2):e00434-20.
DOI: 10.1128/JB.00434-20

BepA is a periplasmic metalloprotease which supports the proper folding of LptD, a component of the Lpt system, responsible for LPS transport to the surface of the OM. In this study, the authors revealed the structure of BepA in *E. coli* showing an active-site plug of the M48 metalloprotease. In more detail, the authors discovered that this active-site plug is crucial for BepA function. In addition, in conditions of stress, the negative pocket and the TRP (tetratricopeptide repeat) cavity are necessary for function and degradation of BamA. Deleting BepA leads to lipid asymmetry of the OM, exposing phospholipids to the surface.

In the paper, the hypothesis that the movement of the active-site plug was raised as being required for the access of the substrates to the active site. So, the authors tried to tether the active site in the conformation observed in the crystal structure by engineering a disulphide bond. Cysteine substitutions were introduced into proximal sites in BepA, specifically at positions E103 and E241 in the active-site plug, either individually or in concert.

My contribution to the paper was to test whether the disulphide bond in the E103CE241C double mutant is formed and whether it prevents activity of the enzyme. It was shown that BepA degrades the BAM complex component BamA under conditions of stress induced by the absence of the chaperone SurA. Therefore, I inserted the plasmids EV (empty vector), WT (wild type bepA), E103C, E241C, E103CE241C in Δ*bepA*Δ*surA* cells by transformation. Next, I did Western blots with these strains grew in media with and without TCEP, a regulatory agent needed to break the disulphide bond and allow movement of the regulatory plug. The primary antibody used was PD5/BamA POTRA SY0121 and the secondary antibody, anti-rabbit HRP antibody. The outcome of the Western blots was that we could see a ~40 KDa band of double cysteine mutation E103CE241C in presence of TCEP corresponding to a break down product of BamA, but not in absence of TCEP (Figure 4c). The data demonstrate that there was a break of the disulphide bond allowing movement of the regulatory plug and that BepA proteolytic degradation of the substrate BamA requires free movement of the active-site plug.

Loss of YhcB results in dysregulation of coordinated peptidoglycan, LPS and phospholipid synthesis during *Escherichia coli* cell growth

Emily C. A. Goodall, Georgia L. Isom, Jessica L. Rooke, Karthik Pullela, Christopher Icke, Zihao Yang, **Gabriela Boelter**, Alun Jones, Isabel Warner, Rochelle Da Costa, Bing Zhang, James Rae, Wee Boon Tan, Matthias Winkle, Antoine Delhaye, Eva Heinz, Jean-Francois Collet, Adam F. Cunningham, Mark A. Blaskovich, Robert G. Parton, Jeff A. Cole, Manuel Banzhaf, Shu-Sin Chng, Waldemar Vollmer, Jack A. Bryant, Ian R. Henderson

PLoS genetics. 2021 Dec 23;17(12):e1009586.
DOI: 10.1371/journal.pgen.1009586

A TraDIS library of *E. coli* K-12 was exposed to polymyxin B, an antibiotic which disrupts the cell envelope, to identify genes responsible for envelope integrity. The gene *yhcB* was identified as essential to polymyxin B resistance. Next, the authors created a TraDIS library of a Δ*yhcB* mutant to identify which genes are or not essential when this gene is deleted. A series of genes were spotted having a synthetic lethal or suppression relationship with *yhcB*. In conclusion, YhcB was placed as an important player in several envelope biogenesis pathways, mainly PG regulation and LPS and phospholipid synthesis.

My contribution to the paper was to validate the data generated by the TraDIS library of Δ*yhcB.* The genes *dacA, lpxM, mepS, wecF, amiD* and *mltG* were identified as synthetic lethal in Δ*yhcB* cells. To confirm these results, I did P1 transduction to

insert the deletion of these genes in WT (BW25113) and Δ*yhcB* cells. The outcome was that there were less colonies or none on the double mutants plates after P1 transduction, confirming the synthetic lethality (Supporting Figure 7d). On the contrary, the genes *mlaD, nlpI and fabF* were identified as suppressor genes, recovering the sensitivity of Δ*yhcB* in vancomycin or SDS and EDTA. To verify this data, single and double deletions were created by P1 transduction in WT (BW25113) and Δ*yhcB* backgrounds. Later, cultures of the strains were serial diluted and inoculated on LB agar plates with or without vancomycin or SDS and EDTA. The plates were incubated and after ~16h we confirmed that Δ*mlaD*Δ*yhcB,* Δ*nlpI*Δ*yhcB* and Δ*fabF*Δ*yhcB* were resistant to the stresses tested compared to Δ*yhcB* (Supporting Figure 8c).

Early midcell localization of *Escherichia coli* PBP4 supports the function of peptidoglycan amidases

Jolanda Verheul, Adam Lodge, Hamish C. L. Yau, Xiaolong Liu, **Gabriela Boelter**, Xinwei Liu, Alexandra S. Solovyova, Athanasios Typas, Manuel Banzhaf, Waldemar Vollmer, Tanneke den Blaauwen

PLoS Genetics. 2022 May 23;18(5):e1010222.
DOI: 10.1371/journal.pgen.1010222

The aim of the paper was to decipher the function of a single PG hydrolase, the DD-endopeptidase PBP4, as *E. coli* present several enzymes with apparent redundant roles during cell elongation and division. The study revealed that PBP4 is localised in the midcell during PG synthesis in the septa and also contributes to the assembly of the division machinery.

My contribution to the paper was to verify the phenotype of deletion of *amiA/B/C, envC* and *nlpD* in a Δ*dacB* (PBP4 encoding gene) background (Figure 7). The authors indicated that the activity of PBP4 could be related to the start of cell division, as there is an augmentation of PBP4 expression in Δ*amiAB,* PBP4 is dependent on FtsEX for septal localisation, and affects the timing of divisome assembly. To test whether PBP4 helps AmiA/B to provide denuded glycan strands that would attract FtsN, I did phase contrast and fluorescent microscopy of the double mutant panel. After the imaging, I analysed the phenotypes by measuring the length and number of septa per cell with MicrobeJ software. The results revealed that when deleting *dacB,* the Δ*envC* chaining

phenotype is exacerbated, presenting double of the length of single Δ*envC* cells. Single amidases or *amiA/B* single deletion were not affected by the deletion of *dacB.* In conclusion, PBP4 and EnvC are important for the function of AmiA and/or AmiB.

LI-detector: a method for curating ordered gene-replacement libraries

Emily Goodall, Faye Morris, Samantha McKeand, Rudi Sullivan, Isabel Warner, Emma Sheehan, **Gabriela Boelter**, Christopher Icke, Adam Cunningham, Jeff Cole, Manuel Banzhaf, Jack Bryant, and Ian Henderson

Spectrum. 2022 Jul 20:e00833-22.
DOI: 10.1128/spectrum.00833-22

In this paper, a method was benchmarked to validate the knock-out mutants of any collection where the genes were disrupted or replaced by uniform linear insertion (LI). This method was applied to validate the Keio collection. As libraries such as the Keio consists of high number of mutants, it is prone to present errors in certain deletions or to be contaminated during long term use. Those errors are important to consider, as subsequent phenotype experiments with a wrong mutant can cause misinformation in future analysis.

Here, it was found that most of the genes had the kanamycin cassette placed in the correct position. However, it was identified discrepancies in the correct collection of 148 genes. Of these, 54 genes did not have the kanamycin cassette identified. My contribution to the paper was to verify if these mutants are indeed incorrect. Therefore, I isolated single colonies of the mutants from our Keio collection. Then, I performed PCR using a primer specific for the kanamycin resistance cassette and a reverse degenerate primer and sequence the PCR product by Sanger sequence using a nested primer specific for the cassette. Afterwards, using Artemis, I could compare if

the sequence from the isolates matched the gene deletion originally designated in the library. We found that most of these isolates were contaminated with nearby isolates of the same Keio collection plate. A table of all knock-outs tested are found in Supplemental material Dataset S1.